THE INTERNATIONAL INTRAVAL PROJECT

Phase 2, Working Group 2 Report

FINNSJÖN, STRIPA AND WIPP2

AEN NEA

SKi

THE INTERNATIONAL INTRAVAL PROJECT

TO STUDY VALIDATION OF GEOSPHERE
TRANSPORT MODELS FOR PERFORMANCE ASSESSMENT
OF NUCLEAR WASTE DISPOSAL

PHASE 2, Working Group 2 Report

Finnsjön, Stripa and WIPP2

P. Andersson, GEOSIGMA
D. Billaux, ITASCA
F. Guérin, BRGM
C.P. Jackson, AEA Technologies
S.P. Neuman, University of Arizona
C.F. Tsang, Lawrence Berkeley Laboratory
A. Winberg, Conterra

The Coordinating Group of the INTRAVAL Project
Swedish Nuclear Power Inspectorate (SKI)

NUCLEAR ENERGY AGENCY
ORGANISATION FOR ECONOMIC CO-OPERATION AND DEVELOPMENT

NEA **SKi**

ORGANISATION FOR ECONOMIC CO-OPERATION AND DEVELOPMENT

Pursuant to Article 1 of the Convention signed in Paris on 14th December 1960, and which came into force on 30th September 1961, the Organisation for Economic Co-operation and Development (OECD) shall promote policies designed:

- to achieve the highest sustainable economic growth and employment and a rising standard of living in Member countries, while maintaining financial stability, and thus to contribute to the development of the world economy;
- to contribute to sound economic expansion in Member as well as non-member countries in the process of economic development; and
- to contribute to the expansion of world trade on a multilateral, non-discriminatory basis in accordance with international obligations.

The original Member countries of the OECD are Austria, Belgium,Canada, Denmark, France, Germany, Greece, Iceland, Ireland, Italy, Luxembourg, the Netherlands, Norway, Portugal, Spain, Sweden, Switzerland, Turkey, the United Kingdom and the United States. The following countries became Members subsequently through accession at the dates indicated hereafter: Japan (28th April 1964), Finland (28th January 1969), Australia (7th June 1971), New Zealand (29th May 1973), Mexico (18th May 1994) the Czech Republic (21st December 1995) and Hungary (7th May 1996). The Commission of the European Communities takes part in the work of the OECD (Article 13 of the OECD Convention).

NUCLEAR ENERGY AGENCY

The OECD Nuclear Energy Agency (NEA) was established on 1st February 1958 under the name of the OEEC European Nuclear Energy Agency. It received its present designation on 20th April 1972, when Japan became its first non-European full Member. NEA membership today consists of all European Member countries of OECD as well as Australia, Canada, Japan, Republic of Korea, Mexico and the United States. The Commission of the European Communities takes part in the work of the Agency.

The primary objective of NEA is to promote co-operation among the governments of its participating countries in furthering the development of nuclear power as a safe, environmentally acceptable and economic energy source.

This is achieved by:

- *encouraging harmonization of national regulatory policies and practices, with particular reference to the safety of nuclear installations, protection of man against ionising radiation and preservation of the environment, radioactive waste management, and nuclear third party liability and insurance;*
- *assessing the contribution of nuclear power to the overall energy supply by keeping under review the technical and economic aspects of nuclear power growth and forecasting demand and supply for the different phases of the nuclear fuel cycle;*
- *developing exchanges of scientific and technical information particularly through participation in common services;*
- *setting up international research and development programmes and joint undertakings.*

In these and related tasks, NEA works in close collaboration with the International Atomic Energy Agency in Vienna, with which it has concluded a Co-operation Agreement, as well as with other international organisations in the nuclear field.

Foreword

Radioactive waste management programmes in OECD countries cover a wide range of activities in research and development with the common purpose to get the necessary scientific basis for disposal of various types of radioactive waste. The concern for the safety of final disposal is shared among the safety authorities and the radioactive waste producers, primarily the nuclear utilities. In some countries, site selection and characterisation programmes for high-level waste disposal are at a relatively advanced stage and several countries already have repositories for low-level waste in operation. Due to the difficulties involved and the amount of work necessary to get the required scientific information, the problems to be resolved have a high priority in national and international co-operative programmes.

INTRAVAL was set up as an international project concerned with the use of mathematical models for predicting the potential transport of radioactive substances in the geosphere. Such models are used to help assess the long-term safety of radioactive waste disposal systems. The INTRAVAL project was established by the Swedish Nuclear Power Inspectorate to evaluate the validity of these models. Results from a set of selected laboratory and field experiments as well as studies of occurrences of radioactive substances in nature (natural analogues) were compared in a systematic way with model predictions. Discrepancies between observations and predictions were discussed and analysed.

The project ran for six years, from 1987 to 1993. It was organised in two phases. The Swedish Nuclear Power Inspectorate (SKI) was managing participant during both phases and the OECD/Nuclear Energy Agency, Her Majesty's Inspectorate of Pollution (HMIP/DOE), United Kingdom, and Kemakta Consultants, Sweden took part in the project secretariat. The project had also observers from the International Atomic Energy Agency and from the State of Nevada.

The first phase of INTRAVAL was finished in 1990. Reports of the results from the first phase were issued in 1990, 1992 and 1993. A summary report of phase one of the project was published in the beginning of 1994.

The second phase of INTRAVAL was initiated in 1990 and finished 1993. Thirty-eight organisations from thirteen OECD countries participated in the second phase. Test cases were divided among four working groups which describe their findings in four separate reports. This report is one of them. In addition a summary report will be issued as well as a report from an independent subcommittee for integration.

Abstract

This report presents the work and conclusions of Working Group 2 within the International INTRAVAL Project. The Working Group focused on the study of ground water and tracer migration in fractured rock formations at three sites. The first field test was carried out at Finnsjön, Sweden, through the use of a number of boreholes in a nearly horizontal fractured zone embedded in a less permeable fractured crystalline rock mass at a depth between 100 to 240 m below the ground surface. A comprehensive series of hydraulic interference tests and tracer migration tests were carried out, with tracer migration distances about 200 m. Both convergent and dipole flow patterns were used.

The second field test was the so-called Stripa-3D experiment, carried out in a drift 360 m underground in fractured crystalline rock in the old Stripa mine in Sweden. Tracers were injected through boreholes at 10 to 55 m above the drift ceiling, and their migration into the drift under supposedly convergent flow field was carefully monitored and evaluated.

The third test case studied by the Working Group was the 8-m thick layer of fractured Culebra dolomite at a depth of 200 m at the WIPP site in New Mexico, USA. This test case is known as the WIPP-2 case within INTRAVAL. An extensive data set of transmissivity, head, and ground water salinity values at more than 40 locations were available for analysis and study.

Each of the test cases was studied by a number of research teams, nine, six and five for the three cases respectively. The teams used a wide range of models and calculational techniques, from equivalent porous and double porosity media, to fracture network and channel models. Of particular note is the application of stochastic models by a number of teams to the study of the large scale WIPP-2 case. The report describes the results of all the efforts of the research teams. Both lessons learned and conclusions from each of the cases and also the general conclusions of the results of the Working Group as a whole are presented.

Table of Contents

1 Introduction and General Comments on INTRAVAL Phase 2, Working Group 2, Test Cases

Chin-Fu Tsang and Shlomo P. Neuman

During Phase 2 of INTRAVAL, Working Group 2 focused on the study of groundwater flow and tracer migration at three field sites in fractured rock, Stripa and Finnsjön sites in Sweden and WIPP (Culebra) site in the USA. The Stripa 3D test case utilized experimental data from a freshly excavated drift at a depth of 360 m in fractured crystalline rock at the old Stripa iron mine in Sweden. The cross-shaped drift was 75 m long with an arm length of 25 m. Tracers were injected passively into the overlying rock between 10 and 55 m above the drift. Groundwater and tracer inflows were monitored in 375 plastic sheets, 2 x 1 m^2 in area, attached to the roof and walls of the drift.

The Finnsjön test case concerned hydraulic and tracer experiments in a low-angle horizontal fracture zone embedded within a less permeable fractured crystalline rock mass. In an area of 500 x 500 m^2, within which there are 7 boreholes, the fracture zone is about 100 m thick and its upper surface lies between 100 and 240 m deep. The zone is composed primarily of three relatively thin layers of enhanced permeability at its top, center and bottom. Three hydraulic interference tests were performed by withdrawing water from isolated intervals in one borehole. During one of these tests, tracer pulses were introduced into the upper high permeability layer through three nearby boreholes and their breakthroughs monitored in the pumping borehole. Following this preliminary tracer test, a radially converging tracer test was conducted by injecting, continuously and as pulses, 11 tracers into isolated intervals within the three high-permeability layers while withdrawing water from a central borehole open throughout the entire zone. Finally, a dipole tracer experiment was performed within the upper high-permeability layer by recirculating water and 15 tracers (both sorbing and nonsorbing) between two boreholes while monitoring their concentrations in these and two intervening boreholes. Two tracers were also injected into one of the intervening boreholes.

The WIPP 2 case study is based on data from site investigations carried out at the Waste Isolation Pilot Plant (WIPP) in New Mexico, USA. This site is being investigated by the United States Department of Energy as the potential location of a radioactive waste repository. Extensive field investigations have been conducted in the fractured Culebra dolomite which lies at a depth of about 200 m, has a thickness of about 8 m, and extends over many kilometers. Transmissivity, head and groundwater salinity have been measured at more than 40 locations in the Culebra dolomite.

Working Group 2 consisted of independent teams which took upon themselves to develop, test and compare models suitable for the interpretation of some of the collected field data. The Stripa 3D data were analyzed by four teams during INTRAVAL Phase 1 and two teams during Phase 2. All six teams considered flow and transport to occur in discrete channels, though the models of some of the teams allowed the transfer of tracer between channels while others did not. In addition to advection and dispersion, some teams also included matrix diffusion in their models. Different teams calibrated their models against different sets of measurements to

different extents by means of various methods. A major obstacle to calibration was the paucity of hydraulic data to define the flow field. This notwithstanding, the various channel models were successful in reproducing various trends in the observed field behavior, such as the appearance of multiple breakthrough peaks. They were however less successful in reproducing consistently all observed behaviors, most notably the apparent loss of tracer mass. It was not possible to meaningfully rank the various models and discriminate among them.

Nine project teams from seven countries worked on the interpretation of data from the Finnsjön site during INTRAVAL Phase 2. Three of these teams had also worked on some of these data during INTRAVAL Phase 1. Five of the seven teams during Phase 1, and seven of the nine teams during Phase 2, used continuum (equivalent porous media) approaches to model the Finnsjön tracer tests. Among these were single- and dual- continuum models as well as deterministic and stochastic continuum models. One team employed a discrete channel network model and one used effective crack tensor theory during Phase 2. The number of space dimensions modelled varied from one to three. Different models were successful in reproducing various aspects of observed field behavior; some were successful in predicting one tracer test after having been calibrated against other test data. The number of space dimensions modelled did not seem to affect the quality of these reproductions and predictions. It was again not possible to rank the various models, and discriminate among them, unambiguously. All teams concluded that advection and dispersion are needed to interpret the test results. However, there was some disagreement among teams regarding the importance of dual continuum models and matrix diffusion for reproduction of the field data. We note in this context that only one among the teams (GEOSIGMA) was successful in using all available hydraulic and tracer test data to calibrate their models and subsequently validate them by predicting observed tracer behavior. This team required neither a dual continuum model nor matrix diffusion to accomplish these tasks. It seems that while these phenomena may occur, they were not able to manifest themselves under the high velocities induced by the test in a medium with a rather low fracture to matrix porosity ratio.

A synthetic natural gradient tracer test was set up based on the Finnsjön data and addressed by some of the teams. Its aim was to compare the ability of various models, calibrated against local tracer tests, to predict tracer migration on much larger scales. The predictions were fairly similar except one made with a model that had included matrix diffusion. One team has shown that calibrating a stochastic continuum model against local data does not necessarily insure its ability to render reliable predictions outside of this area. Another team emphasized the need to consider non-Gaussian models. In such models extreme values of permeability may be more connected than in Gaussian models, increasing the potential for preferential flow paths, which may lead to the main radiological consequence of a repository.

The WIPP 2 case study was addressed by five project teams. All five teams treated the fractured Culebra dolomite as a continuum. As measured transmissivities within this layer vary by more than seven orders of magnitude while porosity remains close to 0.16, all teams accounted for spatial variations in transmissivity and/or hydraulic conductivity while treating porosity as a constant. Two teams did so by means of two-dimensional horizontal stochastic continuum models conditioned on measured transmissivity data. The teams were successful in demonstrating that methods of geostatistical inference and stochastic modelling are at a stage

where they can be applied to real-world problems. They discussed and developed methods to estimate the parameters of stochastic models, showed how statistical hypothesis testing can be used to differentiate between alternative models, illustrated how predictive uncertainty reduces as the model is conditioned on a broader class of hydraulic data (i.e., inclusion of head data), pointed to the need of augmenting such data by geologic information, and stressed again the need to consider non-Gaussian models. Other teams have shown that vertical leakage through formations which overlie the Culebra dolomite may impact horizontal flow within the latter, that both flows are influenced by shallower water table conditions which in turn are sensitive to variations in climate, and that heterogeneity exerts a much greater control on flow than do spatial variations in salinity.

Based on all the field and modelling results encountered by Working Group 2, we may draw the following general conclusions:

1. The geosphere is a complex, multiscale, spatially variable natural environment. It exhibits both discrete and continuum features and phenomenology on all scales. Observed and/or dominant features and/or phenomena are generally scale-dependent.
2. A reasonable understanding and/or interpretation of local field test conditions does not guarantee the ability to make reliable predictions on larger and/or smaller scales. To properly characterize a site, there will be a need to perform numerous measurements and/or experiments and/or observations at multiple locations arranged so as to form a multiscale nested grid of points.
3. Field data and/or experiments typically lend themselves to multiple interpretations and conceptualizations (such as juxtaposed and/or overlapping continua, discrete planar features and/or fractures, discrete channels and/or openings). An unambiguous definition and/or description of the relevant subsurface plumbing system at all scales and locations is not possible.
4. Preferential flow channels in fractured rocks are dynamic entities: They are controlled both by the internal plumbing of the rocks through which groundwater is flowing and by external and/or internal driving forces. Neither these channels nor travel (time) through them can be defined and/or described as intrinsic in-situ properties, as both vary with dynamic conditions and with the scale of observation.
5. Most field (and laboratory) tests can be interpreted with models that are neither too simplistic nor unduly complex. A point of diminishing returns (optimum model complexity) is reached rapidly as complexity increases.
6. Integrated effects (such as dipole pumping well tracer breakthrough) can be modeled more easily than local effects (such as tracer concentrations at a sampling well between the dipole wells). But now the question becomes whether this is all we need for safety assessment?
7. Transport in all the test cases has been dominated by advection along different flow lines which are strongly affected by heterogeneity. This makes clear the need to focus on multiscale spatial variability (heterogeneity and anisotropy) as a key uncertainty to address. Dispersion, known to arise mainly from such uncertainty, has also been shown to be important. Matrix diffusion appears to be a factor in the interpretation of tracer tests within the Culebra dolomite at the WIPP site in New Mexico (this was shown outside of INTRAVAL), but its effect on transport in

crystalline rocks has not been demonstrated.

8. The geosphere can, and where possible should, be characterized statistically and analyzed stochastically in terms of observable and/or measurable intrinsic quantities (rather than nonintrinsic concepts such as flow paths). This requires many observations on multiple measurement and/or sampling scales. It is important for model discrimination, calibration and validation; for the quantification of predictive uncertainty; and for assessment of the worth of data as a means of reducing such uncertainty.

9. There are important differences between rock and/or flow and/or transport behaviors in the interior of intact rock and at (or near) exposed rock surfaces (such as outcrops and underground openings). Hence observations made, and conclusions drawn, based on (near) boundary behavior may not apply to the interior.

10. Modelers, theorists, and experimentalists must together conceive, plan, design, execute, analyze, and interpret experiments. Otherwise, crucial information will almost certainly be lacking when attempting to derive maximum benefit from these experiments.

2 Finnsjön Test Case

2.1 Introduction

This INTRAVAL test case is based on three hydraulic interference tests and two tracer experiments performed in a major low angle fracture zone (Zone 2) at the Finnsjön research area located in northern Uppland in central Sweden [*Andersson et al., 1989*], [*Gustafsson et al., 1990*], [*Andersson et al., 1990*], [*Gustafsson & Andersson, 1991*], [*Gustafsson & Nordqvist, 1993*], [*Andersson (ed.), 1993*], [*Andersson et al., 1993*]. The main objectives with the experiments were to determine parameters important for the understanding of radionuclide transport in major fracture zones and to utilize the results for calibration and verification of radionuclide transport models. An additional objective was to develop and improve equipment and experimental methods for application in future field experiments. These experiments were selected as a test case in the INTRAVAL project since they were designed to study phenomena important in geosphere transport such as advection, dispersion, channelling, dilution, matrix diffusion, heterogeneity on a rather large geometrical scale.

During Phase 1 of the INTRAVAL Project a total of seven project teams studied and analyzed the data with varying amount of detail. The Phase 1 results are reported by *Tsang & Neuman (editors)* [*1992*]. The major conclusion drawn was that data from one or two tracer tests alone are not sufficient to distinguish between different models and/or processes.

The analysis of the Finnsjön test case was prolonged also during Phase 2 of the INTRAVAL Project, this decision partly augmented by the fact that Phase 2 put special focus on field experiments.

Nine project teams from seven countries, including the Pilot Group (GEOSIGMA) who developed this test case, studied and analyzed the data. Two of the groups were also participating in Phase 1, GEOSIGMA (former SGAB) and VTT. The project teams were:

1. GEOSIGMA, Sweden
2. Technical Research Centre of Finland (VTT)
3. Power Reactor and Nuclear Fuel Development Corporation (PNC), Japan
4. Paul Scherrer Institut (PSI), Switzerland
5. University of New Mexico (UNM), USA
6. Hazama Corporation, Japan
7. Conterra/Royal Institute of Technology (KTH), Sweden
8. Bureau de Recherches Géologiques et Minières (BRGM), France
9. Universidad Politecnica de Valencia (UPV), Spain

The processes studied and the conceptual approaches made by the nine teams are summarized in Table 2.1.1. The Phase 2 analysis of the Finnsjön test case is more thoroughly described by *Andersson & Winberg* [*1994*].

Table 2.1.1. Phase 2 analysis of tracer tests at Finnsjön. Conceptual approaches used and processes considered

Modelling team	Conceptual approach	Processes considered
Hazama Corp., Japan	crack tensor theory	advection
Conterra/Water Res. Eng.(KTH), (SKB) Sweden	stochastic continuum multiGaussian	advection
BRGM (ANDRA),	continuum model	advection-dispersion kinematic dispersion radioactive decay
GEOSIGMA,(SKB) Sweden	continuum model	advection-dispersion diffusion sorption matrix diffusion radioactive decay
VTT (TVO), Finland	non-interacting varying aperture channel model	advective diffusion matrix diffusion gen. Taylor multiple flow paths
PNC, Japan	dual porosity continuum model, stream tube concept	advection-dispersion multiple flow paths
UPV (ENRESA), Spain	stochastic continuum multiGaussian non-multiGaussian	advection
PSI (NAGRA), Switzerland	single and dual porosity continuum model	advection-dispersion multiple flow paths sorption matrix diffusion
U. of New Mexico, U.S.A.	single and dual porosity continuum model	advection-dispersion molecular diffusion matrix diffusion

2.2 Description of the Finnsjön Experiments

This section gives a very brief description of the experiments done at the Finnsjön site. The data available for the modelling teams is thoroughly described in INTRAVAL Phase 1 Test Cases [*SKI/NEA, 1991*].

2.2.1 Site Description

At the Finnsjön investigation site, Sweden, two major fracture zones have been identified, the Brändan fracture zone, Zone 1, and a low-angle zone, Zone 2 (Figures 2.1, 2.2). The geohydrology of the site is dominated by these two highly conductive zones. Zone 2, which is the zone utilized for the tracer tests, is trending north with a dip of about 16° to the west and consists of sections with high fracture frequency and tectonisation. The zone is well defined in 7 boreholes located within an area of about 500×500 m (Figure 2.1). In this area the fracture zone is almost planar with the upper surface located between 100 to 240 m below ground. The zone is about 100 m thick and seems to consist of three subzones with transmissivities in the order of 10^{-5} to 10^{-3} m^2/s. The parts in between the subzones have transmissivities similar to the country rock. The magnitude of the hydraulic gradient in the zone is about 0.3%, directed towards ENE.

The rock where Zone 2 is located is dominated by granodiorite. The rock is medium-grained and red in colour. The fracture infillings are dominated by calcite. Other minerals present are hematite, laumontite, asphaltite and clay minerals.

The composition of the groundwater above Zone 2 differs from that in and below Zone 2. The water above the zone is a younger near-surface water, and the water below Zone 2 is an old saline water characterized by a high content of species in solution such as Na, Ca and Cl. The water in Zone 2 is a mixture of these two waters which indicates the appearance of two circulating groundwater systems, one above and one below Zone 2. Both are drained into Zone 2 in the area where Zone 2 is most deeply located and the water is discharged from the shallow parts of Zone 2 into Zone 1.

2.2.2 Experiments Performed

Three hydraulic interference tests were carried out by withdrawing water from different isolated intervals in borehole BFI02 within Zone 2 [*Andersson et al., 1989*]. The pressure responses were registered in 3-6 intervals in all boreholes in the Brändan area and also in 6 boreholes outside the Brändan area up to 1500 m from the pumping well.

During one of the interference tests a preliminary tracer test was performed in order to optimize the design and performance of the planned radially converging experiment. Tracers were injected as pulses in the upper highly conductive subzone of Zone 2 in boreholes BFI01, KFI06 and KFI11. Tracer breakthrough was monitored in the pumping well BFI02.

In the radially converging experiment borehole BFI02 was used as a withdrawal hole and injection of tracers into Zone 2 was made in three peripheral holes, BFI01, KFI06 and KFI11 [*Gustafsson & Nordqvist, 1993*]. In each injection hole three sections were isolated with packers, one in the upper highly conductive part of Zone 2, one at the lower boundary of Zone 2 and one at the most conductive part in between. In the withdrawal hole the isolated section enclosed the whole thickness of Zone 2.

In total 11 different tracers were injected, 8 of them continuously for 5-7 weeks, and three as pulses. The tracers selected, DTPA- and EDTA complexes, fluorescent dyes and anions, are stable and non-sorbing.

The water discharged from the hole was continuously sampled for tracer analysis during the time period of tracer injection. The hydraulic head in the pumped section and also the groundwater level was registered. After the end of tracer injection a detailed sampling of the withdrawal hole was made in order to determine possible interconnections between highly conductive intervals of Zone 2.

The dipole experiment was performed in a recirculating system between BFI01 (injection) and BFI02 (withdrawal) [*Andersson et al., 1993*]. Boreholes KFI06 and KFI11 were used as observation holes. Only the upper highly conductive part of Zone 2 was used for tracer injection in hole BFI01. The two observation holes were isolated with packers in the same manner as in the radially converging test. Water from the isolated section in the withdrawal hole BFI02 was recirculated to the injection section in BFI01 through a pipe system.

In total 15 injections of tracers were made in BFI01. Both radioactive and nonradioactive tracers were used. The radiotracers included both non-sorbing and sorbing species. Two tracer injections were also made in the upper section of the observation hole KFI11.

The tracers were sampled in the upper part of Zone 2 in holes BFI02, KFI06, and KFI11. Occasionally, samples were also taken in the water from the lower intervals of boreholes KFI06 and KFI11. During the experiment the temperature of the water entering the injection hole BFI01 and the oxidation-reduction potential were measured showing that the conditions were stable and reducing. The electrical conductivity and the temperature of the water discharged from the withdrawal hole BFI02 were also registered during the experiment.

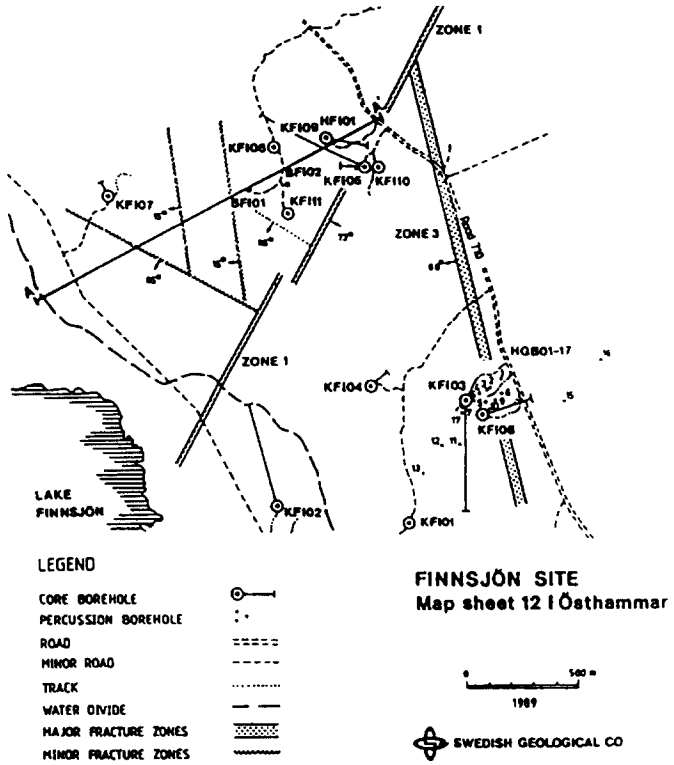

Figure 2.1 Finnsjön site, location of boreholes and major fracture zones.

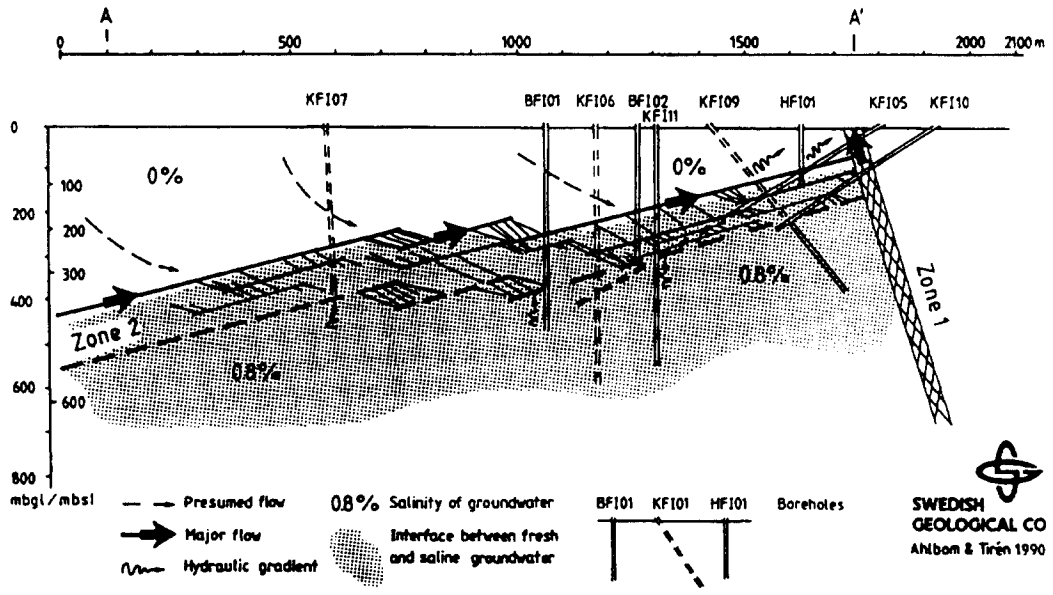

Figure 2.2 Cross-section through the Brändan area showing Zone 2. Profile A-A' is shown in Figure 2.1.

2.3 Summaries of Project Team Analyses

2.3.1 Summary of GEOSIGMA/SKB Analysis

The GEOSIGMA/SKB analysis is a continuation of the original evaluation of the tracer experiments in Zone 2 presented during INTRAVAL Phase 1 [*Tsang & Neuman (editors), 1992*].

Modelling Objectives

The purpose of the two-dimensional modelling of the dipole experiment was to make a direct comparison with earlier predictions and experimental data. Variations of the magnitude and direction of the natural gradient and effects of anisotropy were also examined. The one-dimensional modelling was made in order to evaluate and compare transport parameters for the breakthrough in the observation holes where the transport can be assumed to be one-dimensional. The evaluation also includes parameter estimates from two or more breakthrough curves simultaneously.

Modelling Approach

For both the one-dimensional and the two-dimensional approaches a simple porous medium advection-dispersion model was applied. The breakthrough in the two observation holes KFI06 and KFI11 was modelled assuming constant fluid velocity and no transversal dispersion. The one-dimensional models were solved using analytical solutions as given by *Van Genuchten & Alves* [*1982*]. Variable injection schemes were simulated by superposition of these solutions.

The fitting was generally made for three parameters, dispersion coefficient, D, mean velocity, v, and proportionality factor, f. The f-parameter is the product of injection concentration, dilution in the sampling section, and a weight representing the contribution from each main flow path. The uniqueness of the parameter estimates was assessed by studying the regression statistics of each model run: the correlation coefficients, standard error of the parameters, and the correlation between the parameters. A classification was made on a scale from 1 to 3 where 1 represents a poor model, 2 represents an acceptable model, and 3 a good model.

The one-dimensional modelling also included determination of retardation coefficients for some of the weakly sorbing tracers using simultaneous fits of two or three breakthrough curves, one being conservative and the other(s) retarded. The two-dimensional modelling was made in a 0.5 m thick horizontal plane of the fracture zone covering a region of 500 x 500 m. The transport equation was solved numerically by the 2D finite element code SUTRA [*Voss, 1990*] with a discretization of 10 x 10 m (2500 elements). Simulations were made applying different natural gradients and anisotropy factors trying to simultaneously fit all three breakthrough curves using inverse modelling technique.

Results

The results of the one-dimensional analysis show that the transport between the injection hole and observation borehole KFI11 can be very well described with a single flow path model. The variation in residence times and dispersivities was found to be small for the non-sorbing tracers ($^{82}Br^-$, $^{186}ReO_4^-$, $^{131}I^-$, ^{169}Yb-EDTA, and ^{58}Co-EDTA). ^{140}La-DOTA, ^{177}Lu-DOTA and Rhodamine WT are weakly sorbing and were markedly delayed. The determination of retardation coefficient using simultaneous parameter estimation of two or three curves showed values of 1.3-1.7. ^{51}Cr-EDTA, ^{111}In-EDTA, and In-EDTA (stable) also shows minor delays. Some of the tracers, e.g. $^{24}Na^+$ and ^{160}Tb-EDTA, are not delayed but shows lower peak values and less recovery than others indicating irreversible losses.

The breakthrough in KFI06 is markedly delayed compared to KFI11. The long residence times only enabled detection of the rising part of the breakthrough curves. These model simulations are therefore more ambiguous. No attempts were therefore made to determine retardation coefficients based on breakthrough data from KFI06.

Andersson et al. [1993] also made a comparison of some parameters determined from all three tests using the same concept of linear advective dispersive transport. The results indicate that dispersivity decreases with increased flow velocity. *Andersson et al. [1993]* also concludes that matrix diffusion is likely to have a negligible effect based on estimates of the ratio of fracture to matrix porosity.

The results of the two-dimensional modelling of the dipole experiment shows that it is not possible to fit all three breakthrough curves in the pumping hole and observation holes by applying different magnitudes and directions of the natural gradient. Only minor improvements of the model fits was obtained. However, including an anisotropy factor (K_{max}/K_{min}) of about 8 directed approximately along the strike of the zone, gives a very good agreement between data and model for all three breakthrough curves. The model fits are also slightly improved by including leakage from the lower parts of Zone 2, as indicated by independent information such as head and electrical conductivity data.

Conclusions

The analysis of the whole sequence of interference tests and tracer tests performed both in Phase 1 and Phase 2 of INTRAVAL shows that a relatively simple porous media advection-dispersion model fairly well can predict average flow and transport in Zone 2. The use of the whole sequence of tests with predictions, calibration and verification has proved to be a useful way to obtain consistency.

The analysis of the dipole test shows that good fits and consistent parameter values are obtained for individual observation points within the dipole flow field. Further, by including an anisotropy factor (K_{max}/K_{min}) of about 8 directed approximately along the strike of the zone, gives a very good agreement between data and model. Simultaneous fits of two or three breakthrough curves gives good fits for weakly sorbing tracers applying a linear sorption

isotherm. Finally, the comparison of parameter values determined from the one-dimensional analysis of three different tests shows that dispersivity decreases with increased flow velocity. *Andersson et al. [1993]* suggests that this is an effect of the induced flow geometry.

2.3.2 Summary of VTT/TVO Analysis

The VTT/TVO analysis is a continuation of the work done within Phase 1 of the INTRAVAL Project. The work within Phase 1 included predictions and comparisons with the results of both the radially converging and the dipole experiments. Within Phase 2, also the preliminary tracer test performed in combination with the interference test was analyzed using the same conceptual model as for the other experiments.

Modelling Objectives

The overall objective of the VTT/TVO analysis was to obtain a model which is as realistic as possible for description of groundwater flow and transport in rock fractures and to put the right weights on processes affecting releases and mass fluxes. For Phase 2 a specific objective was to investigate whether the same concept could be applied to all three experiments in Zone 2 at Finnsjön. Based on the results, conclusions regarding groundwater flow and transport are given together with general recommendations for future tracer tests in crystalline rock.

Modelling Approach

A concept of non-interacting, varying aperture channels was applied also in the continuation of the work. Water flow in a fracture is assumed to be concentrated in channels. The three-dimensional tortuous channels can conceptually be flattened and straightened into a two-dimensional channel network in a fracture plane. The channel network is assumed so dense that hydraulic radial symmetry is obtained during pumping. It was also assumed that only one or two routes through fractures and channels contribute significantly to the transport from the injection section to the pumped borehole.

The apertures as well as the widths of the channels may vary strongly along the channel lengths. The aperture variation is taken into account in the transit time calculations. A mean effective width is assumed to describe the possibly varying width of each channel. For further details see *Hautojärvi & Taivassalo [1988]*.

The preliminary tracer test, performed in the same geometry as the radially converging experiment was simulated using one significant route and approximately the same channels widths as for the radially converging and dipole experiments where a channel width was fixed to 5 cm. In the evaluation of the preliminary tracer test the channel width was treated as a fitting parameter using fit by eye method.

Results

The results of the transport simulations show good agreement for two of the flow paths, KFI11-BFI02 and KFI06-BFI02 using approximately the same channel widths as for the radially converging and dipole experiment (5 cm), 3.1 and 4.2 cm respectively. However, for the transport between BFI01 and BFI02 the fit is somewhat ambiguous. The fit is either good in the rising part or in the tail depending on the channel width chosen, 6.58 cm or 1.70 cm. Taking into account differences in the performed experiments and uncertainties in the actual source terms the results can be considered to be essentially the same.

Hautojärvi [1992] also compares the two dominant transport processes in field tracer tests, hydrodynamic dispersion and matrix diffusion. By applying simple analytical solutions to the advection-dispersion and advection-matrix diffusion equations, respectively a relation between flow rate, Q, and the effective diffusion coefficient, D_e, was obtained. In the Finnsjön experiments flow rates through the injection sections were found to be clearly dominated by dispersion.

Conclusions

The modelling, using a relatively simple channel approach, has shown that all three experiments performed in Zone 2 at Finnsjön, can be described with the same concept. Flow is dominated by advection and the only other process needed to explain the breakthrough curves is hydrodynamic dispersion. The high flow rates, measured from tracer dilution during the experiments, in combination with relatively slow transport indicate large cavities in the rock. The modelling has also shown that hydrodynamic dispersion can be described by velocity differences in a channel together with molecular diffusion.

Hautojärvi [1993] also concludes that the transport times within Zone 2 can be predicted reasonably well from hydraulic data e.g. by correcting the parallel plate interpretation of hydraulic data with a factor (possibly increasing with decreasing transmissivity).

2.3.3 Summary of PNC Analysis

Modelling Objectives

The main objective of the PNC analysis was to study the effect of heterogeneity on tracer transport. For that purpose a mathematical model was constructed which also enabled determination of transport parameters. The validity of the model was examined by simulation of the tracer tests performed within Zone 2 at Finnsjön.

Modelling Approach

The basic concept of the PNC analysis was to generate a hydraulic conductivity distribution

which should reflect the heterogeneous nature of Zone 2. This was done in two different ways. In the first analysis the hydraulic conductivity distribution was determined by a trial and error approach based on the measured hydraulic conductivities [*Hatanaka & Mukai, 1993a*]. In the second analysis the hydraulic conductivity distribution was determined using a geostatistical approach. In this analysis single-hole hydraulic test data from all eight boreholes in Zone 2 was utilized [*Hatanaka & Mukai, 1993b*]. Variograms were calculated and a krieged hydraulic conductivity distribution was obtained. Conditional simulations were then performed.

A porous medium, dual porosity system composed of high conductive and low conductive zones was assumed for both analyses. In the first analysis transport was simulated using a stream tube concept and in the second analysis a two-dimensional finite difference method was used. In the high conductive zone, a one-dimensional advection-dispersion transport was considered whereas a two-dimensional situation with transverse dispersion was considered for the low-conductive zone.

The analysis was made by fitting transport parameters to the dipole experiment and then checking the validity of the model by simulation of the radially converging tracer test.

Results

The fitting show a reasonably good agreement for all tracers except Iodide where the model seem to be unable to reproduce the tail of the breakthrough curve. Two parameters were fitted for the high conductive zone, advective porosity ϕ_{wf}, and a lumped parameter $(\phi_{df}/\phi_{wf})\alpha_{Lf}$. By assuming that the advective and dispersive porosities are the same for both low and high conductive zones a similar lumped parameter was determined for the low conductive zone.

Using these parameters breakthrough curves from the three boreholes used in the radially converging test were simulated. The results show a reasonably good fit to the experimental data in the early, rising part of the breakthrough curves whereas the fitting of the tail is somewhat poorer. In order to improve the fit of the tail, a new set of parameters independent of the dipole test were assigned, and a better fit of the tails were obtained.

Conclusions

Based on the results of their analysis the PNC team concludes that transport during both the dipole test and the radially converging test can be explained by the porous medium, double porosity model used. The dipole test breakthrough curves could be satisfactory explained and the radially converging test could be reasonably well simulated. However, the Iodide breakthrough curve could not be well simulated under the parameter constrains. The fit leads to inconsistent parameter values.

2.3.4 Summary of the PSI/NAGRA Analyses

The modelling performed by the PSI/NAGRA team differs from the other INTRAVAL contributions by their use of tracer test data from another part of the Finnsjön site. The analysis is based on a series of radially converging tracer tests, using both non-sorbing and sorbing tracers performed in a minor fracture zone about 1 km south of the Brändan area [*Gustafsson & Klockars, 1981, 1984*]. These tests have earlier been used as a test case for the INTRACOIN study [*SKI, 1986*]. The modelling is presented in more detail by *Jakob & Hadermann* [*1994*].

Modelling Objectives

The main objective of the PSI/NAGRA analyses was to investigate if their relatively simple model could explain tracer transport at Finnsjön or, if not, what criteria could be found for a rejection of the model. Specific objectives were to determine the geometrical assumptions needed, to determine the dominant transport processes, to study the effects of varying flow boundaries, to compare parameter values with values determined in the INTRACOIN study, and finally to find geometrical criteria to choose a unique set of best-fit parameter values for the non-sorbing tracer and then fix these data to determine additional transport parameter for sorbing tracers.

Modelling Approach

The model is based on the assumption that the migration zone may be seen as a part of a larger planar fracture with very flat hydraulic potential. The fracture is represented by a 2D-aquifer of constant values whereas the potential corresponds to that of an unperturbed dipole field. Tracer transport is simulated in a dual porosity system where both fracture and vein geometries for preferential flow paths are considered. Diffusion of tracer into stagnant pore water is also considered. Sorption of the tracer on fracture/vein surfaces and onto inner surfaces of the rock matrix is described by Freundlich isotherms. Both linear and non-linear isotherms are used.

Special emphasis was put on determining the uniqueness of the model fits using the Marquardt-Levenberg method. Thus, regression parameters, their standard deviations and the corresponding correlation was determined.

The modelling was done in a stepwise manner starting with simulations of the tracer breakthrough for a non-sorbing tracer (Iodide). The intention was to find geometrical criteria to choose a unique set of best-fit parameter values for the non-sorbing tracer and then fix these data to determine additional transport parameter for the sorbing tracers (Strontium and Cesium).

Results

The results of a varying source term is clearly visible in the experimental breakthrough data. The modelling performed including all available information on both upstream (source term) and downstream boundaries has a clear influence on extracted best-fit parameter values. *Jakob & Hadermann [1994]* also found that the experimental data were too rudimentary for modelling successfully the finer details of the breakthrough curves. Matrix diffusion was found to play a minor role as transport mechanism. The influence of one or two preferential flow paths was found to be significant. A two path system gave much better fits to the experimental data.

The uniqueness of the obtained transport parameters was checked by repeating the calculations for the same breakthrough curve up to 30 times with different sets of starting values. The resulting best-fit parameters were found not to be unique when two flow paths were introduced. This loss of uniqueness was used as a reason for not introducing more than two flow paths to the system.

The influence of flow path geometry was investigated by applying a vein flow geometry instead of a fracture flow. The vein flow assumption did not yield better fits to the experimental data and was therefore not considered to be more appropriate to use.

The results for the modelling of the Strontium breakthrough gives good fits assuming a two path model both with and without matrix diffusion. However, including matrix diffusion improves the regression statistics. Extracted best fit values for the effective diffusion coefficient are in the order of 10^{-13} m^2/s. The modelling also showed that it was necessary to account for tracer losses due to precipitation. Thermodynamic calculations supported this assumption.

The modelling of the Cesium transport showed that it was impossible to obtain a reasonable fit to the breakthrough curve assuming a linear sorption isotherm. Only by including non-linear sorption, reasonable fits were obtained. The resulting Freundlich parameters were found to be compatible with literature data.

Conclusions

Based on their analysis *Jakob & Hadermann [1994]* conclude that transport is clearly dominated by advection. Matrix diffusion only has a small but non-negligible effect.

The authors also conclude that the concept of a dual porosity medium has proved to be a versatile, efficient, and highly appropriate concept for analyzing these migration experiments. The modelling of the Finnsjön experiments did not reach any serious limitations for the model and no other mechanism than those already incorporated in the model, had to be advocated.

2.3.5 Summary of the University of New Mexico Analysis

Modelling Objectives

The objective of the UNM analysis was to investigate whether a relatively simple porous medium, single porosity model could describe the transport in Zone 2 during the radially converging experiment. Analysis of the dipole tracer test results was performed in order to validate the model. A double porosity model was also used for comparison.

Modelling Approach

Zone 2 and the surrounding bedrock were modelled with 2-D single porosity and double porosity models. In the system, three vertical cross-sections were used to represent the flow paths between each of the three injection holes (BFI01, KFI06, KFI11) and the pumping hole (BFI02). Thickness and hydraulic conductivity was interpreted from the individual borehole data. In the analysis the injection wells and the pumping well were located at the boundaries. No flow boundary was assigned to the pumping well and a Dirichlet type boundary was assigned to the injection well. The flow velocity during the radially converging test was used instead of head distribution and pumping rates and only transport calculations were performed. In the single porosity model, a constant injection rate was assigned while the concentration time history was specified in the double porosity model. About 4000 elements were used to model the entire Zone 2 with the finite difference code TRACR3D [*Travis & Birdsell, 1991*]. The best fit parameters for the single porosity model were: porosity (ϵ), longitudinal dispersivity (α_L), and flow field velocity (u). For the double porosity model three additional parameters were fitted: fracture aperture ($2b$), constrictivity (τ_c), and diffusion coefficient (D_i).

Results

The transport simulations using the single porosity model were performed for 8 of the total 12 tracer injections performed during the radially converging experiment. The results show a reasonably good agreement with observed data for most of the tracers/flow paths. However, some of the model fits are not that good and *Ng & Kota [1993]* indicate that the poor fits may be due to poor recovery or a more complex flow pattern than described in the model. The fitting procedure resulted in longitudinal dispersivities from 10.7 to 13% (α_L/α_T= 100) of the travel distance, porosities in the range of 2-10%, and velocities within a factor of 0.3 to 4.5 of the measured velocity.

The results of the fits with the double porosity model are similar to the results using the single porosity model. Most of the breakthrough curves can be fitted reasonably well with the exception of Er-EDTA and Dy-EDTA where the fits are poorer. The fitting procedure resulted in longitudinal dispersivities from 4.2 to 13% of the travel distance, fracture apertures around 0.01 cm, matrix porosity in the range of 6.9-15%, and constrictivity of 0.155 to 0.5.

The ratios of matrix to fracture porosity, calculated based on the best-fit values, are in the order of 10^{-2}, which suggests that matrix diffusion is an important process at Finnsjön [*Ng & Kota, 1993*]. However, no significant improvement of the fits was found in using the double porosity model compared to the single porosity model although a slightly better fit for the tail of the breakthrough curves was achieved.

The analysis of the dipole test was mainly carried out to validate the models used to interpret the radially converging test. Only the single porosity model has been used. The analysis was performed by assigning the best fit parameters determined from the radially converging test to the upper, 5 m layer, of Zone 2 and using the dipole flow velocity and tracer injection data. The agreement between the simulated and observed data was found to be good and *Ng & Kota* [*1993*] finds it reasonable to say that the single porosity model is validated.

The authors also performed a sensitivity analysis of both models. In both models peak concentrations were found to be sensitive to changes in any of the parameters. The most sensitive parameter was found to be longitudinal dispersivity. Arrival times were found to be sensitive only to changes in porosity and flow velocity in the single porosity model and to longitudinal dispersivity in the double porosity model.

Conclusions

A comparison of the results of the single and double porosity models shows that both models display reasonable agreement with the observed breakthrough curves except in the cases of KFI11:M and KFI11:L, where neither model can reproduce the breakthrough curves. Low recovery of these two tracers may be the reason. The two models yield similar regression coefficients and it cannot be judged which model is best representing Zone 2. However, based on the validation of the single porosity model using the dipole test analysis, such a model can be used for Zone 2.

Ng & Kota [*1993*] also concludes that the interpreted results of the tracer tests strongly depend on the model used. This implies that properties of the medium (e.g. porosity and longitudinal dispersivity) calculated from the two models, are determined by the processes which are included in a certain model. Finally, a three-dimensional analysis is suggested in order to gain a better insight of the transport mechanisms in Zone 2.

2.3.6 Summary of Hazama Corporation Analysis

Modelling Objectives

The Hazama analysis within Phase 2 includes flow and transport analysis of the radially converging tracer test. The objective is to address the problem using a representative elementary volume approach which also includes description of anisotropy and spatial variability in permeability [*Kobayashi & Yamashita 1993*].

Modelling Approach

The first step in the model approach is an estimation of a representative elementary volume on the basis of measured fracture density and an assumed fracture trace length. The fracture frequency (1/[L]) of identified fracture sets is used to solve for the fracture density ($1/[L^3]$) of individual fracture sets assuming three different fracture length distributions. A measure of the representative elementary volume (REV) is subsequently obtained through the Crack Tensor Theory [*Oda, 1986*] using the geometry and properties of the fractures involved in the analysis. The permeability tensor k_{ij} based on single hole data and a matrix Q_{ij} which includes fracture geometrical information is used to calculate an apparent aperture α_{ij} for the REV. The variogram of the three principal components of α_{ij} is calculated as is that of the mean value, assumed to be a scalar.

In the subsequent numerical analysis of flow and transport, a finite element model of fracture zone 2 was devised with a size of 1000x1000x100m. A central 300x300 m area is discretized in more detail with 20x20x20 m blocks. Values of isotropic apparent aperture α are assigned to the FEM model using conditional simulation. A total of 500 realizations were generated. In addition a homogeneous value of Q_{ij} was assigned to all element blocks. Prescribed head boundary conditions are assigned to all faces of the numerical model. The pumping rate applied in BFI02 to simulate the tracer test is 2 litres/s.

For the transport calculations a particle tracking procedure was used. As a first try, the porosity derived from the Crack Tensor Theory was assigned to the model. This porosity is proportional to α and the fracture length squared, and is thus also heterogeneous. A particle is released from various test sections in BFI01, BFI06 and KFI11 and the tracer breakthrough curve is estimated from the ensemble of arrival times for the various realizations. The porosity is calibrated by obtaining an agreement between measured and simulated breakthrough curves.

Results

The analysis showed that the length scale of the representative elementary volume is in the order of 20m, hence the selection of the element size in the densely discretized area. The transport results are presented as figures comparing measured breakthrough with simulated results (ensemble average) for different injection points (upper (U), middle (M) and lower (L) test section in BFI01, KFI06 and KFI11). Because the tracer recovery losses are not explicitly considered in the calculations, the concentration of each particle is multiplied with the recovery rate for each injection point. The much more rapid rise in the simulated breakthrough curves indicates that the calculated velocity field is overestimated for the whole model domain, particularly so for the middle (M) and lower (L) regions.

Conclusions

The authors claim that although the approach to obtain the characteristics of the anisotropic, heterogeneous media may appear complicated and troublesome, the field data have been

processed with care. They admit that there may still be many assumptions which are still unverified theoretically. In order to obtain better agreement between calculated and measured breakthrough curves it is i.e. necessary to revisit the process to infer the fracture length, its standard deviation and distribution function. It is stated that the results appear good although the assumptions regarding the latter three parameters remain unverified.

2.3.7 Conterra/KTH-WRE Analysis

Modelling Objectives

In most practical situations in performance assessment related studies the licensee faces the need to extrapolate a model calibrated (and possibly validated) on a local scale to a larger and more relevant transport scale. In their analysis the authors explore this problem and test whether a stochastic continuum model calibrated on a local test scale also can be validated on a larger, far-field scale [*Kung et al., 1992*]. The analysis is performed using a model with physical conditions similar to those prevailing during the Finnsjön dipole test.

Modelling Approach

At first a reference transmissivity field was conceived over a 1200x1200 m area corresponding to the upper conductive part of Zone 2. This field was constructed through conditional parametric simulation using the turning bands method conditioned on transmissivity values from the field centred on the high-conductive part of Zone 2 in 8 boreholes. The input data which is based on the data from the 8 boreholes are assumed to be log-normal with a mean $Y=\log_{10}K$ of -3.28 ($\log_{10}$ m/s) and a variance of 0.15 ($\log_{10}$ m/s)^2 with an isotropic covariance structure with a 100m correlation length. The dipole tracer test was simulated in the reference field under conditions similar to the actual field conditions including a prevailing linear natural gradient of 3%. The transport simulations were performed using a particle tracking routine assuming conservative particles and only taking advection into account. The resulting breakthrough curves for tracer released in KFI11 and BFI01 were considered as the real system response of the reference field to be used for calibration. Subsequently, a far-field tracer experiment under natural gradient conditions was simulated by releasing tracer along the upstream boundary and monitoring of breakthrough along the downstream boundary of the model. The results of the latter experiment are to be used for validation of extrapolation to the far-field scale of a model calibrated on a local scale.

Following the analysis of the reference field, 100 equiprobable conditioned realizations were generated. The ensemble mean head distribution and the ensemble mean breakthrough for the two local scale test cases were calculated. In the subsequent calibration process only two parameters, the porosity and effective thickness of the aquifer were considered. Yet another calibration approach was utilized whereby a defined index of deviation was used to select the individual realizations which best recreated the response of the local scale tracer test. For the sake of validation the far-field results of the identified realizations were compared with the reference case far-field response.

Results

The results showed that the ensemble mean of the calculated hydraulic head compared well with that calculated for the reference field. The transport calculations on a local scale showed that the ensemble mean breakthrough curve for the tracer release in BFI01 compared well with the reference case results. The corresponding results for tracer release in KFI11 was not as good. In this case the reference case results are not even contained within the one standard deviation envelope. The calibration based on physical parameters showed that a porosity n=0.025 and an effective thickness of b=0.5m are to be used. The alternative calibration based on the index of deviation showed that three realizations best recapture the characteristics of the reference case. The results based on these realizations were compared with the corresponding results based on the reference field. It was found that none of the three realizations gave transport results similar to the reference case results. This was attributed to the fact that there are not enough conditioning points on the far-field scale to recapture the characteristics of the far-field reference case transport response.

Conclusions

The results showed that calibration of the model on a local scale, using the two outlined methods, is insufficient to also validate the model on another larger transport scale. Calibration is better performed using statistical approaches rather than in a deterministic way. Calibration and validation of stochastic continuum models still remain biased through subjectivity, but the work performed by *Luis & McLaughlin* [*1991*] and *Ababou et al.* [*1992*] may provide means to make the calibration process less subjective.

2.3.8 BRGM/ANDRA Analysis

Modelling Objectives

The BRGM/ANDRA analysis has focused on the interference tests and the subsequent converging tracer test. The objectives of the analysis of the interference tests are a) to take boundary effects into account when interpreting the tests in Zone 2 using analytical techniques, b) to take the multilayering of Zone 2 into account using an axi-symmetrical finite difference model, and c) to simulate the interference tests in three dimensions. The objective of the analysis of the converging tracer test are a) to interpret the breakthrough of tracers injected in the upper sections of BFI01, KFI06 and KFI11 using a) an analytical technique, and b) numerical modelling of the solute transport with a 3D particle tracking model.

Modelling Approach

In the analytical approach which addresses the effects of hydraulic boundaries, a Theis scheme accounting for boundaries was utilized [*Schwartz et al, 1993*]. Each of the pumping tests was considered separately. A hydraulic boundary (prescribed constant head or no-flow boundary)

was considered at a specified distance D from the line joining the pump- and observation sections considered. Calibration of transmissivity T, storativity S and distance D was carried out. The axi-symmetrical finite difference approach, which also incorporates boundary effects through "virtual" image theory, allows a simultaneous calibration of the three measurement sections for a given borehole under the assumption that the upper and lower layers have the same hydrodynamic parameters.

The numerical study in three dimensions employs a porous medium finite difference model MARTHE [*Thiery, 1990*] which takes the actual Zone 2 geometry and acting boundary conditions into account [*Schwartz et al., 1993*]. The model has a parallelogram shape with a base length of 2500m and a height of 1200 m corresponding to the model geometry employed by SKB [*Andersson et al., 1989*]. The model consists of 5 layers, representing subzones 1 and 2, the intermediate low-permeable zone, and subzones 3 and 4, respectively. The calibration was carried out on test no. 1 and 2 using an automatic procedure. The calibrated parameter field was validated using the calibrated field to simulate and estimate the corresponding drawdowns during tests no. 3A and 3B.

The analytical approach on the converging tracer test was made using a code CATTI which includes a solution which incorporates bidimensional flow and is valid for a pulse injection in a 2D converging flow field. The premises for the numerical analysis of the converging tests were the hydraulic conductivity and specific storage fields calibrated/validated using the interference tests. The transport simulations were made assuming continuous injection at constant rate. The calibration process was limited to a few parameters to ensure their representativity. Hence, the longitudinal and transverse dispersivities α_L and α_T were assumed homogeneous for the whole model domain and the assigned porosities were assumed homogeneous for each simulated (test) section.

Results

The results of the analytical analysis incorporating hydraulic boundaries show a good agreement between the T and S values obtained and those presented by SKB [*Andersson et al., 1989*]. The axi-symmetric finite difference analysis yielded hydrodynamic parameters in the three layers which were consistent between boreholes, and were also in accord with those obtained through the analytical approach. The results of the three-dimensional numerical analysis showed a good fit between measured and calculated drawdown during the complete test sequence for test sections in KFI05, KFI06, KFI09 and KFI10. The results of the analytical analysis of the converging test in the upper section provided first estimates of porosity n ranging from $1x10^{-4}$ to $3x10^{-4}$ depending on the tracer analyzed. The estimated longitudinal dispersivities α_L range between 15 to 30 m. The analysis of the low recovery of tracers injected into the low-permeable central section showed that the phenomenon could not be fully explained by alteration of dispersion coefficient or porosity. The authors agree with [*Gustafsson et al., 1990*] in that chemical processes, irreversible interactions and clogging and/or the influence of the natural gradient may be the cause of the observed effect. The analysis of the four tracers injected in the upper section yielded the "best" values of the transport parameters through a fitting and reduction of error procedure for all tracers

concerned; dispersivities α_L = 10 m, α_T = 0.25 m and porosities n assigned to the various test sections which vary between $2x10^{-5}$ and $3x10^{-4}$.

Conclusions

Using a hydraulic conductivity and storativity distribution equal to that employed by SKB and further calibration and optimization of the same parameters within the Brändan block using a three-dimensional finite difference model showed that variations in drawdown could be well simulated in KFI05, KFI06, KFI09 and KFI10 during the complete interference test sequence. The equivalent parameters were in accord with those presented by SKB. The analysis of the tracer test shows that it is possible to simulate the behaviour of the four tracers injected in the upper section. Chemical reactions, i.a. irreversible interactions, chemical clogging in the injection sections are possible explanations for the low tracer recovery observed in the middle test section.

2.3.9 UPV/ENRESA Analysis

Modelling Objectives

An assumption of multiGaussianity inherently leads to a low degree of continuity in extreme values. The absence of continuous paths of extreme values of hydraulic conductivity will have a retarding effect on calculated travel times. Underestimation in travel times may lead to decision-making based on inconservative results in performance assessment studies of radionuclide release from a deep geological repository. This fact, and the fact that the multiGaussian model in most cases is selected simply because the supporting data are univariate Gaussian has formed the rationale for the study in which the impact of low continuity of extreme values on travel times is demonstrated by applying two stochastic models, a multiGaussian and a non-multi-Gaussian (the latter displaying high connectivity in extreme values) to a site similar to Finnsjön.

It is shown that for a given univariate Gaussian histogram for $Y=\log_{10}K$ and a covariance $C_Y(h)$ there exist an infinity of combinations of indicator covariances that may yield a given Y-covariance, of which one set of combinations corresponds to a multi-Gaussian model (h is the separation distance). Thus there exist other possible models which can reproduce the Y-covariance. The alternative model used in this study allows significant correlation ranges for indicator covariance corresponding to extreme values. This property is not possible to obtain for a multiGaussian model.

Modelling Approach

The area modelled with the two models is a vertical section through the Finnsjön site which features Zone 1, Zone 2 and the rock mass. The domain is 1000x1000m discretized into 50x50 cells of size 20x20m. The fracture zones are treated deterministically with constant

hydraulic conductivities of $10^{-4.5}$ and $10^{-5.5}$ m/s, respectively. The applied boundary conditions will force groundwater to discharge at the outcrop of fracture zone 1. The hydraulic conductivity of the rock mass is modelled as a random function. The two models applied are univariate Gaussian with a mean $\log_{10}K=Y=$ -8.0 ($\log_{10}$ m/s) and a variance equal to 1 ($\log_{10}$ m/s)^2 and the same anisotropic covariance $C_Y(h)$. However the two models differ in their indicator covariances which have been defined for 9 thresholds. The horizontal continuity in the indicator variable for the last (90%) decile of the non-multiGaussian model is high which cannot be reproduced by a multiGaussian model.

Stochastic travel time analysis for particles released from an idealized repository to the surface via fracture zone 1 was performed. Using the two models 200 unconditional realizations of Y were generated. Subsequently the two fracture zones were superimposed with constant geometry and material properties. Sequential simulation [*Journel, 1989*] was used to generate realizations of rock mass conductivity. In the case of the multiGaussian model, GCOSIM3D [*Gómez-Hernández, 1991*] was used and in the case of the non-multiGaussian model, ISIM3D [*Gómez-Hernández & Srivastava, 1990*] was used. Subsequently groundwater flow and advective transport were simulated in the 200 realizations of each set, producing in each case 200 breakthrough curves of particle arrival at the outcrop of fracture zone 1 following release of particles from a conceived repository area below Zone 2.

Results

The calculated breakthrough curves were used to construct bivariate cumulative probability distribution functions for arrival time and mass concentration, which enable assessment of the uncertainty in these two parameters. The results, for a given probability, show that the non-multiGaussian model gives higher concentrations in shorter time than that of the multiGaussian model. This implies that if a site is considered safe on the basis of uncertainty analysis using a multiGaussian model it may be labelled unsafe if the analysis is carried out using a non-multiGaussian model.

Conclusions

In stochastic continuum modelling of flow and solute transport, the multi-Gaussian model is often chosen on the sole basis of the parsimony principle as the simplest model that can be described by a mean and a covariance. An alternative, non-multiGaussian, model is presented. This model, with the same Gaussian histogram and covariance as the multiGaussian model shows a high continuity in extreme values. This fact renders the non-multiGaussian model to exhibit faster radionuclide transport than the multiGaussian model. The results show that probabilities of exceedence for small concentrations at given times is significantly higher for the non-multiGaussian model than for the multiGaussian model. Thus, the multiGaussian model is not a conservative model for nuclear waste disposal safety assessment.

Before selecting a multiGaussian model it is important to check not only that the data are univariate Gaussian, but also whether they are bivariate Gaussian. The selection of the multiGaussian model should at any rate not be solely made on the basis of the parsimony principle.

2.4 Comparative Discussion

2.4.1 General

The INTRAVAL Phase 2 analysis of the Finnsjön tracer experiments features results from nine different modelling teams using a variety of different approaches. Phase 1 constituted a first contact for the participating teams with the Finnsjön test data and some of these teams have continued their analysis during Phase 2. The Phase 2 results offer explicit attempts to validation of the set up models. A general observation is also that the dimensionality of some of the applications is three-dimensional and in addition stochastic approaches are employed, all of which are new ingredients compared to Phase 1.

Below some aspects of the approaches employed during the Phase 2 analysis of the Finnsjön tracer experiments are discussed and compared in more detail. These are; a) conceptual approaches employed, b) processes studied, c) scale of application, and d) the validation aspects of the studied problem.

2.4.2 Conceptual Approaches

The conceptual models applied by the modelling teams are also in Phase 2 of INTRAVAL focused on porous media approaches, c.f. Table 2.1.1. In Phase 1, five of the seven teams used porous media approaches while in Phase 2 seven of the nine teams used this concept. The two exceptions, in the latter case, are the VTT team, which uses a network of channels where transport is assumed to take place in a few non-interacting channels, and the Hazama team which uses a concept based on a representative elementary volume (REV) obtained through the Crack Tensor Theory.

Some of the teams have also compared different conceptual approaches. The PNC team uses two different ways to determine the hydraulic conductivity distribution and uses both one-dimensional stream tube and two-dimensional finite difference methods to analyze transport. The UPV team compares two stochastical models, Gaussian/non-Gaussian, and the PSI team applies both fracture and vein flow models. The U. of New Mexico team compares single- versus double porosity models. Some of the teams use the comparison to conclude which conceptual approach that gives the best correspondence to the experimental data and which of the models to be, at least partly, rejected.

The models used are mainly two-dimensional which is an obvious assumption given the two-dimensional character of flow in Zone 2. Some teams use one-dimensional transport concepts and two teams use three-dimensional approaches. If all tracer tests are to be considered, a three-dimensional model may be needed, especially if the large scale head responses are to

be incorporated. Experimental evidence of vertical interconnections between different subzones and leakage from the bedrock below the zone also speaks in favour of a three-dimensional approach. However, the relatively simple one-dimensional approaches may also be useful in some cases, like the radially converging test, where variations in source terms and effects of multiple flow paths and matrix diffusion are easily addressed. The dimensionality of the model does not seem to be decisive for the ability to reproduce the field responses at Finnsjön.

A major difference compared to Phase 1 is that geostatistical approaches have been introduced. In Phase 2 three modelling teams, Conterra/KTH-WRE, UPV, and Hazama, have used geostatistical methods to obtain transmissivity or aperture distributions for stochastic travel time analysis. Also the PNC team has initiated a geostatistical analysis of the Finnsjön data. These teams have demonstrated that stochastic approaches may be used within the context of a validation process, although the question remains how to formally validate a stochastic continuum model.

2.4.3 Processes Studied

In the Phase 1 analysis many of the teams studied several processes, trying to separate between them. However, one of the conclusions from Phase 1 was that the tracer experiments at Finnsjön may not be designed to discriminate between processes [*Tsang & Neuman (editors), 1992*]. The results were also somewhat ambiguous where e.g. matrix diffusion was considered to be important by one team while other teams considered it to have none or negligible effect.

In the Phase 2 analysis only four of the nine teams include more than one process, c.f. Table 2.1.1. The GEOSIGMA and PSI teams are the only teams which consider sorption. The reason for this is probably that there are no independent laboratory or field data for the weakly sorbing tracers used in the dipole test. It should also be noted that the PSI team uses a different data set from Finnsjön, previously used in INTRACOIN [*SKI, 1986*], specially addressing sorption processes. The PSI team conclude that sorption parameters determined from these tests agree well with literature data.

The PSI team also made an analysis of the effect of matrix diffusion and came to the conclusion that matrix diffusion has a small but not negligible effect. The U. of New Mexico team also compares a single and a double porosity model and finds that very similar results are obtained and that no definite conclusion regarding matrix diffusion can be drawn although they claim that matrix diffusion is an important process at Finnsjön based on the ratio of fracture to matrix porosity. The GEOSIGMA team draw the opposite conclusion based on the same ratio and therefore they did not consider matrix diffusion at all in their analysis.

In the stochastic continuum approaches, transport is treated as purely advective and these models were designed for other purposes than process discrimination.

The general conclusion drawn by all teams is that flow and transport in Zone 2 is governed by advection and that hydrodynamic dispersion also is needed to explain the breakthrough

curves. The question whether matrix diffusion is important in these experiments or not, still remains open, although most teams agree that matrix diffusion has no, or very small, effect given the high induced velocities and low ratio of fracture to matrix porosity.

2.4.4 Scale of Application

The tracer tests performed at Finnsjön have been conducted in a well-defined borehole array. Thus the experiment scale is also well defined, being on the order of 200x200 m. During Phase 1 mostly analytical tools where employed thus focusing in specifically on the experimental scale. During Phase 2, however, numerical applications dominate and the scale considered is in some instances on the order of 1000x1000m, c.f. Table 2.4.1. This is particularly true for the two stochastic continuum applications which both address transport phenomena on scales larger than the actual experiment scale. Taking scale alone into consideration, the results of most modelling teams can be directly compared.

2.4.5 Validation Aspects

The classical approach to model validation in hydrogeology is calibration of a set of model parameters against a given experiment geometry in a given geological domain for a specific stress of the system. The validation constitutes prediction of model behaviour for another experiment condition (altered stress and/or geometry) in the same geological domain and comparison with field data.

During Phase 1, only three out of seven modelling teams (EdM, GEOSIGMA (formerly SGAB) and JAERI) formally addressed this classical type of validation by first calibrating their model with the radially converging test and subsequently predicting the dipole test [*Tsang & Neuman (editors), 1992*]. The EdM team used a multiple channel model and explicitly addressed validation and claimed proper process and parameter identification but acknowledged poor representation of horizontal heterogeneity. The JAERI team did not explicitly address validation but utilized the parameter set obtained from the calibration of the radially converging test to predict the dipole test. GEOSIGMA was the responsible field organization which conducted and interpreted the field tests conducted at Finnsjön. The GEOSIGMA team in succession used the collected field data to enhance their descriptive models, used that information to predict the subsequent tracer test, and finally attempted and succeeded well to predict the dipole test response.

During Phase 2, various validation aspects have been considered, c.f. Table 2.4.1. Five groups address the classical approach to validation, whereas two groups utilizing the stochastic continuum approach address other validation aspects.

The modelling teams from GEOSIGMA and VTT address parameter consistency between all three tracer tests performed at Finnsjön (including the preliminary tracer test during interference testing). The results show that the average transport behaviour can be acceptably described with one single set of transport parameters. However, for a detailed understanding

of individual transport routes, transport parameters need to be adjusted for different flow geometries. The PNC team utilizes a porous medium, double porosity model to calibrate the transport parameters to the dipole tracer test. The validity of the model was subsequently checked by simulating the radially converging test. The results showed good predictive capability for early times whereas tails in the breakthrough curves are poorly represented. The alternate sequence used by the PNC team, in that they start out with the dipole test in their analysis, may have helped to get a better understanding of the heterogeneity between BFI01 and BFI02. The BRGM team uses the classical approach and succeeds in predicting later interference test results based on calibrations of early interference tests. The U. of New Mexico team uses a single/double porosity 2D model (in vertical sections) to predict the converging test and checks the validity of their model/-s by simulating the dipole test. They conclude that a reasonable agreement between measured and simulated breakthrough is obtained.

The Conterra/KTH-WRE team addresses a performance assessment issue, that of extrapolation of transport models calibrated on a small scale to larger transport scales. Using an exhaustive reference transmissivity field and the stochastic continuum approach they show that a model calibrated on an experimental scale is not validated on a far-field scale when being subjected to extrapolation and simulation of a far-field natural gradient test. The reason being that the local scale conditioning data do not suffice also to describe far-field scale heterogeneity.

With the more and more frequent use of stochastic continuum models the UPV team raises an important issue relating to the inherent choice of statistical model when generating hydraulic conductivity/transmissivity fields. The UPV work shows that when, and if, the multiGaussian model is used this should be preceded by a check whether the data also are bivariate Gaussian and with the understanding that the multiGaussian approach intrinsically suppresses connectivity of extreme values. The latter is of paramount interest from a performance assessment perspective since an unwarranted use of the multiGaussian model may transform an "unsafe" site to a "safe" one.

In summary the approaches on model validation are versatile and focus in on other issues than the classical validation issue, which may be equally important in improving our predictive capability of solute transport phenomena in crystalline rock.

Table 2.4.1. Phase 2 analysis of tracer tests at Finnsjön. Scale of problem and validation aspect of problem studied.

Modelling team	Scale of problem	Validation aspects of problem
Hazama Corp., Japan	1000x1000x100m (far-field) 300x300x100m (local scale) 20x20x20m discr.	Use of REV concept in analysis of flow and transport in fractured rock.
Conterra/KTH-WRE (SKB), Sweden	1200x1200m (far-field) 200x200m (local scale) 20x20m discr.	Extrapolation of a model, calibrated on a local scale to a larger far-field scale.
BRGM/ANDRA, France	2500x1200x100m parameters.	Consistency in evaluated flow and transport
GEOSIGMA, Sweden	2500x1500m (far-field) 500x500m (local scale) 10x10m discr.	Same conceptual model used for all analyzed tracer tests. Check whether it is possible to simulate tracer test results in various geometries with the same transport
VTT (TVO), Finland	< 200m	Same conceptual model possible to explain all tracer test results.
PNC, Japan	< 200m	Calibrated dipole model tested by simulating the radially converging tracer test.
UPV (ENRESA), Spain	1000x1000m 20x20m discr.	Is use of a Gaussian model a conservative choice!?
PSI (NAGRA), Switzerland	~ 30m	Consistency in evaluated transport parameters. Comparison between laboratory test results with field test results in granitic rocks performed at different sites and in various geometries.
U. of New Mexico, U.S.A.	~ 200x200m	Model(-s) calibrated using the radially converging tracer test are tested by simulating the dipole tracer test.

3 Stripa Test Case

This report summarizes the modelling and model validation programmes performed on the Stripa 3D data as part of the INTRAVAL project. The three-dimensional tracer test experiment performed in the Stripa mine in Sweden was part of INTRAVAL phase 1. A summary of the works of the project teams who analyzed the available data has already been presented. In addition to the 3D experiment data from two other experimental programmes performed in the Stripa mine were also available during INTRAVAL phase 2: the "Site characterization and Validation Programme (SCV)" and the "Channelling Experiment". At the time of the writing of this review, results concerning the modelling of these two experiments have not be presented as part of INTRAVAL.

Four project teams were involved as part of INTRAVAL phase 1 :

- KTH[1]/SKB[2]
- LBL[3]/USDOE[4]
- KTH[1]/SKI[5]
- INTERA[6]/AEA[7]/NIREX[8]

The contribution of these project teams is reviewed by *Hodgkinson and Grindrod [1991]*. Two other project teams have analyzed the Stripa 3D data as part of INTRAVAL phase II :

- VTT[9]/TVO[10]
- BRGM[11]/ITASCA[12]/ANDRA[13]

The current review includes the models used and the results obtained by the six project teams. The Stripa 3D experimental set-up, the available data and the main purposes of this experiment are outlined in section 3.1. These points were extensively documented by the KTH/SKB project team and full details are available in *Abelin et al. [1987]*. Section 3.2 presents the alternative models used by each group and the relevant parameters. In sections 3.3 and 3.4 the data processing and calibration strategies are reviewed. Section 3.5 gives details of the results and parameter estimations, whilst in section 3.6 we present a summary of the results and of what was learnt.

---

[1]KTH ; Royal Institute of Technology, Sweden

[2]SKB ; Swedish Nuclear Fuel and Waste Management Co, Sweden

[3]LBL ; Lawrence Berkeley Laboratory, USA

[4]USDOE ; US Department of Energy, USA

[5]SKI ; Swedish Nuclear Power Inspectorate

[6]INTERA ; Intera Information Technologies Ltd UK

[7]AEA ; AEA Technology, Harwell Laboratory, UK

[8]NIREX ; UK Nirex Ltd, UK

[9]VTT ; Technical Research Centre of Finland, Finland

[10]TVO ; Industrial Power Company Ltd, Finland

[11]BRGM ; BRGM/4S, France

[12]ITASCA ; Itasca Consultants S.A., France

[13]ANDRA ; French Agency for Nuclear Waste Management, France

3.1 The Stripa 3D experiment

3.1.1 Experimental set-up

The Stripa mine is a disused iron mine adjacent to a body of granite. The main experimental activities were performed within the granite body at the 360 m level. An experimental drift was excavated, starting about 100 m from the nearest drifts and extending 75 m due to north, into the undisturbed granite. The test site consists of a 75 m long main drift and a crossing arm 25 m in length.

The whole ceiling and the upper part of the walls were covered with around 375 plastic sheets (about 2 m^2 each) which were used to collect the water seeping in from the rock.

Three vertical boreholes for injections of tracers were drilled upwards with lengths of 70 m. From these boreholes, nine different conservative tracers were injected into nine 2.5 m long separate sections located between 10 and 56 m above the test site. The tracers were continuously injected for more than 20 months with a "constant" overpressure, less than 10 % above the natural pressure. Water entering the test site was sampled for tracers during the time of injection and an additional 6 months after the end of injection. Water samples were taken every 16 hours from all sampling areas with a high enough water flow rate. Figure 3.1 shows the lay-out of the experiment.

The injection flow rates varied during the time of the experiment. The decrease in the injection flow rate at the start of injection was not only caused by the natural pressure build-up, but also due to the closing of an adjacent borehole N1 some 100 m distant. If the injection flow rate decreased below a certain level, the injection pressure was increased to get an acceptable mass inflow rate of tracers.

3.1.2 Field results - Available data

The available data from the 3D experiment were such as:
- Daily logs, rock characteristics and fracture data, water chemistry, hydrostatic pressures, water flow rates, injection pressures and injection flow rates, tracer concentration in water to test site.

Some of the main field observations are outlined below.

Fracture mapping

About 100 major fractures were mapped in the test site, excluding the floor. For each of the mapped fractures in the drift the following features have been noted: location and extension, direction and dip, infilling and coating materials, surface characterization, and signs of water flow.

Water flow rates in the drift

The total water inflow to the covered area of the site was about 0.7 l/h. Of the 375 sampling sheets 145 yielded measurable amounts of water, with 50 % of the total inflow coming from approximately 3 % of the covered area. The wettest sheet carried about 10 % of the total inflow. The water inflow rate distribution from the rock (prior to the drilling of the three injection holes) was monitored for 6 weeks. Water inflow was concentrated within a few zones, with large dry areas in between (Figure 3.2). Areas with a higher number of fracture intersections were found to have higher water flow rates.

Tracer occurrence in the drift

Only five of the nine tracers were found in significant concentrations in the different plastic collection sheets during the first 30 months of the experiment. These were Eosin B, EosinY, Uranine, Elbenyl and Iodide. Figure 3.3 shows the parts of the test site to which the different tracers have migrated. It can be seen in Figure 3.3 that tracers from 6 of the 9 injection zones have emerged into the test site. During the last period of reduced sampling a seventh tracer was found which is illustrated with dashed lines. This occurrence might be due to the preparations for Stripa project phase III.

No tracers were found in the right part of the arm, which is the area with the highest water inflow rates. The right arm is also closest to the injection zones in hole III, but the tracers injected at these zones emerged at the central part of the main drift.

Figure 3.4 shows the locations where the individual tracers emerged. Only those sampling areas with high water flow rates, i.e. connected to fractional collectors, are included in the figure. All tracers emerge in the central part of the main drift over a length of 35 m. Note that one tracer, Eosin Y, has been found in an another drift 150 m distant.

3.1.3 Aims

The Stripa 3D experiment provides a good opportunity to examine tracer transport through a three dimensional block of granite containing a drift and various boreholes. The development of the plastic sheeting technique allowed a detailed monitoring of the water flowrate and tracer path distribution so that the interpretation of both temporal and spatial variations constitutes a major challenge for the modelling project teams.

The main purposes of the 3D experiment and its analysis can be summarized as follow:
a) Develop techniques for large tracer experiments in low permeability fractured rock.
b) Determine flow porosity and longitudinal and transverse dispersion.
c) Obtain information on channelling.
d) Obtain data and other information for:
e) Validation and/or modification of models.
Points b), c) and e) were the first aims of the project teams who have analyzed the Stripa 3D data.

3.2 Models used by each group and relevant parameters

3.2.1 Introduction

The concept of "channelling" has been particularly studied during the last 10 years. Until the Stripa 3D experiment several observations were made indicating that flow is not uniform inside the fracture planes: see for example, *Neretnieks et al.* [*1982*] who performed a series of tracer tests in a core with natural fractures, *Abelin et al.* [*1985*] who observed water flow in three fractures intersecting drifts as part of the Stripa 2D experiment, *Gentier* [*1986*] who studied the hydromechanical behaviour of a single fracture under normal stress. Since the Stripa 3D experiment, observations that flow and solute transport are strongly channelled globally as well as in the fracture planes have led to the development of the channelling concept and relevant models: see for example *Bourke* [*1987*], *Neretnieks* [*1987*], *Tsang and Tsang* [*1987*], *Billaux and Long* [*1988*], *Cacas et al.* [*1990 a,b*].

Furthermore two others experiments performed on the Stripa site, Channelling Experiment and Site characterization and Validation (SCV), also confirmed the fact that the transport of solute in fractured rocks is dominated by a few pathways (see [*Abelin et al., 1990*], [*Birgersson et al., 1992*]).
According to these observations, most of the groups who analyzed the Stripa 3D data used models which take channelling into account, in one way or another. The word "channelling" implies here that there exists a scale at which flow is considered as one-dimensional. Such models can be described by two types of characteristics called single channel properties and channel arrangements.

Assuming that the flow regime in the channel is known, single channel properties define the type of transport processes which are incorporated into the channel : advection only, advection - dispersion (with or without retardation), advection-dispersion - matrix diffusion.
Channel arrangement defines the assumptions about geometry which are incorporated into the model : one channel, several discrete parallel channels, a "large" number of parallel channels, a network of interconnected channels. The last type of arrangement assumes that the flow is not purely one - dimensional at the scale of the rock mass under study, and that network connectivity effects are important in order to reproduce the behaviour of the system.

One group, INTERA/AEA/NIREX project team, did not assume a priori what the dimension of flow is at any scale, and in fact considered this dimension as being the main unknown of the system, using a fractal approach.

The parameters describing each of the transport models that were used are reviewed below. The governing transport equations describing single channel properties are presented by order of increasing number of parameters required. The different models of channel arrangement are presented in order of increasing complexity. Concerning the last model type, i-e network of interconnected channels, the initial parameters required for using it towards a mass transport simulation are also reviewed.

3.2.2 Single channel properties

Advection only

This model describes the tracer movement trough a channel with negligible longitudinal dispersion. The governing equation is:

$$\frac{\partial C}{\partial t} = -v\frac{\partial C}{\partial x} \tag{3.1}$$

where v is the advective fluid velocity [LT^{-1}] and C is the tracer concentration [ML^{-3}] as a function of the spatial coordinate, x, and time, t.

Only one parameter is therefore required to describe the physics, given the channel geometry. The usual form for this parameter is the water residence time, $t_w = x/v$. This model type was used by two project teams who both assumed that dispersion in the direction of flow is only caused by channelling:

- The KTH/SKB used this model as part of the "advection - channelling" model (large number of parallel channels, see sub-section to section 3.2.3).

- The KTH/SKI used this model as part of transport calculations performed with the DISCFRAC code [*Dverstorp et al., 1992*] in which equation (3.1) is solved in each channel using the particle-tracking algorithm.

Advection-dispersion

This model describes the hydrodispersive transport of tracer through a channel (when the volumetric flux remains constant in time and space). The governing equation is:

$$R\frac{\partial C}{\partial t} = D_L\frac{\partial^2 C}{\partial x^2} - v\frac{\partial C}{\partial x^2} \tag{3.2}$$

where v and C have been previously defined, D_L is the dispersion coefficient [L^2T^{-1}], and R (dimensionless) is generally called the retardation factor due to sorption and accounts for the interaction between the tracer and the solid material ($R = 1$ corresponds to the zero retardation scenario).

For a surface reaction:

$$R = R_a = 1 + K_a \cdot a_w \tag{3.3}$$

where K_a is the surface equilibrium constant [L^3L^{-2}] which assumes that the surface reaction is linear, entirely reversible and instantaneous. a_w is the specific surface area per volume of mobile water [L^2L^{-3}].

Rewriting (3.2) in dimensionless form shows that only two parameters are needed to fully define the solution:
- The water residence time : t_w
- The dimensionless Peclet number : *Pe*

$$Pe = x \cdot v \; / \; D_L = \frac{x}{\alpha} \qquad (3.4)$$

where α is known as the intrinsic dispersion coefficient or dispersivity (L), x is the length in flow direction (over which the transport model is used).

Most project teams used the advection-dispersion model at some point:

- the KTH/SKB team used it as part of the "single channel arrangement" (sub-section to section 3.2.3)

- the LBL/USDOE team used an advection-diffusion model with governing equation identical to (3.2), and $R = 1$. D_L was defined by the team as a channel longitudinal dispersion coefficient which arises from the slightly different velocities of the various flow paths that compose the channel, and Taylor dispersion was neglected [*Tsang et al., 1991*].

- The KTH/SKI team fitted the advection-dispersion model to the cumulative breakthrough curves resulting from transport calculation performed with the discrete model DISCFRAC.

- The BRGM/ITASCA/ANDRA team used the advection-dispersion model in two ways : a) firstly as part of transport calculations performed with the TRIPAR code which is a part of the CHANNET (previously named FETICHE) programs chain [*Guérin and Billaux, 1993*]. Equation (3.2), with $R=1$, is solved for each channel using the particle tracking algorithm (or the particle following one when the Peclet number in each channel is high, $Pe > 100$). Simulated breakthrough curves were then calibrated on the experimental data; b) secondly by fitting the advection-dispersion model to these calibrated breakthrough curves.

A common analytical solution of (3.2) [*Lapidus and Amundsen, 1952*] was used by three teams (KTH/SKB, KTH/SKI and BRGM/ITASCA/ANDRA):

$$C(x,t) \,/\, C_o = \frac{1}{2}\{ \; erfc \left[\frac{Pe^{0.5}\,(1-t_R)}{2t_R^{0.5}} \right] + e^{Pe} erfc \left[\frac{Pe^{0.5}\,(1+t_R)}{2t_R^{0.5}} \right] \} \qquad (3.5)$$

where $t_R = t/R_a\, t_w$. (3.5) is valid for: $C(x, 0) = 0$, $C(0, t) = C_O$, $C(\infty, t) = 0$.

Advection-dispersion - matrix diffusion

This model is similar to the advection-dispersion except that the possibility for the dissolved species to diffuse from the fracture into the surrounding porous matrix (and vice versa) is incorporated. Thus equation (3.2) becomes :

$$R_a \frac{\partial C}{\partial t} = D_L \frac{\partial^2 C}{\partial x^2} - v\frac{\partial C}{\partial x} + a_w D_e \frac{\partial^2 C_p}{\partial z^2} \qquad (3.6)$$

$$x \geq 0,\ t > 0$$

where C, v, D_L, a_w and R_a have been previously defined. D_e is called the effective diffusivity of the tracer into the matrix [L^2T^{-1}], and C_p is the solute concentration in the pore water in the matrix.

A further partial differential equation is required to describe the linear diffusion of the species into the rock matrix.

$$\frac{\partial C_p}{\partial t} = \frac{D_e}{K} \frac{\partial^2 C_p}{\partial x^2},\ x \geq 0,\ z \geq 0,\ t \geq 0 \qquad (3.7)$$

(3.6) and (3.7) are coupled by the condition that the concentration in the fracture water is equal to that in the matrix pores at the fracture surface.

Here K is the sorption coefficient and includes the capacity of micropore water to hold nuclide:

$$K = \varepsilon_p + (1 - \varepsilon_p)\, K_d\, \rho \qquad (3.8)$$

where ε_p is the rock matrix porosity, K_d is the sorption coefficient per mass of rock minerals

$[L^3M^{-1}]$, ρ is the rock density $[ML^{-3}]$. The product $K_d\,\rho$ represents the sorption capacity of the solid minerals which constitute the rock [*Neretnieks, 1980*].

Several analytical solutions are available for various boundary conditions (see for example *Tang et al, [1981]*, for the case when there initially is no solute in the system and when at time zero a constant concentration of the solute is input).

- The KTH/SKB used this model, neglecting sorption, as part of the single-channel arrangement. Compared to the advection-dispersion model, one extra parameter in required, the A parameter defined by :

$$A = \frac{\delta}{2(D_e \cdot \varepsilon_p)^{1/2}} \tag{3.9}$$

where δ is the channel aperture [L].

3.2.3 Channel arrangement

Single channel

For this arrangement, single channel parameters are obviously the only ones needed.

- The KTH/SKB project team used this model in directly fitting the theoretical curves given by the appropriate analytical solutions to the experimental breakthrough curves. Two single channel properties were compared, advection-dispersion and advection-dispersion matrix diffusion.

- The KTH/SKI project team also used the single channel arrangement in comparing the theoretical solution (3.5) with the synthetic breakthrough curves generated from the discrete model.

- The BRGM/ITASCA/ANDRA project team used this arrangement to analyze, with the theoretical solution (3.5), the breakthrough curves generated from the discrete model and fitted to the experimental results.

Using the single channel arrangement assumes that the different pathways taken by a tracer from its injection zone to a given observation sheet in the drift can be represented by an equivalent channel with properties representative of the medium.

As the corresponding analytical solutions are one-dimensional, it is furthermore assumed that the transverse dispersion caused by the fracture network and the heterogeneity of the velocity field is negligible.

Several discrete parallel channels

In this case, differing single channel parameters are explicitly assigned to a small number of tortuous one-dimensional channels. These channels do not interact with each other. Each channel possesses its own hydraulic conductivity controlled by constrictions along its length and has variable apertures along its length. Such channels are not pipes, but rather arise naturally as paths of low resistance through fracture planes, which themselves have widely ranging and variable apertures:

- The LBL/USDOE project team used this arrangement coupled with the advection-dispersion model. The implicit and crucial assumption was that the travel distances corresponded to only a few fractures spacings so that a full three-dimensional network effect could be ignored and the transport was dominated by a few variable aperture channels.

"Large number" of parallel channels

This arrangement also called "channelling model" [*Abelin et al, 1987, 1991*] is based on the assumption that all channels conduct the flow from the inlet to outlet without mixing between channels on the way. Thus, such an arrangement is close to the one previously presented. At the outlet, the fluid from all channels is instantaneously mixed.

The KTH/SKB project team used this arrangement assuming that dispersion in the direction of flow is only caused by channelling, so that the "advection only" single channel property is applied. A further assumption is that channel properties obey some probability distribution function. Here the channel apertures have a lognormal distribution. Using the usual cubic law leads to the flow rate through each channel.

Let Q the water flow rate in one channel [L^3T^{-1}] and $f(Q)$ the density distribution of the channel flow rates, the mean flow rate $\overline{Q}$ is obtained from:

$$\overline{Q} = \int_0^\infty Q f(Q) dQ$$

The tracer outflow concentration a time t of the mixed effluent from all the channels is then of the form :

$$C(t) = \frac{1}{\overline{Q}} \int_0^\infty f(Q) C(t,Q) Q dQ$$

Note that in each channel the solute transport $C(t,Q)$ could be modelled by any of the models describing the single channel properties. As the KTH/SKB project team used advection only, two free parameters are required: the usual water residence time (t_w) and the standard deviation of the lognormal distribution for channel aperture (σ).

Channel Network

The Channel Network assumes that the solute transport takes place in a three-dimensional network of interconnected one-dimensional channels. The specification of a channel network requires much more geometric information than the other channel arrangements. Also, because the flow geometry in such a model is complex, transport cannot be apprehended directly and the flow must be solved first.

An assumption common to most channel network models is that the channels are located within planar fractures. The two project teams (KTH/SKI, BRGM/ITASCA/ANDRA) who used the channel network concept have taken the assumption of disc-shaped fractures. Other options are available to simulate the shape of the fractures (see for example, [*Dershowitz et al., 1985*], [*Grindrod et al., 1991*]) and the flow in the fracture planes (see for example [*Nordqvist et al., 1992*], [*Herbert and Lanyon, 1992*]).

The geometrical parameters can then be separated into disc network geometry, and channel arrangement on each disc.

Disc network geometry

Models used by the two teams share common assumptions:

a) all fractures are planar; b) all fracture locations are equally probable, i.e. the fracture disc centres constitute a 3D Poisson point process; c) all fracture orientations are independent of fractures locations

The parameters needed to build the network were:

a) the definition of the fracture sets, as fractures are separated into several sets according to their orientations; b) the orientations (strike and dip) distribution for each set; c) the disc diameters distribution for each set; d) the 3D density of disc centres for each set

These parameters were assumed uncorrelated and were derived from fracture traces observations. Note that fracture aperture has not been taken as a parameter of the geometrical model.

In addition, the model of the BRGM/ITASCA/ANDRA project team was conditioned to the actual fracture traces observed on the ceiling and walls of the experimental drift. Therefore the specification of each observed fracture (trace endpoints and orientation) becomes part of the parameter field.

Channel arrangement on each disc

Two channel arrangement models were used.

- The KTH/SKI and BRGM/ITASCA/ANDRA project teams used the technique proposed

by *Cacas et al.* [*1990*] in which the flow is assumed to occur through "bonds" joining the centre of each disc to the centre of the adjacent disc. The bonds are made up of two parts, one for each fracture, meeting at the intersection of the two discs. Thus the number of internal nodes in the network is equal to the number of fractures and the channel network reproduces the connectivity of the disc network.

- The previous model was called "Simplified Disc Model" (SDM) by the BRGM/ITASCA/ANDRA project team. This team also used the "Random Channel Model" (RCM) proposed by *Billaux and Long* [*1988*] where one-dimensional channels are thrown at random on the fracture discs and where fracture intersections may or may not be considered as channels. The SDM is, geometrically, fully specified by the fracture network, and therefore requires no extra parameter. On the other hand, the RCM needs several extra parameters. One or several sets of channels may be defined for each fracture set so that one must define: a) the orientation distribution for each set; b) the length distribution for each set; b) the density of each set.

Here, two orthogonal sets of channels were defined on each fracture plane. The length of the channels was constant and set to 10 m (i.e channels were truncated at the fracture boundaries according to their location on the fracture plane). Three successive values of the channel density, λ [L^{-2}], of each set were considered for the calibration of the flow model:
a) case 1, $\lambda = 0.02$ m^{-2}; b) case 2; $\lambda = 0.03$ m^{-2}; c) case 3, $\lambda = 0.04$ m^{-2}.

For all cases, fracture intersections were also considered as channels The lower density case (i.e, case 1) was only considered for the calibration of the transport model.

For both channel network models, the assumption of a perfect mixing of the different fluxes entering a note was made.

3.2.4 Flow channel geometry

Most project teams considered explicitly or implicitly that the flux, Q_c [L^3T^{-1}] through the channels could be described by the "cubic law". For a channel with rectangular cross section:

$$Q = constant \cdot w \cdot \delta^3 \, | \, \vec{grad} H \, | \tag{3.10}$$

where w denotes the channel width, δ denotes the channel aperture and *grad H* is the hydraulic head gradient.

In addition, the KTH/SKI project team also used tube flow channels where the flux was calculated by means of the Hagen - Poiseuille law :

$$Q = constant \cdot r_c^4 \, | \, \vec{grad} H \, | \tag{3.11}$$

where r_c denotes the radius of the tube channel.

3.3 Data processing

3.3.1 Introduction

The main data used for transport parameters fitting were the experimental breakthrough curves. However, one problem made the use of these curves difficult: they represent the response of the medium to time-varying tracer injections.

Whereas there are known analytical or semi-analytical solutions of the 1D convective-dispersive solute transport equation when simple injection histories (i-e pulse, step, exponentially decaying, see for example *Van Genuchten and Alves*, [*1982*], one needs to resort to numerical schemes when studying more complex injection patterns. This is definitely the case for the Stripa 3D injections.

The alternatives are then as follows.
- either one tries to compute from the real data what the response would have been if a simple (pulse) injection had been performed. One can then fit a model to the "simplified" breakthrough curves. Finding the impulse response necessarily involves a deconvolution technique.
- or one computes the response of the system to the time-varying injection, using a convolution technique, and fits the parameters directly without the intermediate step of deconvolution.

The first approach was used by the LBL/USDOE and VTT/TVO project teams and is reviewed below. The second approach was used by the KTH/SKB project team when fitting the theoretical analytical models to the experimental results. This approach was also used by the BRGM/ITASCA/ANDRA for the calibration of the channel network on the experimental data, and for interpreting the results with the analytical solution (3.5).

Two other approaches were also used :
- As a preliminary analysis of the Stripa 3D field data, the LBL/USDOE team studied the first peak early arrival data, modelling the time-varying injection flow rates by an exponential decay curve followed by a period of stabilization.
- The KTH/SKI team generated synthetic breakthrough curves with the channel network model using a pulse injection and integrated the simulated curves over time in order to simulate a constant step injection of tracer.

3.3.2 Deconvolution of the breakthrough curves

The basic assumption inherent in this technique is that the system under study is linear and time-invariant. Also, the technique must be constrained to yield only non-negative "pulse" breakthrough curves concentrations : whereas "perfect" measurements should lead to non negative concentrations, the errors contained in the measurements may cause the resulting impulse curve to contain negative concentrations. The LBL/USDOE and VTT/TVO project teams used deconvolution techniques to analyze the experimental breakthrough curves. The impulse responses obtained by the LBL/USDOE were composed of distinct peaks. These peaks

were considered as the result of solute transport in independent channels and the solution of the one-dimensional advection-diffusion equation, for a delta pulse injection, was fitted to each peak. The VTT/TVO project team focused on the detailed analysis of the impulse responses given by deconvolution of the experimental breakthrough curves and injection pulses, taking into account the effects of measurement errors and other disturbances on the deconvoluted results. The impulse responses obtained by the VTT/TVO project team were also composed of various peaks. These peaks did not necessarily correspond to those previously identified by the LBL/USDOE team.

The deconvolution techniques used by the two teams are reviewed below. Results of the fit of the advection-diffusion model by the LBL/USDOE team are given in section 3.5. The VTT/TVO project team did not fit a given transport model to the estimated impulse responses.

Toeplitz analysis

The LBL/USDOE project team [*Tsang et al., 1991*] used the Toeplitz method to perform the deconvolution. This technique is briefly described here.

First, tracer injection and tracer breakthrough curves are discretized into constant time intervals. Let M_i be the mass flow rate for the discretized breakthrough during the i^{th} time interval and m_i the mass flow rate for the discretized injection during the i^{th} time interval, then, from linearity and time invariance, we can write :

$$M_i = \sum_j a_{ij}\, m_j$$

where the coefficients of the "Toeplitz matrix", a_{ij}, only depend on the difference $(i - j)$. Because of this property, the above equation can be rewritten, taking $s = i-j$:

$$M_i = \sum_s a_s\, m_{i-s}$$

where a_s becomes a vector describing the response to a unit pulse injection during the first time interval, and the m_{i-s} coefficients now define a matrix $\boldsymbol{M}$:

$$\begin{aligned} \boldsymbol{M}_{ij} &= m_{i-j} \quad i \geq j \geq 0 \\ \boldsymbol{M}_{ij} &= 0 \qquad\quad i < j \end{aligned}$$

In matrix form, one can the write:

$$M = \boldsymbol{M} \cdot a$$

where M and a are the vectors formed with the M_i and a_s coefficients respectively. Finding the pulse response then amounts to computing vector a by solving the linear system above. However, some of the coefficients a_i found in this way are negative. Because such results are unphysical, the procedure is modified and vector a is computed using least square optimization:

$$minimise \ \| M - Ma \|^2 \ subject \ to \ a \geq 0$$

This procedure was applied to five sets of tracer data, using 500 hour time steps. Later, 1000 hour steps were also used with little effect upon the solutions. To test the stability of the Toeplitz analysis method with respect to errors in injection data, nonsystematic random errors were introduced into the discretized data (up to 20% of their value). These also had little effect upon the solution and thus it was concluded that the solution is stable and unique.

The Extreme Value Estimation method

The VTT/TVO project team [*Ilvonen et al., 1993*] used the Extreme Value Estimation method (EVE) to perform the deconvolution. EVE is a general purpose tool for solving a linear set of equations in cases where all the unknowns are required to be non-negative. EVE estimates the lower and upper bounds of the unknowns or any user-defined linear expressions formed from them (thus the name of the method). The equation solved here is $y = M a + e$, where the vector y contains the measured breakthrough curve pulse of the tracer, M is a kernel matrix formed from the injection pulse (here a Toeplitz type lower triangular matrix), and a is the impulse response. Measurement errors associated to y are represented by e, assuming that they are independent random variables with known standard deviations. The EVE method performs all estimations among a set of acceptable solutions. This set of solutions is defined as a subset of an n-dimensional space assuming the unknown vector a has n components [*Ilvonen et al., 1993*]. As part of this study a confidence parameter D was selected and all those solutions which led to a chi-2 value at most D units greater than a "minimum" were accepted. This minimum (i.e, the closest solution) was obtained by using least-square optimization, as in the Toeplitz analysis performed by the LBL/USDOE project team.

The VTT/TVO analysed six tracers : Eosin B, Iodide, Bromide, Elbenyl, Eosin Y and Uranine. Injection flowrates were discretized into constant time intervals of length 125 hours. The impulse responses were estimated using the rates of mass accumulation. For Eosin B both concentrations and rates of mass accumulation were used.

Figure 3.5 displays representative responses obtained for Eosin B. The impulse responses are presented as confidence belts. In each case, the plot on the right-hand side indicates the goodness of the fit, with the measurements as stars and the convolution of the least squares solution with the injection as a solid curve. The impulse responses were computed using the 125 h discretizations of the measured pulses. As the kernel had a high condition number, the estimated functional was chosen to be the sum of the components of the impulse response in a window 1000 hours wide, moved in steps of 250 hours. A smoothed solution was then

obtained. The belts shown on Figure 3.5 are based on the assumption that the standard deviation of the errors is always 10 % of the breakthrough. Each impulse response is represented by two confidence belts. The wider belt is plotted with solid double lines and corresponds to value 4.0 of the confidence parameter D. The narrower belt, whose individual intervals are the vertical segments between the stars, corresponds to value 2.5 for D. The analysis was also performed with a 500 h discretization of the initial data and a step of 500 h instead of 250 h for the window. It was found that the density of discretization seems to have very little effect upon the results. In the same way, it was observed that the shape of the belt is not substantially changed by the value of the confidence parameter. The effect of small changes in the injection pulse was then studied. The impulse responses obtained with the 500 h discretization of the Eosin B injection pulse used in this study were compared with those obtained using the discretization employed by the LBL/USDOE project team. The most obvious differences found in nearly all sheets were the number and the locations of the peaks, and the shape of the first peak. An example of such a comparison is shown in Figure 3.6. It was observed that the use of the LBL/USDOE data usually yields better fits.

In order to study the physical relevance of multiple peaks identified from the impulse responses a sensitivity analysis was performed using singular value decomposition of the kernel matrix, $\boldsymbol{K}$, and test runs with an artificial impulse response.

It was concluded that the interpretations of the impulse responses should be made with great care and the following points were underlined [*Ilvonen et al., 1993*]:

- in the Stripa 3D experiment, the validity of the assumptions related to the use of the deconvolution procedure (linearity and time-invariance of the system) is poorly known.
- the basic properties of the solutions may be changed by quite minor changes in the injection functions.
- the available data are not sufficient to discriminate between the various possible solutions.
- the physical relevance of multiple peaks appears rather uncertain in some cases (especially for Eosin B) and the apparent peaks seem most probably due to the mathematical appearance of the injection flow rate data.

3.4 Calibration strategy

The strategies employed for calibrating the alternative transport models are reviewed below. In the case of the channel network arrangement, fracture network calibration and flow calibration were required before running transport; both calibrations are also reviewed. Note that the geometries of the flow and diffusion paths were treated as the unknown quantities by the INTERA/AEA/NIREX project team. However, we have decided to present the strategy of this team in section 3.4.3: "Calibration of the transport model".

3.4.1 Calibration of the geometrical model

The two teams who used the channel network arrangement have first calibrated their discrete fracture networks on the observed trace geometry.

- The KTH/SKI project team [*Dverstorp and Andersson, 1989*] used the fracture traces observed in the long section of the drift roof. Fracture sets were identified from a visual inspection of the Schmidt stereo net and Fisher orientation distributions where fitted to the experimental data assuming that fractures belong to one of the fracture sets defined. The mean fracture radius was obtained, assuming exponentially distributed fracture radii, from the mean fracture trace length. This was estimated using the circular sampling and scanline techniques [*Andersson and Dverstorp, 1987*]. Fracture centre densities were then estimated, wet fractures being those retained for the estimation. From this "direct" estimation of the parameters, the network was calibrated on the measured data by generating fractures with the desired statistics until the number of fractures intersecting an observation window agreed with the number of traces observed on the roof. For each realization statistical measures of the fracture traces (mean length, total trace length and degree of censoring) were recorded. Simulation results were then compared with the observed trace lengths.

- The BRGM/ITASCA/ANDRA project team used the fracture traces observed both on roof and walls of the total drift. A visual inspection of the Schmidt diagram was also used to identify the fracture sets.

Fracture orientations were defined by the peak density value observed on the Schmidt diagram except for the subhorizontal fracture set for which a uniform distribution was employed. The fracture radii distribution was "analytically" derived from the true trace-length distribution taking into account the main biases (censoring, truncation and size) affecting the experimental histogram of trace length (see for example the review of *Chiles and de Marsily*, [*1993*]). All the available sampling area surveys (roof and walls) were used. Fracture traces observed on the walls were preferably used when estimating parameters of the subhorizontal fracture set. Lognormally distributed fracture radii were assumed for the derivation of the fracture size distribution. Results were then numerically verified, with a Monte Carlo technique, by generating fracture networks with the obtained parameters. In order to take into account the actual location of the fractures intersecting the drift, the simulations were conditioned on the observed fractures [*Chiles et al., 1992*]. Only one sampling surface (roof or wall) was considered in conditioning. If a fracture intersected just one sampling surface, the fracture trace was then exactly reproduced. If a fracture intersected more than one sampling surface, it was decided to exactly reproduce the trace observed on the roof. The total number of fracture traces, considering roof and walls, was simulated. A parametric study of the generated fracture network was then performed in order to study how the network could be simplified to save computer effort.

Results of the two previous approaches are presented in section 3.5.2.

3.4.2 Calibration of the flow model

The objective of this calibration was to determine the "channel transmissivity distributions" of the channel networks. Two approaches were used which both assumed lognormally

distributed channel hydraulic properties, flow rates into the drift being the calibration criterion.

- THE KTH/SKI project team calibrated the lognormal distribution of the "parallel-plate fracture disc" transmissivities [L^2T^{-1}] on the inflows observed in the drift roof assuming that the hydraulic gradient was unity and that all fractures reaching a nonzero flow sampling sheet were equally conductive. To calibrate the flow model, flow simulations were made in a right-angled box with sides $X=20\ m$, $Y=10\ m$, and $Z=20\ m$. Flow through a 4.5 m wide strip at the bottom of the box was treated as simulated flow into the drift; boundary conditions which would produce a unit gradient in a homogeneous porous medium were used. A Monte Carlo procedure provided a statistical ensemble of flow estimations. Criteria used for the calibration were: ensemble log mean of total flow into the drift, total wet trace length, cumulative frequency plots of the flow into a 2 m sections of the drift roof, statistical measures of the areal distribution of flow. The validity of the calibrated flow model was then explored by predicting the flow into the three vertical "tracer boreholes" and comparing the resulting inflow distribution with the measurements. For the transport simulation, the transmissivities were interpreted in terms of channel conductances (C [L^3T^{-1}], $C = Q/|grad\ h|$). The calibrated fracture transmissivity distribution was assigned to the channel conductance distribution.
- THE BRGM/ITASCA/ANDRA project team calibrated the lognormal distribution of the channel conductances (with log mean μ_c and log standard deviation σ_c) assuming also a lognormal distribution of the inflow rates into the drift (with log mean M_Q and log standard deviation S_Q for the observed values, m_Q and s_Q being the corresponding simulated values). The calibration procedure used by the team was derived from the one used by *Cacas et al. [1990 a]*. It can be summarized as follows. The procedure makes use of the fact that the fitting of σ_c is independent of those of μ_c: if μ_c is kept constant, Q is only a function of σ_c.

$$Ln(Q) = \alpha + \beta\sigma_c$$

In practice, finding σ_c simply consists in solving :

$$S_Q^2 = A\sigma_c^2 + B\sigma_c + C$$

using n realizations of fracture networks, each realization providing m simulated inflow rates (m being equal to the actual number because of conditioning). A first set of n×m inflow rates is obtained using $\mu_c = 0$ and σ_{c1}. A second set is obtained with $\mu_c = 0$ and σ_{c2} (σ_{c1} and σ_{c2} must define the interval in which the solution lies, i.e the interval must be large enough initially and then iteratively reduced). Once σ_c is found, which is not always the case, μ_c can be determined analytically from:

$$\mu_c = M_Q - \frac{\sum_i^n \sum_j^m Ln(Q_{ij})}{n.m}$$

where Q_{ij} is one of the inflow rates calculated with $\mu_c = 0$.

Flow simulations were made in a right-angled box with $X=190m$, $Y=160m$ and $Z=150m$. The total 3D drift was simulated by two rectangular parallelepipeds entirely contained within the flow domain and located at the centre of the box. The following boundary conditions were imposed: an atmospheric pressure in the drift, a constant pressure, derived from the measurements performed in the three vertical boreholes, at the top of the domain (70 m above the drift roof) and a no-flow condition on all the other sides of the box. The influence of these boundary conditions on the total flow into the drift was studied using a porous medium numerical flow model. It was found that with this location of the no-flow boundaries, the total flow into the drift is underestimated by 10% compared to the total flow obtained when the no-flow boundaries are located 1 km far away from the drift. The two channel network arrangements (SDM and RCM models) were calibrated using the previous method and 18 realizations of fracture networks. Pressure values resulting from the calibrated models were then compared with pressure values measured in the "tracer boreholes" in order to verify the calibration.

3.4.3 Calibration of the transport model

Among the six project teams, three calibrated their transport model on the experimental breakthrough curves, in one way or another. The calibration strategies of these teams, are reviewed first then the options used by the other teams will be presented.

Calibration on the experimental curves

-The KTH/SKB project team fitted the solutions of the alternative mathematical models (section 3.2) to the experimental results by a nonlinear least squares method. Each observed breakthrough curve was smoothed by eliminating outliers containing obvious errors, and then fitting a curve by hand through the remaining data. This resulted in a continuous smooth curve which was then transferred to the computer. A convolution technique was employed to relate the outflow to the time-varying inflow after first representing the inflow curves by a sequence of square (step) pulses. 167 individual concentration breakthrough curves were fitted using the "single channel - advection-dispersion" model. A subset of five curves for each tracer were then fitted using the "single channel - advection-dispersion-matrix diffusion" model and the "large number of parallel channels - advection only" model. According to the physical model used, one to three parameters were fitted (section 3.2), plus an extra scaling proportionality factor (called DF) accounting for dilution at steady-state conditions. Five tracers were

considered : Eosin B, Uranine, Elbenyl, Eosin Y, and Iodide.

-The LBL/USDOE project team performed two types of calibration. First, an exponentially decaying injection rate was used to approximate the sharply decreasing injection rates at the start of the experiment. Since the "single channel-advection-dispersion" model has an analytical solution in this case (see *Van Genuchten and Alves*, [*1982*], and *Javandel et al.*, [*1984*]), fitting was performed by an iterative process involving: guess at parameters, computation of resulting early time breakthrough curve and modification of the parameters. The first peak analysis represented a straightforward analysis of the early behaviour, itself reflecting the flow properties of the fastest channel. Secondly, the "pulse" response derived by the Toeplitz method was used to fit a "several parallel channels - advection-dispersion" model. In fact the response vector a obtained from the Toeplitz method was expected to be given by:

$$a_j = \frac{C_0}{\sqrt{4\pi D_L t_j}} \exp\left[-(x - vt_j)^2 / 4Dt_j\right] \qquad (3.12)$$

which is the Green's function to a one-dimensional "advective diffusive" equation for a unit injection at $t = 0$ and where C_0 is a constant proportional to the initial mass injected per unit channel cross-section area. The other parameters have been previously defined.

The number of channels was chosen to match the number of peaks in the pulse breakthrough curves. The two parameters defining each advection-dispersion channel were then fitted. The rates of tracer mass accumulation were used as the observed quantity rather than the tracer concentrations. This analysis was performed on total tracer breakthrough (sum over all sheets), and repeated for several single sheets or smaller groups of sheet. The five tracers analysed by the KTH/SKB project team were also considered.

- The BRGM/ITASCA/ANDRA project team first fitted the SDM and RCM channel network transport models to the experimental breakthrough curves. As a preliminary analysis the team calibrated the models using only two tracers and without considering the time-varying injection flow rates. [*Guérin and Billaux, 1993*]. In the final analysis four tracers (Eosin B, Eosin Y, Uranine and Elbenyl) were analysed and the time-varying injection flow rates were explicitly treated. The observed quantity used for the calibration was also the total collection mass flux calculated from the smoothed concentration curves of the KTH/SKB project team and the time-varying inflow rates observed in the plastic sheets. Two parameters were used to calibrate the models. The first one was a microdispersivity coefficient, α [L], introduced in each channel, which accounted for the local dispersion in the flow channels due to Taylor dispersion but also to the different pathways of various residence times which constitute a channel. α was assumed constant over the whole network. The second was a parameter allowing to calculate the volume of each channel available for transport. A shape factor, C_f (dimensionless), was defined assuming that the width, w, of the "parallel plate channel" was proportional to its length, L ($C_f = L/w$). Once again C_f was assumed constant over the whole network. Thus, using the cubic law, the calibration of C_f allowed to find the distribution of apertures and widths characterizing the transport model. *Cacas et al.* [*1990b*], presented a

procedure to calibrate a stochastic transport channel model on experimental data. They performed several realizations of each in-situ tracer test. The calibration parameter was a factor, C_r, allowing to obtain the volume of each channel available for transport. The times of the peak arrival were used as a calibration criterion. Thus they adjusted the C_r value (the same one for all the calculations) so that the central part of the histograms of simulated peak arrival times was as close as possible to the experimental values of arrival times. Here the calibration of the stochastic transport model was different. For each tracer test and for each channel network only five realizations of conditioned fracture network were considered. Each realization was characterized by its own lognormal distribution of channel conductances. The aim was to perform a "deterministic" calibration of each realization on the experimental data and then to study the variability of the calibrated parameters from realization to realization, from tracer to tracer and from channel network to channel network. The procedure for one calibration was by trial and error, as follows : a) choose an injection node with coordinates as close as possible to the actual location of the injection zone. b) compute a starting value for C_f based on first arrival times in case of pure advection. This was done using the "shortest path" algorithm [*Baase, 1978*]. c) Perform a transport simulation with an initial value of α equal to 10% of the mean channel length. d) change the two parameters according to discrepancies between the simulation and the calibration curve, and simulate transport again. e) Iterate step d) until a satisfactory fit was obtained. The goodness of the fit was appreciated (i.e, iterations were stopped) using an usual correlation criterion, R^2. Due to the relatively small distance between the injection zones and the drift, and due to the boundary conditions of the model (section 3.4.2), 100% recoveries were simulated when the total 3D drift was used to record the particles. Therefore , for each tracer, the mass effectively recovered at the end of the experiment was injected in the model, in order to mimic the field experiment.

In a second step, the fitted total breakthrough curves (normalized to the maximum simulated mass flux) were analysed with the analytical solution (3.5), i.e advection-dispersion model, in order to obtain estimations of *Pe* and t_w parameters, such as defined in section 3.2. A non linear optimization procedure was employed.

Other options

- The KTH/SKI project team employed the flow-calibrated discrete model to perform synthetic transport experiments in a channel network (sub-section to section 3.2.3). The validity of the use of effective transport parameters within an appropriate continuum model was analysed by fitting one-dimensional breakthrough curves to the synthetic breakthrough curves generated from the discrete model. The 1D advection-dispersion model (eq. 3.5) was used as continuum model. Transport simulations in the channel network were performed neglecting local dispersion in the flow channels of the fractures. Three different flow-channel geometries were compared assuming either " channel parallel plates" or circular tubes:
  - Type 1 channels : tube flow channels (Poiseuille law) where the channel radius was chosen to give each channel the desired conductance.
  - Type 2 channels: parallel plate channels (cubic law) with a constant width equal to 0.2 m.
  - Type 3 channels : parallel plate channels with the width of each channel equal to the length of the intersection line between the two fractures connected by the channel.

Transport simulations were performed over a rectangular domain with length X varying for different simulation cases from 10 to 30 m, and constant cross-sectional area ($Y.Z$ = 30×30 m^2). A hydraulic head difference (equal to 10% of X) between the two faces perpendicular to the x direction was imposed. All the other faces were impermeable boundaries. Particles were injected into the domain through one or more fractures intersecting the upstream face within a central, 10×10 m^2, square. Particles were sampled on the entire outflow face providing a spatially breakthrough curve. A pulse injection was used. For comparison with the analytical solution the simulated curves were integrated over time in order to simulate the mass breakthrough curves resulting from a constant step injection of tracer. Estimates for effective parameters were then performed using transport simulation results and the continuum model. Peclet numbers were estimated from the fit of the continuum equation. Porosity and specific rock surface available for sorption were estimated from geometrical calculations, transport simulations and the continuum model. Four values of the natural log standard deviation σ_c were tested (0, 2, 4, and 6) in order to highlight the effects of various channel conductances. For each simulation case 30 Monte Carlo realizations were used providing an ensemble of the transport parameters determined from individual realizations.

- The approach employed by the INTERA/AEA/NIREX project team was based on the hypothesis that the rock mass acted as a self-similar system by virtue of the hydraulic discontinuities at a number of different length scales (grain boundaries, microcracks, pores, channels, small fractures, fractures zones, fault zones, etc.). Thus, in this approach the geometry (geometries of the flow and diffusion paths) was treated as the parameter to be estimated. The objective was to develop improved ways of describing the structures within which transport occurs in saturated fractured rocks without committing the model to a particular flow path regime a-priori. The main data used were the tracer transit times to a given location. Concentration profiles were examined and twelve sheets for which five tracer arrivals were measured were found. For these twelve sheet the arrival times (T) for five tracers were estimated. The distance between the injection and collection points (R) was determined from published geometric information [*Abelin at al., 1987*].

The five tracer arrival times and distances for each sheet were fitted to the equation :

$$Log_eT = a + Dlog_eR$$

where D is the hydraulic, possibly non-integer, dimension. This equation arises by computing the arrival time from the relation:

$$v_R = c/R^{D-1}$$

where v_R is the radial velocity and assuming that, for a given sheet, c is constant for all tracers. A further assumption was that the strength of the effective sink at each sheet is the same for all tracers. Thus, if there were a straight channel connecting the injection and collection points, the velocity along the channel would be constant. If a planar fracture connected them (and did not connect with anything else), then the radial velocity would increase inversely with the distance to the collection sheet. If the medium were uniformly permeable then the flow would take place in three dimensions towards the drift (ignoring the

effect of adjacent sheets) so that the radial velocity would vary like $1/R^2$. Given the intermittent and sparse distribution of fractures observed within the rock, and the spatial variation in the experimental breakthrough curves, a flow path dimension, D, close to one was anticipated, which would suggest that the flow was highly channelled. Practically the data were collected for small differences in the injection times, and for each sheet, the five tracer arrival times, T, were plotted against the flow distances, R, on a log-log graph. A line was fitted by the method of least squares, yielding an estimate for D.

3.5 Results - estimation of parameters

The results obtained by the various project teams are reviewed below. Sections 3.5.1 and 3.5.2 give results concerning the geometric and hydraulic properties of the rock mass. Results concerning transport and the estimation of relevant "effective parameters" are given in sections 3.5.3 to 3.5.7. Note that we treat here the flow path dimension determined by the INTERA/AEA/NIREX project team as a transport parameter.

3.5.1 Fracture network properties

The two project teams (KTH/SKI and BRGM/ITASCA/ANDRA) who used the channel network arrangement first estimated the fracture network parameters assuming disc-shaped fracture. Methods relevant to the estimate were outlined in section 3.4.1. Table 3.1 summarizes the parameters of the calibrated model geometry, for the two project teams. These parameters were used for simulating flow and transport. In order to characterize the obtained network, the BRGM/ITASCA/ANDRA project team defined a connectivity index of the fracture network, I_c, equal to the mean number of intersections per fracture, weighted by fracture diameter [*Billaux and Guérin, 1993*]. The definition of this index is consistent with parameters defined by *Robinson* [*1984*] for 2D networks and the weighting is also consistent with numerical studies performed on percolation invariants (see for example [*Charlaix, 1987*]).

Given that the size of the simulation domain was large enough compared to the fracture sizes, I_c was found to decrease with the network connectivity. The team used this index to study how the network could be simplified, in order to save computer effort, without significantly affecting the medium connectivity.

The network was reduced by keeping only the generated fractures with a radius over a selected value. From the behaviour of I_c it was found that the connectivity of the simulated Stripa network was not significantly changed when the fractures with a radius below 2.0 m were removed (3 % reduction in I_c, $I_c \sim 7$).

Table 3.1 shows that the parameters obtained by the two teams are in some cases quite different. Whatever the methods used, the number of fracture traces (about 100) was probably too small to obtain statistically representative estimates.

The two estimates clearly underlined sparsely fractured networks, with a total density, λ, of fracture centres less than 0.1 m^{-3}. For comparison the following values were obtained on other sites also simulated with 3D Poisson point processes:

- Fanay-Augeres Mine, $\lambda > 5$ [*Cacas, 1990a, Billaux, 1990*], $17 \leq I_c \leq 33$.
- Stripa "SCV" site, fractured zone H, $\lambda \approx 30$ [*Herbert et al., 1991*], $I_c \sim 12$.
- Stripa "SCV" site, average rock, $\lambda \approx 4$ [*Herbert et al., 1991*]

3.5.2 Channel conductances - Hydraulic conductivity

Channel conductances

The KTH/SKI and the BRGM/ITASCA/ANDRA project teams assumed that channel conductances $[L^3T^{-1}]$ followed a lognormal distribution with log mean conductance μ_c and log standard deviation σ_c.

-The KTH/SKI project team first calibrated the lognormal distribution of fracture transmissivities $[L^2T^{-1}]$. A calibrated value of the log mean lying between -20.5 and -18.5 was found [*Dverstorp and Andersson, 1989*]. Four values of the natural log standard deviation were compared (sigma equal to 0, 2, 4, 6). As part of the transport simulations, a value of μ_c = -20.1 was used and it was found that a value of σ_c close to 4 best represented the investigated rock [*Dverstorp et al., 1992*].

-The BRGM/ITASCA/ANDRA project team directly calibrated the distribution of channel conductances for the SDM and RCM models. Using 18 conditioned fracture network realizations, the following distributions were obtained:

- Simplified Disc Model (SDM) : μ_c = -21.03 , σ_c= 1.69
- Random Channels Model (RCM) - Case 1 : μ_c = -18.92 , σ_c= 0.36
- Random Channels Model (RCM) - Case 2 : μ_c = -20.42 , σ_c = 0.88
- Random Channels Model (RCM) - Case 3 : μ_c = -21.93 , σ_c = 1.13

Thus the log standard deviation of the conductance distribution, σ_c, was found to increase with the channels density on each fracture plane (from case 1 to case 3).

As expected, the conditioning procedure reduced the variability of conductance distribution from realization to realization and therefore the uncertainty due to the stochastic process [*Guérin and Billaux, 1993*]. This observation was used as part of the transport simulations where calculations were performed using the conductance distributions calibrated for each realization instead of using the mean distributions.

For the SDM model, the two project teams estimated relatively similar distributions although different assumptions were used. For comparison, a quite different distribution was calibrated by *Cacas et al.* [*1990a*] for the highly fractured medium of the Fanay-Augere mine: μ_c = - 26.7, σ_c = 7.4.

Hydraulic conductivity

Two approaches were used to estimate the hydraulic conductivity of the rock mass.

-The KTH/SKB project team evaluated the hydraulic conductivity of the rock adjacent to the drift assuming a homogeneous porous medium where Darcy's law applies. The following expression was used:

$$K_p = \frac{Q\ln(r_2/r_1)}{2\pi L\Delta h f} \tag{3.13}$$

where Q is the flow rate to an L meter long part of the drift where the water flow rate is measured over a fraction f of the area (the sheets cover 50% of the area of the drift). Δh is the hydraulic head difference between the drift and points at a distance r_2 from the centre of the drift of radius r_1. The hydraulic head was measured in the three vertical injection holes. Two estimates of the gradient were deduced from the measured heads. Table 3.2 summarizes the values of the hydraulic conductivities of the different parts of drifts (values averaged over more than 100 m of drift). Table 3.2 shows that the difference of the hydraulic conductivity between the access drift and the experimental one is a factor of 2. This may indicate that the 100-m scale is not large enough to obtain reasonably constant average values [*Abelin et al., 1991*].

- The BRGM/ITASCA/ANDRA project team evaluated the equivalent permeability tensor of the rock mass using the channel conductance distributions calibrated with the SDM and RCM channel networks. Several methods have already been proposed to compute large-scale equivalent conductivities of a continuum using stochastic fracture network models (see *Long*, [*1983*], for 2D networks of lines; *Cacas et al.*, [*1990*]; *Herbert et al.*, [*1991*]; for 3D networks). These authors used square or cubic flow regions, boundary conditions being either linear pressure variations or prescribed constant head on two opposite faces and a no-flow condition on the (two or four) others. Here the permeability tensor was estimated using spherical instead of cubic flow regions. 180 orientations uniformly distributed on the half sphere were defined and for each orientation linearly varying heads were imposed at the boundaries of the sphere. For each orientation the induced flow was recorded on a centred disc orthogonal to the head gradient orientation. Thus a set of directional permeabilities was obtained and the equivalent permeability tensor was defined as the one giving the best least-square fit to these directional permeabilities.

In order to check the adequacy of the obtained tensor, a dimensionless "variability index for permeability", *Ivk*, was then defined as follows:

$$Ivk = \frac{\sum (K.u_i - k_i)^2}{n.\left[(K_1 + K_2 + K_3)/3\right]^2}$$

where n is the number of gradient orientations considered, u_i is the unit vector defining orientation i, k_i is the directional permeability computed for orientation i, K is the best fit

permeability tensor and K_1, K_2, K_3 are the principal permeabilities of K. The sum is over n.

Ivk is a normalized mean square error (NMSE) and can be regarded as the 3D equivalent of the NMSE defined in 2D by *Long [1983]*. *Ivk* was found to decrease when the medium under study comes closer to a homogeneous porous medium behaviour. On the other hand the continuum approximation for flow was found to be not valid any more when *Ivk* becomes greater than 10^{-3} (average value). This conclusion was obtained using pumping test interpretations as a criterion [*Billaux and Guérin, 1993*]. Table 3.3 displays the mean tensors of hydraulic conductivities calculated using the calibrated distributions of conductances, and the corresponding *Ivk* values. These values were obtained considering 80 m - radius spherical flow regions (i.e; a volume of rock close to the one used for the calibration of the flow model) and ten realizations of fracture networks. Figure 3.7 displays the value of *Ivk* as a function of the flow domain size, for the four channel networks. As expected *Ivk* decreases when the volume of the channelled medium increases. The best "hydraulic continuity" is obtained for the SDM model which represents an upper bound of connectivity. The 10^{-3} value is reached only for large volume of rock so that equivalent hydraulic properties cannot be derived at the scale of the tracer tests, whatever the channel network model.

Estimates performed by the two teams show that the hydraulic conductivity found in the Stripa 3D site is two orders of magnitude larger than that obtained for the average fractured rock of the SCV site, and one and half order of magnitude lower than that obtained for the highly fractured H zone of the SCV site (see [*Birgersson et al., 1992*]).

3.5.3 Fitting of breakthrough curves: results

Three project teams calibrated their transport model on the experimental breakthrough curves using the calibration strategies previously described. The calibration results are reviewed below.

The KTH/SKB project team

Tables 3.4 to 3.6 give results obtained using the three transport models employed. These results correspond to the subset of five representative sheets selected for each tracer. The right column in the tables contains the standard deviation of the fit.

In fitting the "single channel - advection-dispersion" model (AD) and the "single channel - advection-dispersion-matrix diffusion" model (ADD), the Peclet number was limited to values greater than 4.0 by introducing a penalty function in the fitting process. In the same way, the standard deviation in the lognormal distribution was limited to values below 0.318 in fitting the "advection-channelling" model (AC).

Figure 3.8 shows some selected response curves (sheet 108) and the corresponding fitted curves with the AD model for Eosin B, Uranine, Elbenyl, Eosin Y, and Iodide. The results from the model fits indicated that :

- the fits were generally good for Eosin Y and Iodide and showed poor agreement for Uranine.
- the theoretical models did not reproduce all the several ups and downs observed in the experimental curves.
- the values of the transport parameters required for fitting the experimental curves in adjacent sheets with the same tracer were in some cases quite different.
- the A-parameter that accounts for the matrix diffusion effects (ADD model) varied over several orders of magnitude. It was found that this parameter could not be determined by the calibration method because it influenced the curves in a way similar to dispersion, and the two processes could not be distinguished sufficiently with the data available [*Neretnieks, 1993*]. When matrix diffusion was included, the curve fits improved only marginally.
- the dispersion for many of the breakthrough curves was very high; the Peclet numbers being, in average, between 4 and 5 except for Iodide where they were in the neighbourhood of 30.

The LBL/USDOE project team

The results of the first peak breakthrough analyses are given in Table 3.7. A typical fit is shown in Figure 3.9. The distance x was taken to be the mean linear distance from the injection point to the weighted centre of exit locations in the drift ceiling; t_p is the time of arrival of the first peak. The mean arrival time t, corresponding to a delta pulse injection at time t = 0, was calculated from the fitted D and v values.

The results of the Toeplitz analysis are given in Table 3.8. The solutions are shown in Figure 3.10 which represents the normalized breakthrough behaviour, given the input data and the optimal choices for the transfer coefficients $\boldsymbol{a}$ (see section 3.4.3). The solid lines show solutions of the 1D advection-diffusion equation (with delta function tracer injections) surimposed so as to fit the Toeplitz output data. Here, the number of peaks observed corresponds directly to the number of independent channels. Thus for each tracer, a value for v and D was obtained for each channel. Then a Peclet number was calculated for each peak. The results from the model fits indicated that:

- the fit was very good (correlation coefficients between 0.936 and 0.989)
- the number of "channels" determined by the Toeplitz analysis ranged from two to four
- the values for the dispersion length, α, calculated by the Toeplitz analysis for the first channels (early behaviour) ranged from 0.6 to 2.9 and were globally consistent with those defined via the first peak analysis (α between 1.8 and 6.8).
- the dispersion length calculated for the first channels was between 2 (Uranine) and 75 (Iodide) times greater than the one calculated for the other channels.

Table 3.9 displays the calibration results obtained with the two channel network models. For each case, the calibrated values of the channel microdispersivity, α, and of the channel shape factor, C_f, are given.

The correlation coefficient R^2 was used to test the goodness of the fit: $R^2 = 1 - (1/N\sigma^2)\sum(obs - sim)^2$ where *obs* and *sim* denote respectively the observed and simulated mass fluxes, σ^2 is the variance of the observations. The sum is over the number of values N. The values of the effective parameters, Pe and T_w, obtained by fitting the continuum model to each simulated curve are also given. Figure 3.11 shows the results obtained with the SDM model, for the four tracers, and the "Eosin Y fits" obtained with the SDM model. An example of fit of the solution (3.5) to a simulated curve (Eosin Y, RCM model, realization 5) is also given on this figure. The results from the model fits indicated that:

- the fits were generally good for Eosin Y; satisfactory fits of the first behaviours were obtained for Eosin B; the beginning of the build-up was only well reproduced for Elbenyl; fits showed poor agreement for Uranine.
- the variability, from realization to realization, of the two calibrated parameters was of a factor 10, at the most.
- in most cases the best-fit dispersivity α values were not negligible. The highest values of α were obtained for the tracer Elbenyl whereas the smallest ones were obtained for Uranine. α values lie between 0.2 and 2.2 for the SDM model (with a mean around 0.9) and between 0.3 and 1.7 for the RCM model (mean around 0.7).
- the best-fit shape factor C_f values were generally low, with a mean around 0.7 for the SDM model and 1.2 for the RCM model. Considering the mean channel length in both models, such values would correspond to channels of width equal to 10 m, on the average, for the SDM model and 0.8 m for the RCM model.

These results are discussed in the following sections.

3.5.4 Porosities

Three project teams estimated "porosities" using different methods : KTH/SKB, KTH/SKI, BRGM/ITASCA/ANDRA. Table 3.11 summarizes the various estimates.

- THE KTH/SKB project team estimated the flow porosity, ε_f, assuming radially convergent flow into the drift and a homogeneous porous medium where Darcy's law applies:

$$\varepsilon_f = 2t_w Q / A_0 (r_2^2 / r_1 - r_1) \qquad (3.14)$$

where A_0 is the collecting area of the drift defined as the area covered by, and between, sheets in which tracers were found, t_w is the residence time, r_2 is the distance to the injection (the

shortest distance between the injection point and the drift), and r_1 is the collecting radius (the radius of a cylinder having the same surface area as the drift, taken here to be 2.2 m). Q was taken to be the flow-rate of water in which tracers were located and t_w was estimated from the fitting of the models to the breakthrough curves of the different tracers. Considering the uncertainties in the basic assumptions the project team mentioned that the resulting flow porosities would differ by more than a factor 2 if other extreme combinations of the assumptions were used. Table 3.10 shows the data used for evaluating the porosities and the obtained values. It was found a tendency for the porosity to decrease with distance from the drift.

A similar trend was observed as part of the Stripa SCV project [*Birgersson et al., 1992*]. This was ascribed to a local disturbance due the drift itself.

- The KTH/SKI project team estimated porosities from the channels network and the transport runs performed with the code DISCFRAC. Three types of estimate were done:
  - a geometrical estimate of the global flow porosity, ε_{geom}:

$$\varepsilon_{geom} = \frac{\sum V_c}{V_{dom}} \tag{3.15}$$

in which V_c denotes the volume of an individual channel, and V_{dom} denotes the volume of the simulation domain. The sum is over all conductive channels in the simulation domain

  - an estimate of the flow porosity, ε_{fds}, from transport runs:

$$\varepsilon_{fds} = Q_{tot}\, t_{0.5} \,/\, V_{dom} \tag{3.16}$$

in which Q_{tot} is the total flux through the simulation domain and $t_{0.5}$ is the time taken for 50% of the mass to break through (the median particle transit time).

The flow porosity was estimated in one direction through the fracture network using boundary conditions described in section 3.4.3.

  - an estimate of the flow porosity, ε_{fct}, by fitting the breakthrough curves from the discrete model to that given by the continuum model (1D advection-dispersion):

$$\varepsilon_{fct} = Q_{tot}\, t_w \,/\, V_{dom} \tag{3.17}$$

where t_w is water residence time and Q_{tot} is also the flow rate determined from the code.

The transport simulations were performed in a cubic domain with a side length of 25m and particles were injected with equal concentration in all fractures intersecting the injection area

on the upstream face of the domain. Boundary conditions described in section 3.4.3 were also used. Porosities were estimated for the three different flow channel geometries (channel type 1 to 3) and for different values of σ_c (σ_c = 0, 2, 4 and 6). The channel apertures, or channel radii in case of tube flow channels, were back calculated from the channel conductances. Figure 3.12 displays ensemble mean values of simulated porosity at the scale of 30 Monte Carlo realizations. Solid curves represent the flow porosity ε_{fds} while dashed curves represent the flow porosity ε_{fct}.

This figure demonstrated the importance of the local flow geometry in the fracture plane. For the channel type 2 case and for σ_c = 4 the ratio between the flow porosity obtained from the transport simulations and the corresponding total available flow porosity in the simulation domain was found, on average, equal to 0.42. In some realizations the values obtained from the transport simulations were reduced to only a few percent of the medium average values. Table 3.11 displays representative values of effective flow porosity estimated from the fitting of the 1D advection-dispersion equation. Results correspond to the case where μ_c = -20.1 and σ_c = 4 which gave the best fit to field data.

The flow porosity varies by several orders of magnitude depending on the geometry of the local flow channels. Only the results for channel type 3 (see section 3.4.3), which give the largest porosity values, fall within the range of the values obtained by the KTH/SKB project team.

- The BRGM/ITASCA/ANDRA project team estimated porosity using the results of the calibration of their transport models on the total breakthrough curves. Two types of estimate were done.
  - a geometrical estimate of the global flow porosity, ε_{geom}, as previously defined.
  - an estimate of the flow porosity, ε_f, and of its gradient direction dependence.

The flow porosity was computed using the same flow simulation method as for estimating permeability tensors. In addition to directional permeabilities computation, mass transport simulations were performed without considering the microdispersivity inside the channels. For each of the 180 gradient orientations, particles were injected on an upper segment of the sphere, i.e located upstream, and followed down to a lower segment. The flow porosity was then estimated from:

$$\varepsilon_f = q \cdot T/L \tag{3.18}$$

where q is the specific discharge recorded on a centred disc orthogonal to the gradient, T is the mean travel time for particles to reach the lower segment of the sphere, and L is the corresponding mean travel length. As for permeabilities, using several radii of the sphere allowed to study the scale dependence.

For 2D fracture networks, *Endo et al.* [*1984*], *Endo and Witherspoon* [*1985*] examined the directional nature of the "hydraulic effective porosity" to test the equivalent porous medium behaviour for mechanical transport; porosity having to be independent of the gradient direction in an equivalent continuum. The same procedure was employed here and a criterion was

defined to verify that the 3D surface corresponding to the "directional porosities" could be fitted by a sphere. Similar to the *Ivk* index defined in section 3.5.2, this criterion was called variability index for porosity , *Ivε*:

$$Iv\varepsilon = \frac{\sum [\varepsilon_0 - \varepsilon_i]^2}{n\varepsilon_0^2}$$

where n is the number of gradient orientations considered, ε_i is the directional flow porosity calculated for orientation i, and the sum is over $n \cdot \varepsilon_0$ is a reference value for porosity which here was taken equal to the mean of the ε_i. *Ivε* was found to decrease when the fractured medium comes closer to a porous medium behaviour for mechanical transport [*Guérin and Billaux, 1993*]. Figure 3.13 shows a 3D view of the surface representing the values of ε_f as a function of the gradient orientation. The calibrated SDM flow model was used for this calculation and a spherical flow region of radius 80 m was considered. This figure shows that, in this case, the flow porosity can vary by a factor 2 or 3 depending on the orientation of the gradient and therefore the distribution of porosities cannot be fitted by a sphere ($Iv\varepsilon = 4.1 \cdot 10^{-2}$).

The surface described in Figure 3.14 is particulary degraded when the RCM channel model is considered ($Iv\varepsilon = 10^{-1}$). Table 3.11 summarizes the values of flow porosity estimated using the shape factors, C_f, calibrated on the experimental curves (see Table 3.9).

Two values are given for each estimate, corresponding to the smallest and the highest directional porosity at the scale of ten realizations of fracture networks. In some cases the variability from a directional porosity to another inside a given network realization was greater than the variabilility from realization to realization. The maximum porosity values estimated with the SDM channel network parameters are comparable to the values obtained by the KTH/SKB project team.

Values obtained with the RCM model are from 5 to 7 times lower than the ones obtained with the SDM model. The geometric porosity ε_{geom} was found to be greater (by a factor 1.5 to 2) than the mean value of "directional flow porosity".

3.5.5 Specific surface - Matrix diffusion

We have regrouped here the estimation of specific surface and matrix diffusion. Specific surfaces have been estimated by the KTH/SKB, KTH/SKI and BRGM/ITASCA/ANDRA project teams using different methods. These estimates provided an opportunity to evaluate the potential for matrix diffusion. The VTT/TVO project team evaluated whether the experimental breakthrough curves revealed matrix diffusion or not. Table 3.12 summarizes the various estimates.

- The KTH/SKB project team determined the specific surface a_r (average fracture or channel surface wetted area per volume of rock) by comparing the experimental recovery and the

recovery obtained from model calculations. Several calculations were made using the "single channel ADD" model to fit the recovery. Fitting the three unknown parameters t_w, Pe, and a_r at the same time gave erratic values of Pe and t_w, but relatively stable estimates for a_r. If Pe or t_w were fixed to give values previously obtained, the value obtained for a_r did not change much from its value when all parameters were fitted.

Table 3.12 contains the compilation of obtained specific surfaces. The values obtained for the dyes are clearly greater than those obtained for Iodide. The large values obtained for the dyes seem unreasonable because they imply that spacing of conductive fractures should be between 0.07 and 0.4 m, using $2/a_r$ [*Abelin et al., 1991*]. This seems to contradict the observations in the drift. Matrix diffusion effects alone cannot explain the low recoveries if the large fractures alone are assumed to carry most of the flow. Both matrix diffusion and diffusion into stagnant water were suggested.

- As for porosities the KTH/SKI performed three estimates for specific surfaces.
  - a geometrical estimate of fracture surface area per volume of water, a_w, and fracture surface area per volume of rock, a_r :

$$a_{w.geom} = \sum A_c \,/\, \sum V_c$$

and

$$a_{r.geom} = \sum A_c \,/\, V_{dom} \qquad (3.19)$$

where A_c and V_c are respectively the wetted area and the volume of an individual channel. V_{dom} denotes the volume of the simulation domain and the sums are over all channels in the domain.

  - an estimate of specific channel surface from transport simulations.

The particle transit time in each flow channel of the model was corrected to take into account linear sorption, using the relationship:

$$t_{cs} = t_c\,[1 + (A_c/V_c)K_a]$$

where t_c is the particle transit time in the absence of sorption and t_{cs} is the corrected transit time. The ratio (A_c/V_c) in this formula is the local specific channel surface. Each transport simulation was run twice, once with and once without sorption ($K_a = 0$). K_a was set to one for "sorption runs". Then the median particle transit times were used to give the estimate

$$a_{w.ds} = \frac{(t_{0.5.s}/t_{0.5}) - 1}{K_a}$$

and subsequently

$$a_{r.ds} = a_{w.ds}\varepsilon_{f.ds}$$

where $t_{0.5.s}$ is the median transit time estimated from a sorption run, and $\varepsilon_{f.ds}$ the flow porosity previously defined.

- an estimate of specific surface parameters by fitting the continuum model to the breakthrough curves generated from the discrete model. Using a sorption run, the value of t_s (= $R_a t_w$, see eq. 3.3) is obtained. Since t_w is known from the corresponding "no-sorption run", the continuum estimates are:

$$a_{w.ct} = (t_s + t_w)/K_a t_w$$

and

$$a_{r.ct} = a_{w.ct}\varepsilon_{f.ct} \qquad (3.20)$$

Specific surfaces were estimated using the simulation domain and the boundary conditions employed for estimating porosities. Figure 3.14 displays ensemble mean values of simulated specific channel surface area per volume of rock, a_r, for the three different channel types and four values of the log standard deviation of conductances distribution, σ_c. Solid curves represent the estimate of $a_{r.ds}$ while dashed curves represent the estimated of $a_{r.ct}$. Figure 3.14 shows that specific surfaces differ by several orders of magnitude depending on the different channels types used. The fitted continuum model overestimated ensemble mean specific channel surface area, $a_{r.ds}$, by a factor of 2 to 3, depending on the value of σ_c.

The ratios $a_{w.ds}/a_{w.geom}$ and $a_{r.ds}/a_{r.geom}$ showed that the results from the transport simulations on the average differ by a factor 2 from the medium average properties. As for porosities, the case of channel type 2 with $\sigma_c = 4$ was considered. Here again, the values obtained from the transport simulations in some realizations were reduced to only a few percent of the ones obtained from geometrical estimate. Such results show that network effects must be taken into account when estimating specific surfaces. As for porosity, only simulations with channel type 3 result in an ensemble mean specific surface that falls within the range of the values obtained by the KTH/SKB project team.

- The BRGM/ITASCA/ANDRA project team did not consider matrix diffusion when simulating transport in the channel networks and therefore only estimated the "geometric channel surface area per volume of rock", $a_{r.geom}$. As for porosity, higher specific surfaces are obtained with the SDM channel network (i.e. the 10 m wide "unrealistic channels").

- The VTT/TVO project team [*Hautojärvi, 1993*] analysed the "dispersive powers" of hydrodynamic dispersion and matrix diffusion in order to study if matrix diffusion effects could be identified from breakthrough curves. The analysis was based on the comparison of a 1D analytical solution for the advection-dispersion equation to the corresponding solution for the advection-matrix diffusion equation. Considering the flow rate Q through a channel of width W, the team obtained the following relation:

$$D_e = Q^2 / (0.4 \cdot W^2 \cdot x \cdot v \cdot \varepsilon) \tag{3.21}$$

where D_e is the effective diffusion coefficient into the matrix, v is the velocity, x is the transport distance and ε is the matrix porosity. One of the assumptions used to obtain this relation is that the dispersion length is equal to 10% of the transport distance. The team used (3.21) to define in a $D_e=f(Q)$ plot two areas where hydrodynamic dispersion or matrix diffusion dominates. (3.21) was applied to the Stripa 3D site with x = 20 m, v = 0.006 m/h, W = 0.1 m and ε = 0.01. It was concluded that matrix diffusion seems not to play an important role in the transport of the Stripa 3D experiment and that matrix diffusion effects can hardly be seen or measured in breakthrough curves type of measurements due to the extremely low flow rates required.

3.5.6 Dispersive behaviour - Channelling

Three mechanisms were considered for modelling "dispersion": hydrodynamic dispersion, channelling and matrix diffusion. The project teams showed, in one way or another, that it was necessary to take into account an important dispersion to simulate most of the tracer tests. This dispersion was quantified in an usual way by a Peclet number, *Pe*, a dispersion length α or a dispersion coefficient, D_L.

- The KTH/SKB project team evaluated Peclet numbers using the tracer breakthrough curves in their entirety. The evaluated Peclet numbers range from very low values, less than 4, to about 35. In some cases values of Pe $<$ 1 were required to fit the experimental curves. Such an "unreasonable result" seems to show that the models used do not describe some of the important causes of dispersion and attempt to force the parameter values to account for processes which they cannot account for [*Abelin et al., 1991*].

The team mentioned that the mechanisms that govern diffusion into stagnant pools of water, matrix diffusion, the frequency of mixing, and especially the non-mixing of channels need further study.

- The LBL/USDOE project team evaluated Peclet numbers for each peak of the deconvoluted breakthrough curves (see Table 3.8). Therefore the results cannot be directly compared to those obtained by the KTH/SKB project team. There was no clear dependence of Peclet number on travel time, which would be a sign of scale dependent dispersion. However on a log-log plot, there appears to be a general increase of *Pe* as a function of mean travel time *(t)* which implies a decrease of dispersion in each flow channel with travel time. Values obtained from the Toeplitz analysis and from the first peak fit analysis display the same trend

(see Figure 3.15). Relationships of the form

$$Pe \propto (t)^n \quad and \quad \alpha \propto (t)^{-n}$$

with n $\approx$ 2, are suggested to explain such scale effects.

The mean travel time is strongly affected by the local heterogeneity around the injection location. However this mean time could be correlated to the basic aperture probability distribution parameters. Thus the scale effect for travel time distribution would be consistent with the local heterogeneities in the rock geometry, as represented by the variable-aperture channel model used by the team.

- The KTH/SKI project team evaluated Peclet numbers by fitting a continuum model to the cumulative breakthrough curves simulated with the channel network model. Figure 3.16 illustrates the evolution of the Peclet number with transport distance in simulations with $\sigma_c = 0$ and $\sigma_c = 4$. For $\sigma_c = 0$, a linear increase in the Peclet number with transport distance is observed (i.e constant dispersion length). For $\sigma_c = 4$, this trend disappears indicating the presence of non-Fickian dispersion and a dispersion length proportional to the transport distance. Here the transport distance was taken equal to the length of the simulated domain. Occasionally, very high Peclet number (Pe $>$ 100) were evaluated, indicating extreme channelling. For $\sigma_c = 4$, which gave the best fit to the field data, the average Peclet number estimated from the simulation varies from 0.2 to 7.

- The BRGM/ITASCA/ANDRA evaluated first a channel microdispersivity α, constant over the whole network, from the calibration of the channel network models on the experimental curves. In a second stage, Peclet numbers were estimated by fitting a continuum model to the simulated curves (Table 3.9). From the Peclet numbers obtained with these fits, "global" dispersion lengths can be estimated using, as a first approach, the travel distances taken by the LBL/USDOE project team. The ratios between the dispersivity obtained by this method and the microdispersivity introduced to calibrate the models can be used to appreciate the importance of network effects. Ratios between 1.1 (Elbenyl, SDM, rea 5) and 18 (Uranine, RCM, rea 1) were obtained with a mean around 4.6 for the SDM model and 6.6 for the RCM models. Such results clearly show that in some realizations the transport pathways were reduced to only one or a few channels poorly connected and therefore a high channel microdispersivity was required to reproduce (or at least attempt to) the dispersion revealed by the experimental curves.

In this case such a microscopic dispersion clearly cannot be neglected in a channel network. Note that, on the contrary, *Cacas et al.* [*1990b*] found that microscopic dispersion had negligible effects on the macroscopic dispersion created by the velocity differences along the different fractures that composed the densely fractured network of the Fanay-Augeres mine. However they used a value of α equal to 0.8 to obtain smooth simulated breakthrough curves. In the present study removing the smallest fractures of the network probably affected the initial dispersive behaviour of the channel network.

3.5.7 Estimation of flow dimension

Most teams assumed an underlying one-dimensional geometry for the flow paths and therefore this dimension was not estimated. Only the INTERA/AEA/NIREX project team calculated fractional dimensions of the flow paths using the method described in section 3.4.3. The results are shown in Table 3.13. The closeness of the data to the fitted is indicated by the correlation value (shown as "cor" in Table 3.13). It was noted that the slope of the fitted lines is generally close to unity. Such a slope suggests that the basic premise of transport through a simple geometric structure is appropriate, and that the dominant structure is pipe-like. Sheet 64, which has the highest correlation, has a slope of 1.34, suggesting an influence of planar fractures, and less channelled flow. On average, the data indicated that the effective dimension is slightly greater than unity. The average slope $< D >$ was given by $< D > = 1.1$ to three significant figures. Note that the average slope becomes 1.25 if the data with lower correlation (i.e, correlation below 0.6) are discarded. This new value was evaluated more in line with the pattern [*Hodgkinson and Grindrod, 1991*]. An additional estimate of D was done using estimates for flow porosity given by the KTH/SKB project team. These estimates showed a trend for porosity to decrease with flow path distance. Using the fractional-dimension flow model, the porosity was derived as a function of distance, R, as follows:

- As R increases from zero, the volume filled by the inflow paths is of the form :

$$R^D W$$

where W is a constant (3-D) dimensional width.

- Thus the volume fraction available to the flow was obtained from:

$$\phi \sim R^{-3+D}$$

A graph, on a log-log scale, of the porosity data obtained by the KTH/SKB team (sub-section to section 3.5.3), was then fitted by a linear curve having slope $-3+D$. On the basis of these results (Figure 3.17), an estimate of $D = 1.6$ was made. The generalized D-dimensional cylindrical geometry may well be inappropriate at very large distances from the sinks, i.e. the sheets. Nevertheless, the team mentioned that it was encouraging to see that a value between 1 and 2 was obtained using independent estimates. The closer to unity D becomes, the closer the idealized fractional cylindrical flow paths come to the one-dimensional channels concept used, in one way or another, by the other project teams. It was underlined that it should be possible to build a generalized radial transport model which includes generalized geometric descriptions of flow and diffusive paths.

Such an approach would be based upon the work of *Barker* [*1985, 1988*] who notably derived an analytical expression of flow in the case of a medium with a noninteger dimension.

3.5.8 Spatial variability

Spatial variability of the tracer recovery is one of the important results of the Stripa 3D experiment. This variability has not been considered as a quantitative calibration criterion by the project teams who calibrated their models on total or cumulative breakthrough curves (LBL/USDOE, KTH/SKI and BRGM/ITASCA/ANDRA). However results obtained by the two project teams who employed the concept of interconnected channels can be used to verify the ability of these models to reproduce field observations. Figures 3.18 and 3.19 display examples of spatial variability simulated by the KTH/SKI and BRGM/ITASCA/ANDRA project teams.

3.6 Conclusion - what was learnt

Experiment

The Stripa 3D experiments provided a good opportunity to study the advective flow and dispersion of soluble tracers through saturated fractured rock. The use of a multitude of plastic sheets in a long underground drift allowed a detailed survey of the spatial and temporal variability of flow and transport. This survey notably showed; a) the uneven distribution of water inflow rates into the drift; b) a relationship between areas having a higher number of fracture intersections and areas having higher water flow rates; c) the uneven distribution of tracer concentrations underlined by the fact that experimental curves in adjacent sheets for the same tracer were in many cases quite dissimilar. The very uneven distribution of flow and tracer paths points to one difficulty with this experiment : our lack of knowledge about flow patterns in the volume under study. Another difficulty was the variation of the injection flow rates with time.

Assumptions

To reproduce such observations most project teams based their analysis upon the assumption of one-dimensional channelled flow. Therefore it was assumed that one-dimensional governing equations could be used to reproduce flow and transport processes, at least at the channel scale. The assumption about mixing between channels may be used to differentiate between the different approaches.

- Three teams used one-dimensional models assuming no mixing of tracer between the channels over the migration domain.
- Two teams used models of interconnected one-dimensional channels assuming a perfect mixing at each channel intersection.
- One team did not assume any mixing and flow dimension a priori and considered this dimension as the main unknown.

The assumption about connections between channels conditioned in some cases the assumption about transport processes. For example, the KTH/SKI project team assumed that dispersion was only due to network effects (i.e, mixing between channels of various velocities) whereas

the LBL/USDOE assumed that a three-dimensional network effect could be completely ignored and that dispersion was due to the slightly different velocities of the various flow paths that compose the channel.

The assumption about channel mixing also conditioned the number of parameters required to simulate transport. Both project teams (KTH/SKI and BRGM/ITASCA/ANDRA) who used models of interconnected channels assumed that these channels were located within planar fractures; each channel having its own hydrodispersive properties (conductance, volume available for transport and possibly microdispersivity). Thus specifications of the fracture network and hydrodispersive properties of the channels were needed for simulating transport. As all values of these parameters could not be directly derived from observations a stochastic approach was used. One of the channel models used by the BRGM/ITASCA/ANDRA project team was not geometrically fully defined by the fracture network and therefore additional parameters were required. The "large" number of parameters required for using channel network models constitutes an obvious drawback. However, once calibration of the model is done, one can expect to reproduce the variability of flow and transport, at least statistically.

The project teams who simulated transport assuming no mixing between channels on the way (KTH/SKB and LBL/USDOE) used few "effective" parameters. Thus one or several sets of parameters were estimated for each tracer experiment, depending on the number of channels used to explain the breakthrough curves. The relatively low number of parameters required in this approach constitutes an obvious advantage for predictive purposes. However calibrated values of the parameters may vary largely from a tracer experiment to another, and therefore hindering the predictive value of this approach.

The INTERA/AEA/NIREX project team calculated fractional dimensions of the flow paths for each part of the medium between the injection sites and sheets, each sheet containing several tracer arrivals. Thus just one parameter was calibrated which also could vary from sheet to sheet.

Approaches

The calibration strategies used by the project teams were designed to estimate effective parameters representative of the Stripa flow system, in one way or another.

Different and complementary approaches were used from which several results can be pointed out. The time-varying injection flow rates made the interpretation difficult in some cases. Thus deconvolution techniques appeared to be an interesting tool to treat such disturbed data although, as noted by the VTT/TVO project team, physical interpretation of the deconvoluted results should be made with great care. Considering only the fitting of the experimental breakthrough curves, the use of sophisticated numerical transport models with a large number of parameters did not improve the fits obtained with simple analytical models. However, in such a sparsely fractured medium, conditioning appeared to be a potential tool to improve the calibration of stochastic transport models (see the BRGM/ITASCA/ANDRA project team). Both channel network models have shown their capacity to reproduce the strongly heterogeneous behaviour observed in the experiment. However only unrealistic flow channel

geometry (channel with large width) have allowed to obtain effective transport parameters comparable to those evaluated by the KTH/SKB project team. Dependence of the medium properties with scale, particulary concerning dispersion, and in some cases with direction were observed.

Calibration and validation

Although the assumptions used by the project teams were in some cases quite different, the various channel models were able to reproduce most of the trends observed in the experiment. Such a conclusion would point out that the experimental data could not be used to discriminate between the various channel models. All of the teams validated highly channelled flow path models; an independent validation of the one-dimensional flow path approach was provided by the INTERA/AEA/NIREX project team. However, one problem remains open : we do not know why low recovery rates, and sometimes complete loss of tracer, were observed. Possible explanations have been given, mostly by the KTH/SKB team : diffusion into the matrix or into stagnant pools of water, of flow paths not leading towards the experimental drift. The data needed to evaluate these hypotheses is lacking. Indeed, it is true that these models have been able to reproduce some of the field observations, nevertheless it can hardly be seen how they could have predicted them. To overcome these difficulties, future tracer transport experiments should include a more detailed investigation of the flow conditions.

Acknowledgement

The financial support of ANDRA, France, for the work of the editors is gratefully acknowledged.

Table 3.1 Fracture Network Parameters obtained from the Stripa 3D Experiment (KTH/SKI, BRGM/ITASCA/ANDRA).

Fracture set	Fracture orientation		Fracture radius		Fracture centre density
KTH/SKI Project team					
Visual inspection of the stereonet	Fisher distribution fitted to each fracture set		Exponential distribution Mean (m)		Poisson space process density, λ (m^{-3})
1	sub-vertical		2.3		$3.9\ 10^{-3}$
2	sub-vertical		2.3		$4.5\ 10^{-3}$
3	sub-horizontal		2.3		$18.4\ 10^{-3}$
4	random		2.3		$1.8\ 10^{-3}$
BRGM/ITASCA/ANDRA Project team					
Visual inspection of the stereonet	Peak density value		Lognormal distribution		Poisson space process density λ (m^{-3})
	Théta (deg)	Phi (deg)	Mean (m)	St.Devia (m)	
1	156 ± 10	16 ± 10	0.53	0.975	0.061
2	106	83	2.30	0.55	0.010
3	216	75	1.575	1.78	0.0083

Table 3.2 Hydraulic Conductivities in the Stripa Three Dimensional Drifts (KTH/SKB)

LOCATION	Conductivity x 10^{11} m/s	
	Steep Gradient	Low Gradient
Experimental Drift		
- Ceiling + upper sides	0.56	1.07
- Floor + lower sides	1.9	3.6
- Average	1.3	2.3
Access drift	0.7	1.3

Table 3.3 Average hydraulic conductivity tensors for the Stripa 3D rock mass (BRGM/ITASCA/ANDRA)

Channel network	Permeability tensor			Ivk
	Phi	Théta	K (m/s)	
SDM	57.7	- 22.4	$2.0\ 10^{-11}$	
	104.1	- 103.3	$1.3\ 10^{-11}$	$2.13\ 10^{-3}$
	35.9	- 173.1	$6.56\ 10^{-12}$	
RCM - 1	66.3	- 33.3	$2.55\ 10^{-11}$	
	120.4	- 108.4	$6.51\ 10^{-12}$	$1.17\ 10^{-2}$
	40.2	- 154.5	$3.76\ 10^{-12}$	
RCM - 2	67.9	- 35.2	$1.18\ 10^{-11}$	
	111.3	- 116.1	$4.46\ 10^{-12}$	$1.06\ 10^{-2}$
	31.5	- 166.6	$2.19\ 10^{-12}$	
RCM -3	68.0	- 36.3	$7.11\ 10^{-12}$	
	116.8	- 114.6	$4.73\ 10^{-12}$	$5.04\ 10^{-3}$
	35.9	- 160.3	$1.46\ 10^{-12}$	

. SDM = Simplified Disc Model
. RCM = Random Channel Model

Case 1 = Density of channels in each channel set, $\lambda = 2.0\ 10^{-2}\ m^{-2}$
Case 2 , $\lambda = 3.0\ 10^{-2}\ m^{-2}$
Case 3 , $\lambda = 4.0\ 10^{-2}\ m^{-2}$
. Phi, Théta : orientations (poles) of tensor components

Table 3.4 *Calibration results obtained using the advection-dispersion model. The condition that the Peclet number should be greater than 4.0 was imposed (KTH/SKB).*

NUMBER	PECLET NUMBER	RESIDENCE TIME (hours)	DILUTION FACTOR	STANDARD DEVIATION
Tracer	Eosin B			
571	5.1	7045.0	151.3	0.14
601	4.0	20470.0	181.7	0.11
661	4.0	5004.0	313.3	0.22
1081	4.2	5331.0	797.4	0.32
1201	4.0	7077.0	135.5	0.09
Tracer	Uranine			
642	4.7	2273.0	1152.0	0.38
712	4.0	4223.0	695.0	0.25
902	4.0	7445.0	1670.0	0.19
1082	4.0	3634.0	2194.0	0.29
1342	12.0	11810.0	190.0	0.03
Tracer	Elbenyl			
603	4.0	2112.0	285.8	0.15
643	6.1	2014.0	247.7	0.22
663	4.0	1969.0	202.3	0.20
683	5.6	1978.0	382.2	0.11
1083	6.3	1636.0	583.6	0.29
Tracer	Eosin Y			
646	6.6	5090.0	130.7	0.10
686	5.5	7320.0	94.9	0.07
716	5.3	7381.0	93.5	0.07
906	4.7	8933.0	72.4	0.03
1086	6.0	6324.0	277.6	0.08
Tracer	Iodide			
618	18.6	7209.0	126.8	0.08
628	4.0	11160.0	40.3	0.05
1038	34.0	7558.0	98.6	0.06
1088	54.5	7113.0	82.3	0.06
1108	34.5	7031.0	76.2	0.06

Table 3.5 *Results obtained using the advection-dispersion-matrix diffusion model. A Peclet number greater than 4.0 was imposed (KTH/SKB).*

Number	Peclet number	Residence time (hours)	A-parameter	Dilution factor	Standard deviation
Tracer:	Eosin B				
571	5.1	7035.0	$3.10 \cdot 10^{5}$	150.1	0.14
601	4.0	20470.0	$2.00 \cdot 10^{5}$	181.7	0.11
661	4.0	1944.0	1039.0	168.9	0.07
1081	4.2	3118.0	1636.0	465.7	0.17
1201	4.0	4687.0	2987.0	78.2	0.03
Tracer:	Uranine				
642	19.8	15.1	28.9	946.1	0.29
712	6.5	26.5	22.5	470.4	0.15
902	4.0	11170.0	$1.18 \cdot 10^{5}$	1052.2	0.16
1082	4.0	1979.0	2309.0	1645.3	0.21
1342	11.7	12000.0	$9.44 \cdot 10^{4}$	173.0	0.03
Tracer:	Elbenyl				
603	5.8	1402.0	3632.0	239.9	0.11
643	6.1	2014.0	$7.62 \cdot 10^{16}$	247.7	0.22
663	4.0	1941.0	$2.00 \cdot 10^{5}$	203.6	0.20
683	5.6	1978.0	$1.25 \cdot 10^{13}$	382.2	0.11
1083	6.3	1636.0	$4.51 \cdot 10^{16}$	583.6	0.29
Tracer:	Eosin Y				
646	6.5	5067.0	$1.81 \cdot 10^{7}$	130.4	0.10
686	5.5	7274.0	$3.93 \cdot 10^{5}$	94.4	0.07
716	5.4	7758.0	$2.82 \cdot 10^{5}$	92.7	0.06
906	34.8	2829.0	1669.0	43.1	0.03
1086	6.0	6325.0	$2.02 \cdot 10^{5}$	277.6	0.09
Tracer:	Iodide				
618	18.6	7206.0	$4.94 \cdot 10^{7}$	126.8	0.08
628	4.0	11090.0	$5.00 \cdot 10^{5}$	40.2	0.05
1038	34.0	7557.0	$4.49 \cdot 10^{6}$	98.6	0.06
1088	54.5	7113.0	$5.28 \cdot 10^{8}$	82.8	0.06
1108	34.5	7030.0	$2.50 \cdot 10^{7}$	76.2	0.06

Table 3.6 *Results obtained using the advection Channelling model. The standard deviation was limited to values lower than 0.318 (KTH/SKB).*

Number	Standard deviation in model	Residence time (hours)	Dilution factor	Standard deviation in fit
Tracer:	Eosin B			
571	0.301	7794	150.0	0.14
601	0.318	19870	201.6	0.12
661	0.318	4994	318.8	0.23
1081	0.318	5191	800.4	0.33
1201	0.318	7774	135.9	0.09
Tracer:	Uranine			
642	0.318	3039	1162	0.39
712	0.318	4225	692	0.25
902	0.318	7445	1666	0.19
1082	0.320	3555	2325	0.31
1342	0.194	12080	193	0.03
Tracer:	Elbenyl			
603	0.318	2329	284.9	0.14
643	0.281	2194	246.6	0.22
663	0.318	2187	202.2	0.20
683	0.287	2160	380.2	0.11
1083	0.273	1762	581.4	0.28
Tracer:	Eosin Y			
646	0.267	5468	130.2	0.10
686	0.285	7899	95.1	0.08
716	0.286	8409	94.0	0.07
906	0.296	9476	73.7	0.03
1086	0.275	6801	277.8	0.09
Tracer:	Iodide			
618	0.165	7450	126.2	0.08
628	0.318	11970	41.1	0.05
1038	0.121	7677	98.5	0.06
1088	0.096	7180	82.3	0.06
1108	0.120	7136	76.0	0.06

Table 3.7 Results of the first peak analysis (LBL/USDOE)

Tracer	x, m	t_p, h	D m mm/h	v mm/h	x/t_p, mm/h	$\bar{t} = (x/v) + (D/v^2)$, h	$\alpha = D/v$, m	$Pe = vx/D$
Elbenyl	10.7	2500	17	3.7	4.3	4200	4.7	2.2
Eosin Y	24.6	8500	7.5	3.2	2.9	8300	2.3	11
Eosin B	33.3	4000	67	9.8	8.3	4100	6.8	4.9
Uranine	36.4	7000	15	5.6	5.2	6900	2.7	13
Iodide	42.8	9000	9.5	5.3	4.8	8400	1.8	24

Table 3.8 Results of the Toeplitz analysis (LBL/USDOE)

Tracer	x, m	Channel	$\bar{t}$, h	D, m mm/h	v, mm/h	$Pe = xv/D$	$\alpha = D/v$, m
Elbenyl	10.7	1st	2612	8.1	4.7	6.3	1.7
		2nd	14447	0.02	0.74	323	0.03
Eosin Y	24.6	1st	6478	12.4	4.2	8.4	2.9
		2nd	10440	0.2	2.4	314	0.1
Eosin B	33.3	1st	2814	24.8	12.5	16.8	2.0
		2nd	7198	1.9	4.7	82.6	0.4
		3rd	11980	0.2	2.8	411	0.1
		4th	16212	0.1	2.1	507	0.1
Uranine	36.4	1st	3640	5.9	10.2	62.2	0.6
		2nd	6053	1.8	6.1	119	0.3
Iodide	42.8	1st	7473	9.0	5.9	28.3	1.5
		2nd	14990	0.06	2.9	1980	0.02

Table 3.9 Calibration results obtained using the channel network models. (BRGM/ITASCA/ANDRA)

Channel Network	Network Realization	Channel Micro dispersivity (m)	Shape Factor cf	R^2	Pe	t_w
Tracer :	Eosin B					
SDM	1	0.8	0.5	0.79	8.1	1967
	2	0.7	1.1	0.78	9.5	2008
	3	1.0	0.7	0.80	5.1	1899
	4	0.8	0.4	0.81	7.9	2006
	5	1.1	1.2	0.76	13.9	1919
RCM 1	1	0.6	2.4	0.83	5.5	2045
	2	0.6	2.2	0.84	6.9	1936
	3	0.3	1.1	0.74	7.4	1768
	4	0.7	1.3	0.78	10.3	1967
	5	0.4	0.9	0.80	4.8	2017
Tracer :	Eosin y					
SDM	1	1.1	1.1	0.93	7.6	5532
	2	0.4	0.2	0.95	10.9	6099
	3	2.2	0.7	0.93	5.3	5803
	4	0.5	0.5	0.94	12.0	5817
	5	1.0	0.3	0.93	13.6	6162
RCM 1	1	0.8	1.1	0.97	11.3	5561
	2	0.6	0.9	0.92	11.1	5137
	3	0.9	1.0	0.97	7.1	6038
	4	0.7	0.9	0.95	9.8	5976
	5	0.3	0.4	0.96	8.9	5644
Tracer :	Uranine					
SDM	1	0.3	0.7	0.79	9.5	2942
	2	0.2	0.2	0.71	11.7	2943
	3	0.7	0.9	0.62	8.9	2882
	4	0.3	1.3	0.71	9.5	2745
	5	0.4	0.4	0.58	19.3	2689
RCM 1	1	0.3	1.8	0.72	6.6	2676
	2	1.5	0.9	0.79	5.3	2884
	3	0.5	1.4	0.58	19.2	2688
	4	0.4	1.3	0.71	5.2	2706
	5	0.3	1.2	0.59	21.2	2885
Tracer :	Elbenyl					
SDM	1	1.2	0.5	0.68	7.6	1178
	2	0.6	1.3	0.66	10.3	1012
	3	1.2	0.2	0.69	4.8	1179
	4	1.6	0.7	0.69	4.8	1178
	5	1.0	0.6	0.67	10.1	1036
RCM 1	1	0.6	0.6	0.68	8.0	1145
	2	0.9	0.4	0.69	8.0	1206
	3	0.6	1.5	0.67	7.6	1179
	4	1.7	0.9	0.66	4.1	1317
	5	0.6	1.9	0.65	9.7	1216

SDM = Simplified Disc Model
RCM 1 = Random Channels Model with density of channels in each channel set = $2.0.10^{-2}$ m^{-2}

Table 3.10 Porosities and basic data used in the calculations (KTH/SKB)

Tracer	Residence time (hours)	Flowrate in section (ml/h)	Length of section (m)	Distance to injection point (m)	Porosity x 10^5
Eosin B	3000	175	22	19	3.4
Uranine	5500	153	23	32	2.0
Elbenyl	2000	178	10	10	15.5
Eosin Y	6000	198	27	18	6.9
Iodide	7000	200	31	29	3.0
Bromide	2500	200	31	13	4.5

Table 3.11 Summary of estimated porosities (KTH/SKB, KTH/SKI, BRGM/ITASCA/ANDRA)

Tracer	Eosin B	Uranine	Elbenyl	Eosin y	Iodide	Bromide
KTH/SKB Project team						
Flow porosity ε_{f1}(x10^5)	3.4	2.0	15.5	6.9	3.0	4.5
KTH/SKI Project team						
Effective Flow Porosity ε_{f2} (x10^5)	Global estimate Channel type 1 : 0.022 ± 0.023 Channel type 2 : 0.51 ± 0.45 Channel type 3 : 3.4 ± 2.8					
BRGM/ITASCA/ANDRA Project team						
Flow porosity ε_{f3} (x10^5)	0.3 - 2.3 0.02 - 0.3	0.8 - 2.0 0.01 - 0.3	0.5 - 3.2 0.04 - 0.5	0.7 - 2.9 0.04 - 0.4	No estimate	No estimate

- ε_{f1} = flow porosity (eq. 14)
- ε_{f2} = flow porosity (eq. 17)
- ε_{f3} = flow porosity (eq. 18) (First line = SDM network, 2nd line = RCM)

Table 3.12 Summary of estimated specific surfaces (KTH/SKB, KTH/SKI, BRGM/ITASCA/ANDRA)

Tracer	Eosin B	Uranine	Elbenyl	Eosin y	Iodide
KTH/SKB Project team					
Injection Distance (m)	19	32	10	18	29
Specific surface (m^{-1})	14-27	5.1-12	15-20	4.7-7.7	0.49-11
KTH/SKI Project team					
Specific surface (m^{-1}) $a_{r.ct}$	Global estimate Channel type 1 : $7.4.10^{-4} \pm 7.1.10^{-4}$ Channel type 2 : 0.15 ± 0.14 Channel type 3 : 2.7 ± 2.6				
BRGM/ITASCA/ANDRA Project team					
Specific surface (m^{-1}) a_{geom}	2.9 - 6.2 0.1 - 0.4	3.0 - 6.9 0.3 - 0.6	3.4 - 7.4 0.3 - 0.7	3.9 - 8.6 0.3- 0.9	No estimate

- $a_{r.ct}$ = estimate from the continuum model (eq. 20)
- a_{geom} = geometrical estimate (eq. 19)

First line = SDM network, 2nd line = RCM network.

Table 3.13 Calculated fractional dimensions of the flow paths, between the injection sites and sheets. Each sheet yielded arrival times for five tracers. (INTERA/AEA/NIREX)

Sheet	Dimension, D	Cor	Sheet	Dimension, D	Cor
66:3+1	1.3642	0.698	64:31+2	1.3404	0.749
62:33+1	0.90126	0.565	60:33+2	1.1353	0.744
110:29-1	0.95826	0.565	108:29+0	1.1676	0.625
65:29+1	1.1885	0.681	67:29+2	1.0437	0.613
106:27-1	0.75843	0.506	68:27+1	1.4777	0.682
69:27+2	1.2779	0.633	70:27+2.5	0.69144	0.544

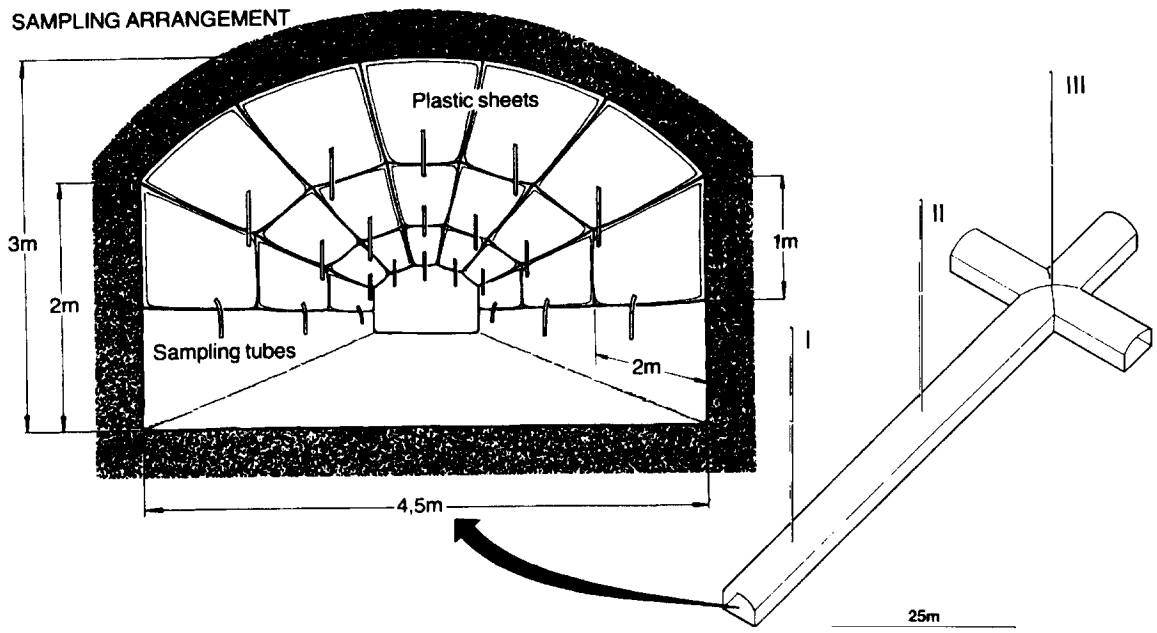

Figure 3.1 Lay-out of experimental 3-D Drift at Stripa and sampling arrangement.

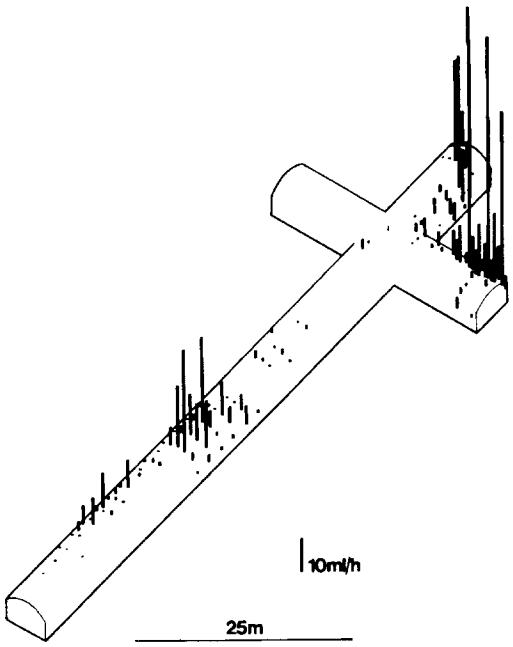

Figure 3.2 Water inflow rates into the test site before drilling of the injection holes.

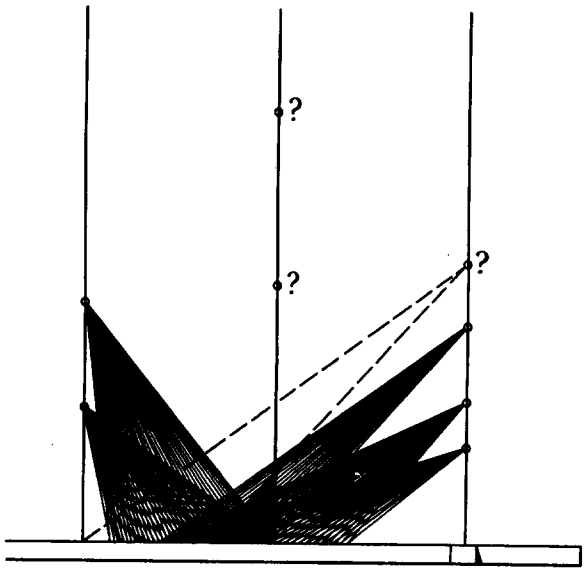

Figure 3.3 Areas in the test site where the different tracers have emerged.

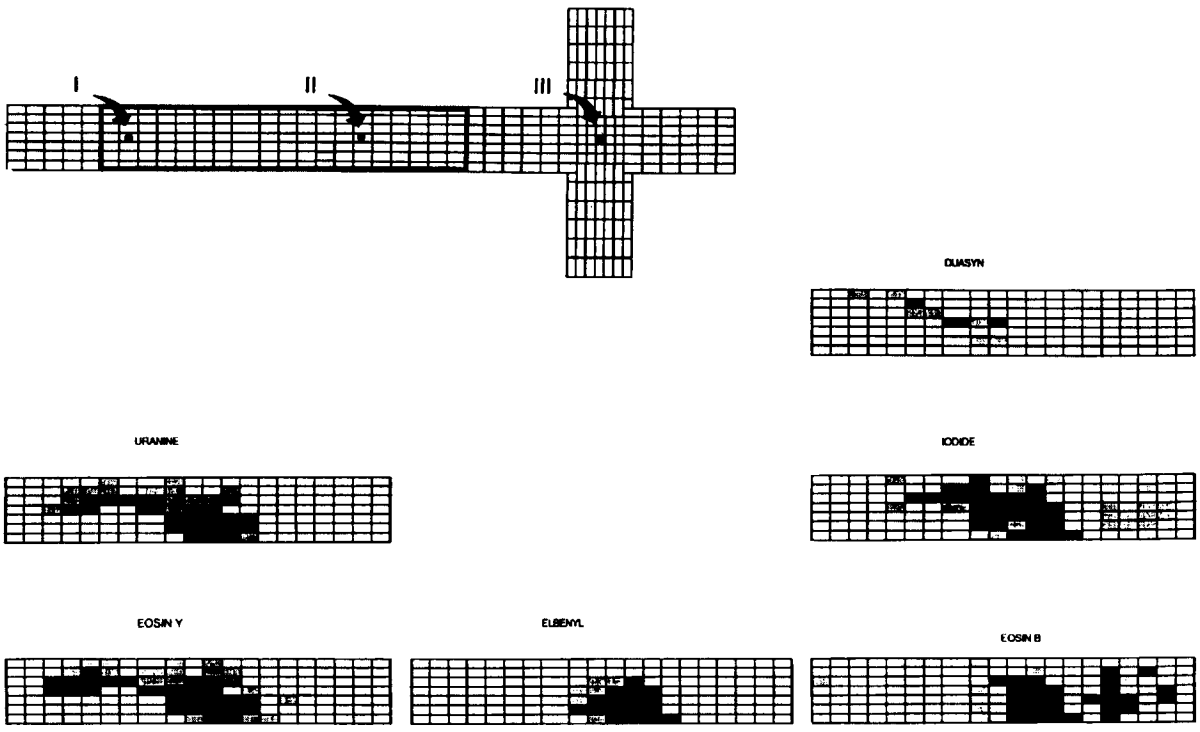

Figure 3.4 Tracer occurrence in the main drift for the individual tracers.

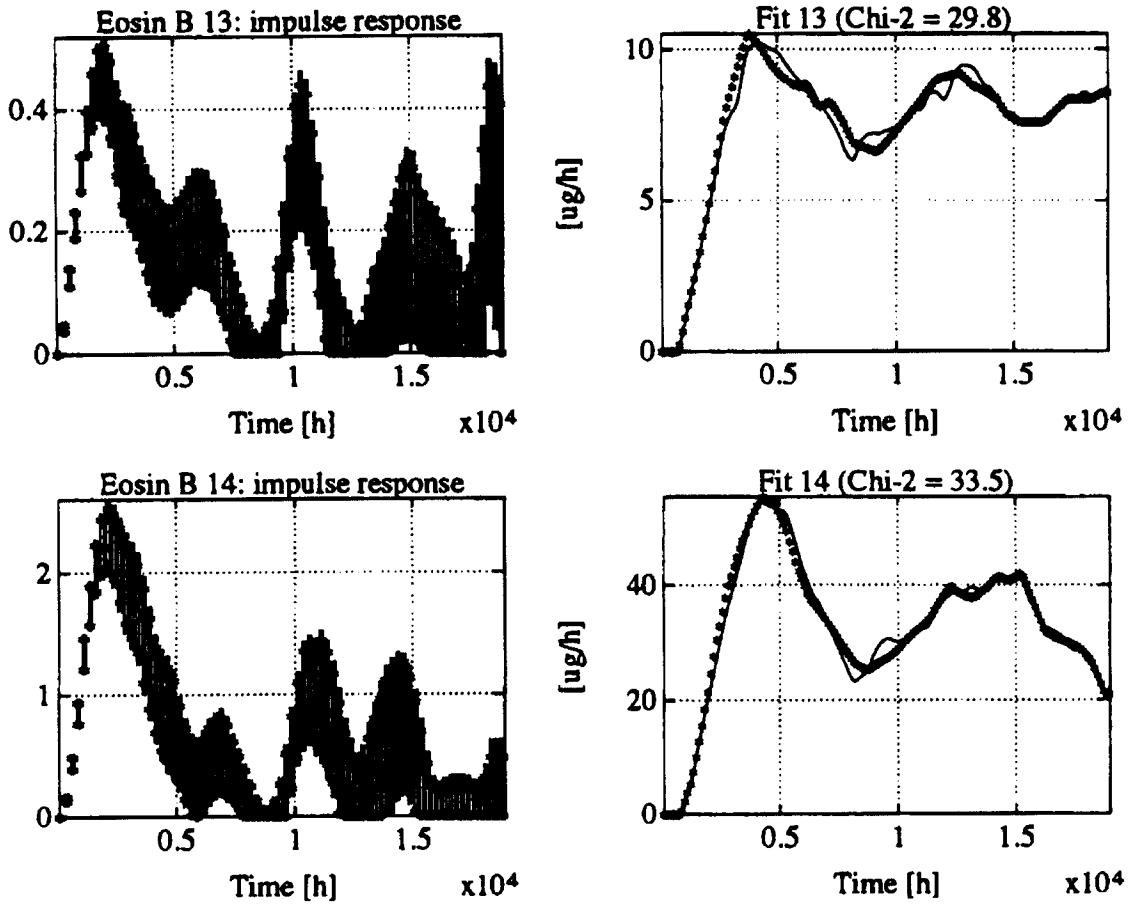

Figure 3.5 Representative results of EVE analysis method for Eosin B.(VTT/TVO)

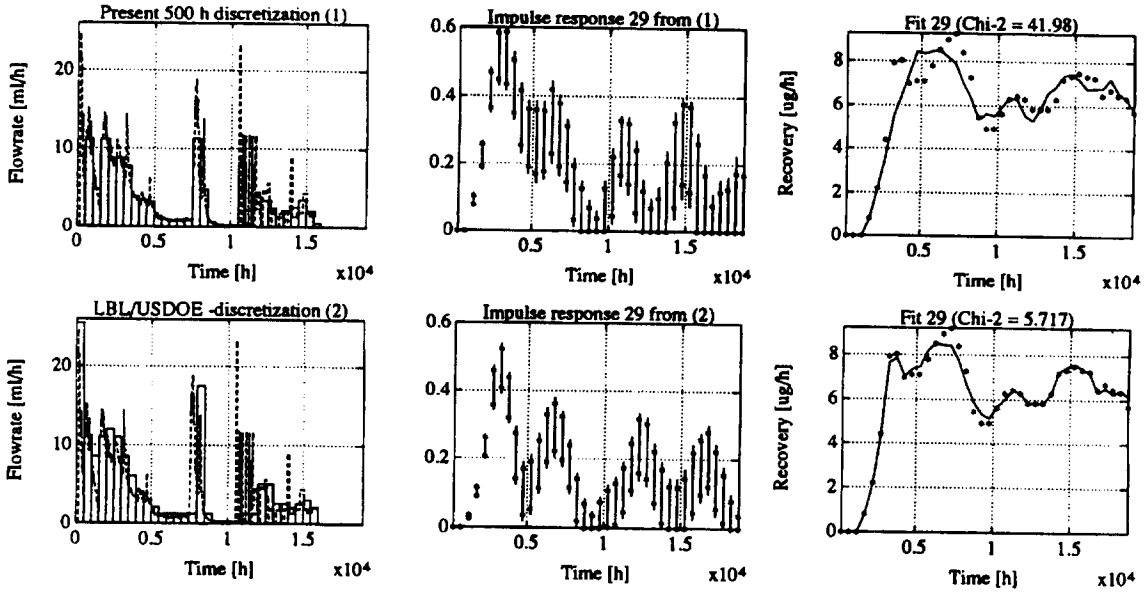

Figure 3.6 EVE analysis method influence of the injection pulse on the impulse response. Eosin b case.(VTT/TVO)

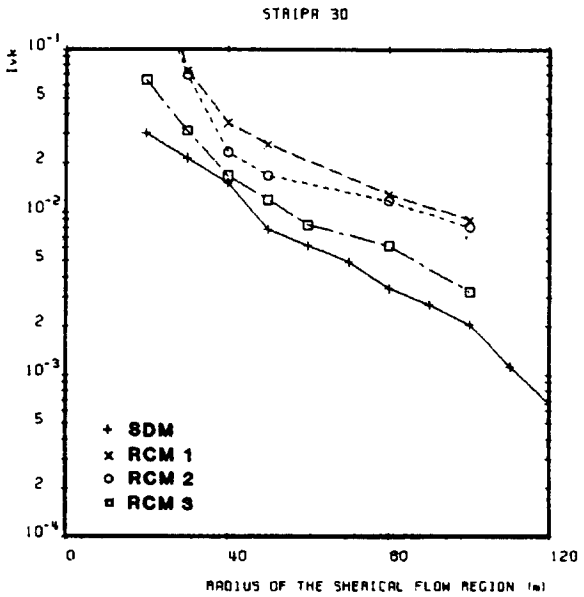

Figure 3.7 Value of the variability index for permeability, Ivk, as a function of the size of the flow domain, for the various channel networks. (BRGM/ITASCA/ANDRA).

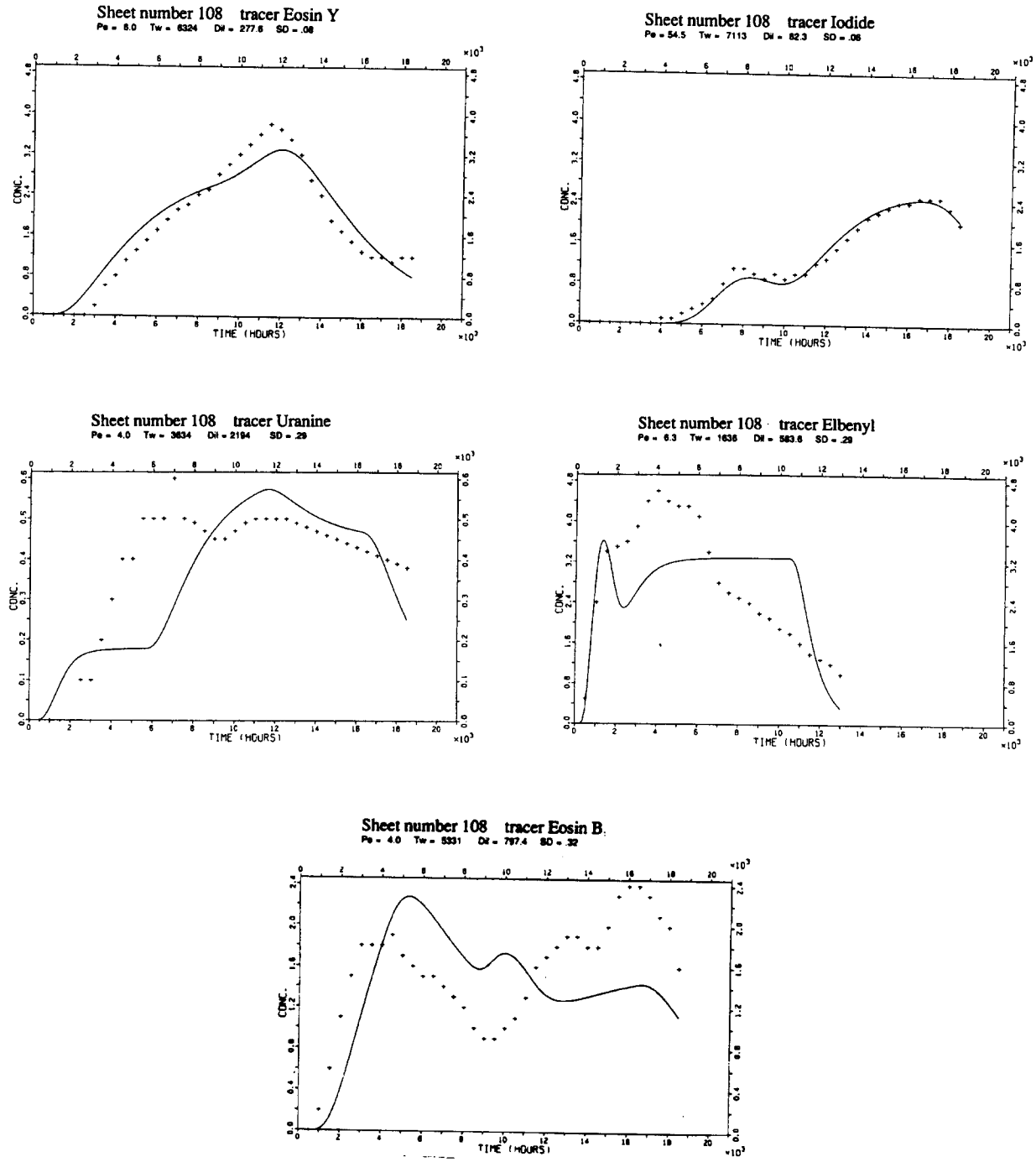

Figure 3.8 Breakthrough curves in sheet 108. The solid lines give fitted curves by the AD model and the crosses show selected experimental points. (KTH/SKB).

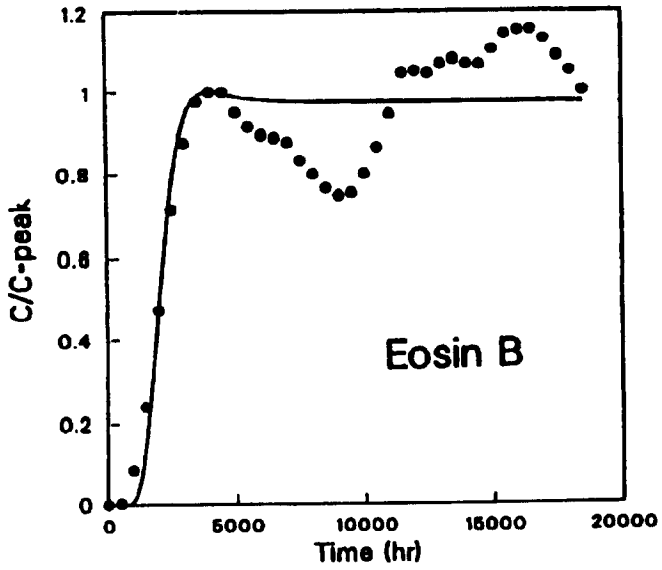

Figure 3.9 Example of a first peak fit to the early break through behaviour (LBL/USDOE)

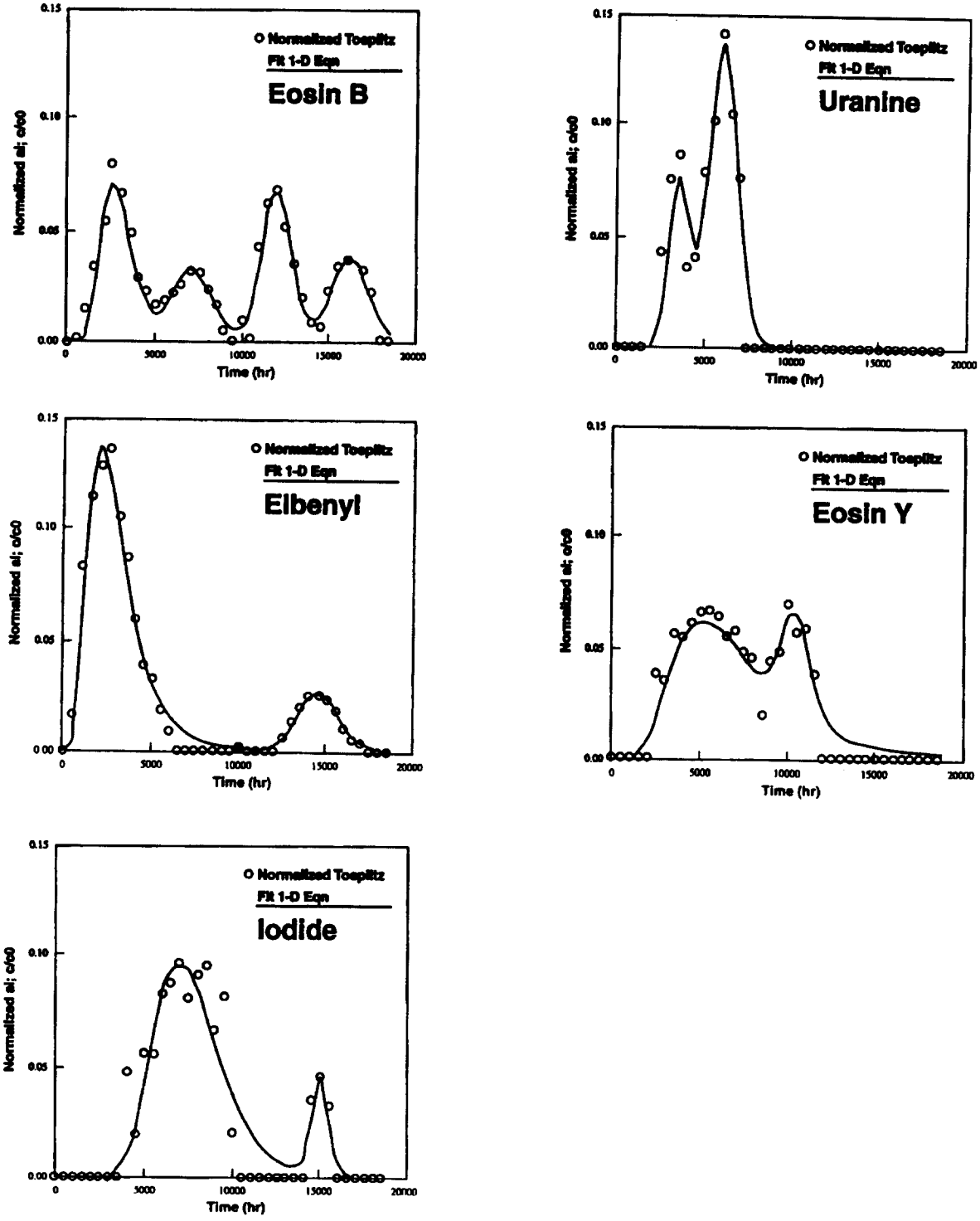

Figure 3.10 Normalised breakthrough curves derived from the Toeplitz analysis, together with subsequent fits using one-dimensional, pulse injections, solutions (LBL/USDOE)

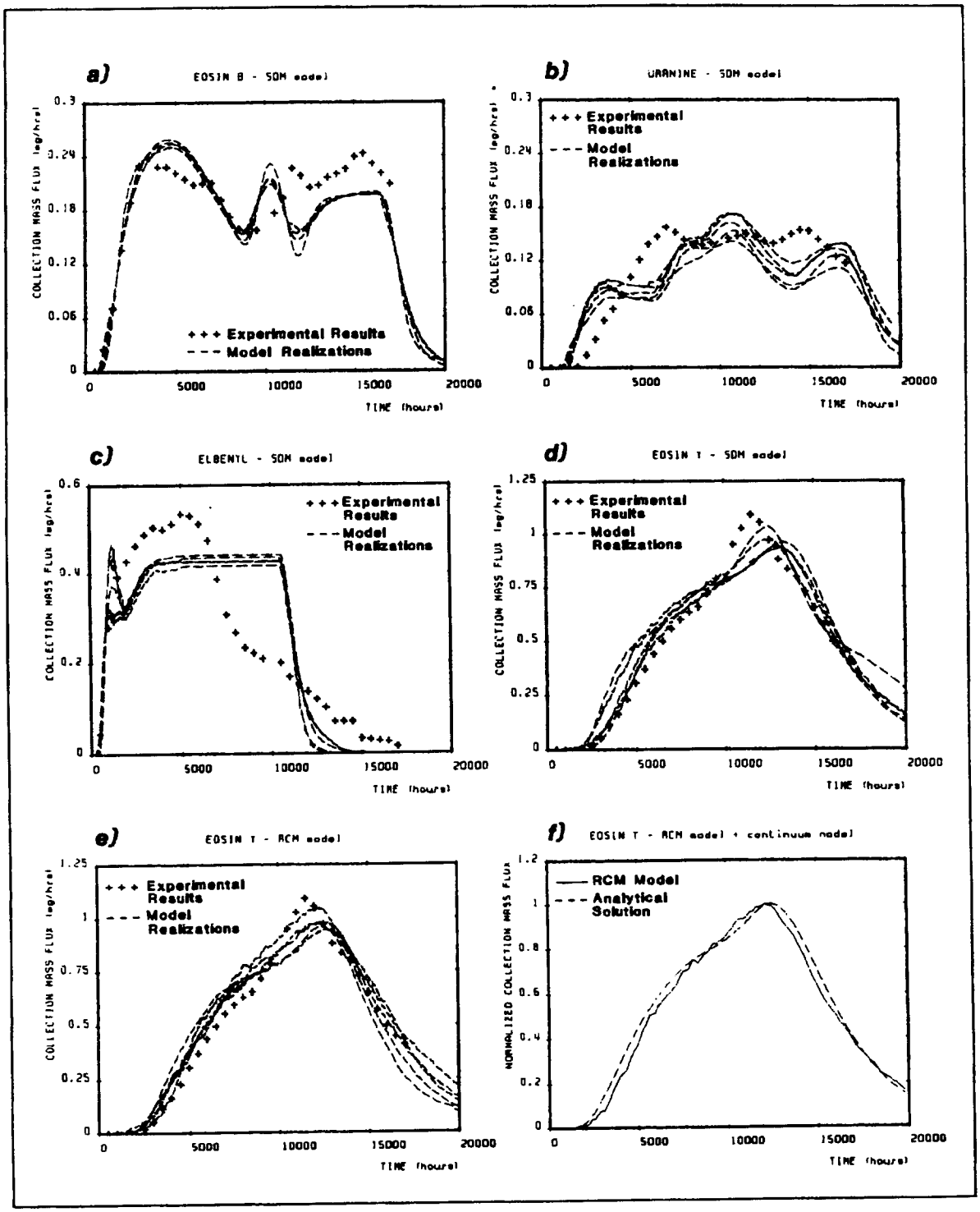

Figure 3.11 Fit of the channel network models to the mass collection rates.
a), b), c), d) = Simplified disk model e)= Random Channel model
f) fit of the analytical solution (BRGM/ITASCA/ANDRA)

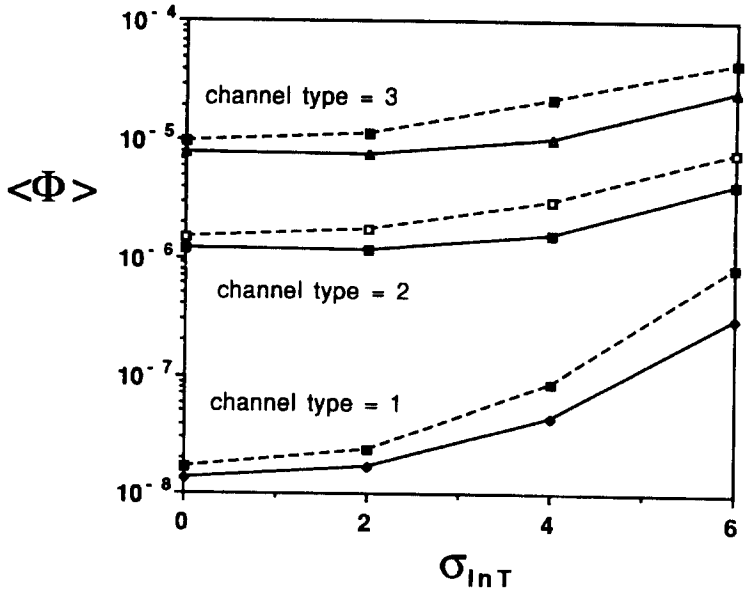

Figure 3.12 Ensemble mean of simulated porosity as function of the natural log standard deviation of the channel conductances, σ_c. Solid curves represent direct estimates determined from simulations in the discrete model and dashed curves represent values determined by fitting a continuum model to the simulated breakthrough curves (KTH/SKI).

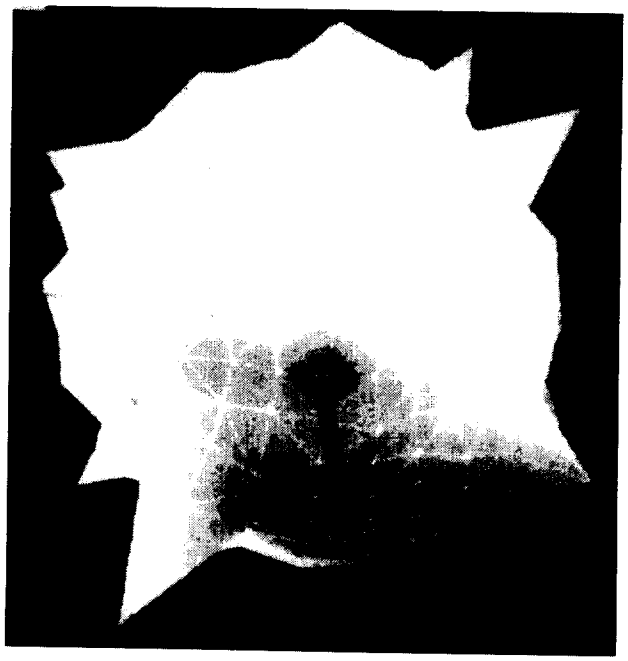

Figure 3.13 3D view of "directional hydraulic effective porosity". Simplified Disc model. (BRGM/ITASCA/ANDRA)

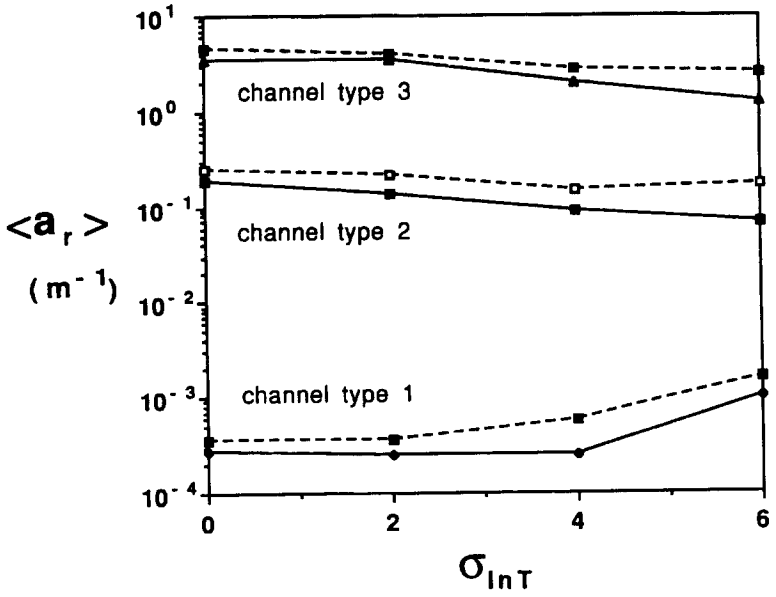

Figure 3.14 Ensemble mean of estimated specific fracture surface area as function of the natural log standard deviation of the channel conductances, σ_c. Solid curves represent direct estimates determined from simulations in the discrete model and dashed curves represent values determined by fitting a continuum model to the simulated breakthrough curves. (KTH/SKI)

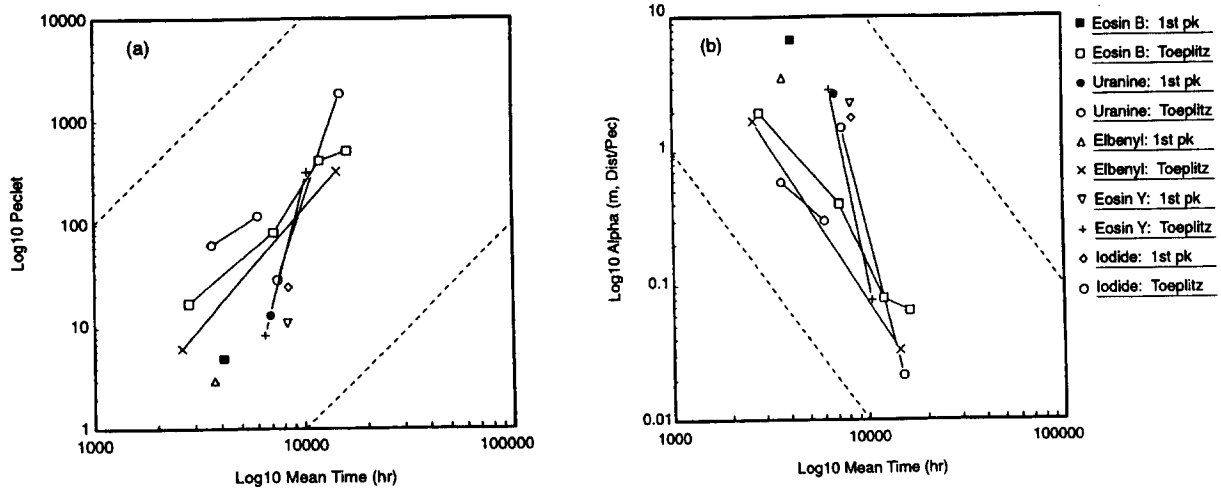

Figure 3.15 Log-log plot of Peclet numbers and Dispersion length versus mean arrival time of each channel. Points representing channels for the same tracer are jointed by solid lines (LBL/USDOE).

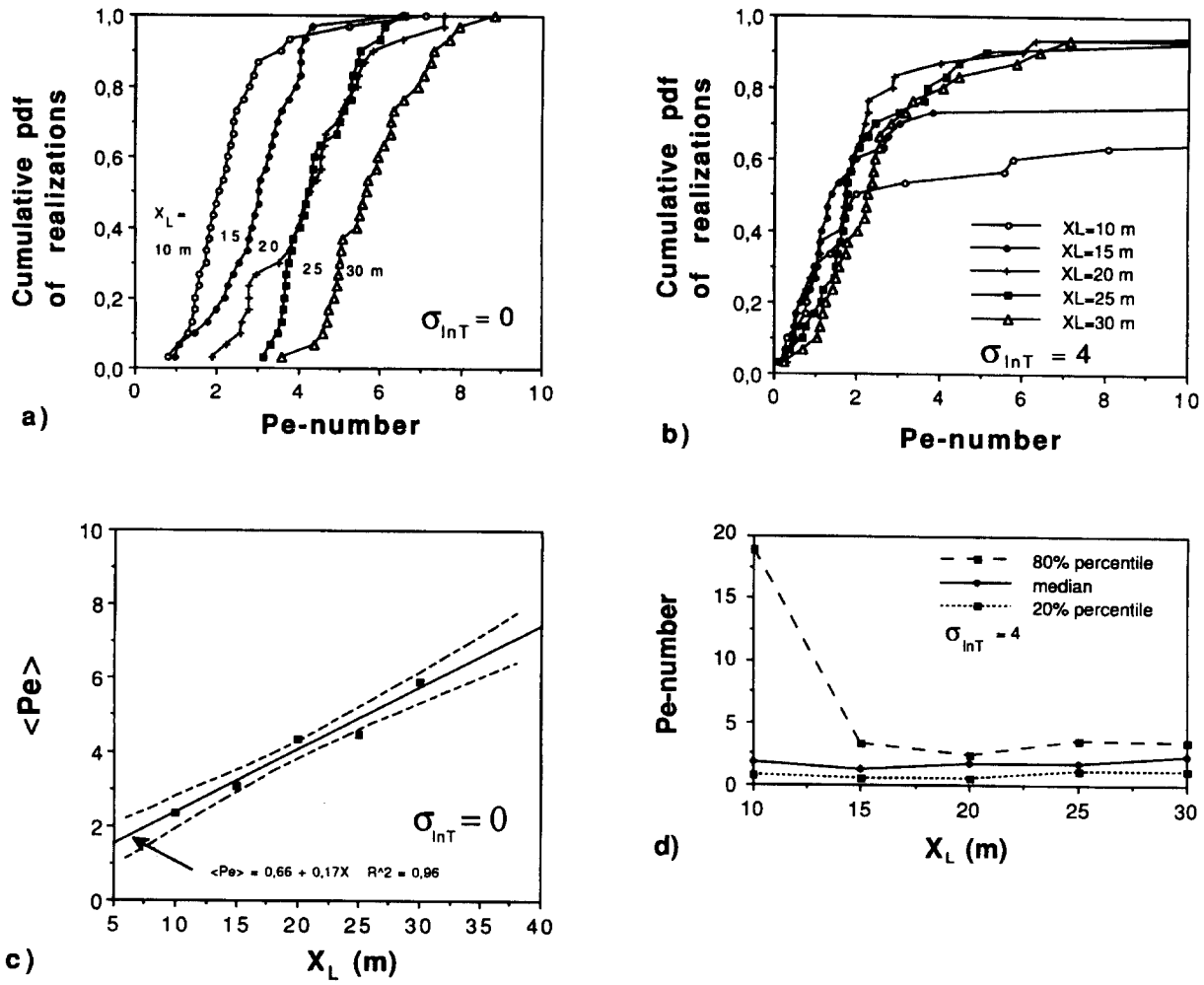

Figure 3.16 Peclet numbers evaluated by fitting a continuum model to breakthrough curves simulated in the DISCFRAC channel network model, a) and b): distribution of estimated Peclet numbers in individual network realisations with natural log standard deviation of channel conductances, σ_c equal to 0 and 4, respectively, and c) and d): ensemble mean Peclet number as a function of transport distance for σ_c equal to 0 and 4, respectively. (KTH/SKI)

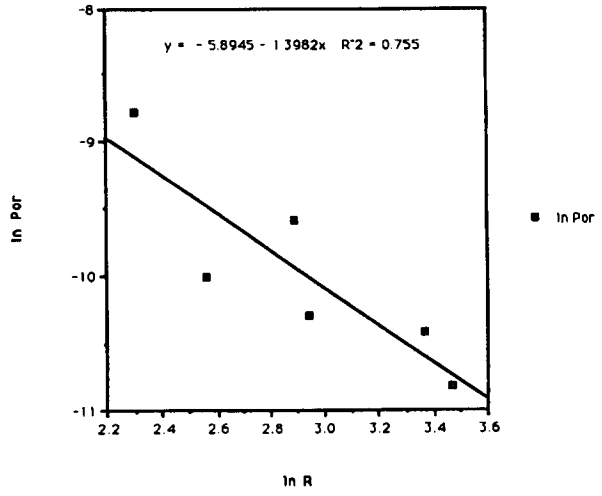

Figure 3.17 Porosity variation with travel distance (INTERA/AEA/NIREX)

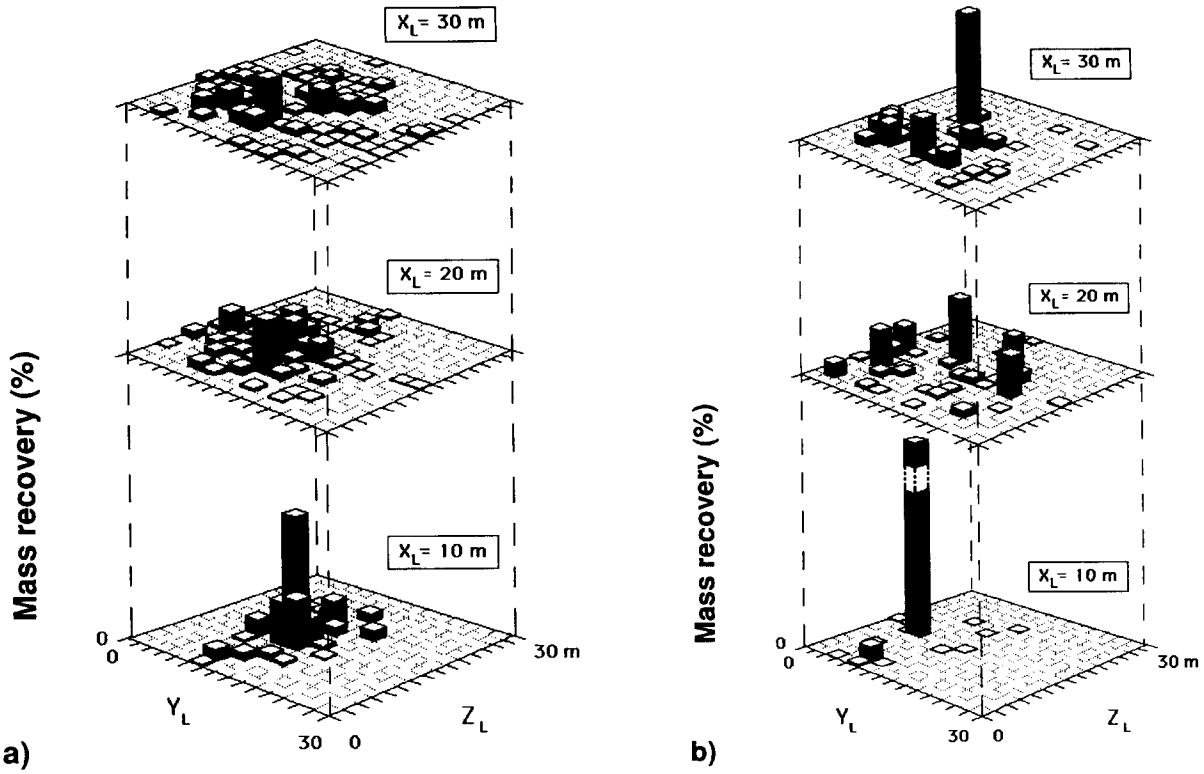

Figure 3.18 Simulated tracer recovery in a fracture network realization with $\sigma_c = 0$ (a) and $\sigma_c = 4$ (b), for three domain lengths. Each bar represents the recovery in a 4 m^2 sampling area on the outflow face of the simulated domain (KTH/SKI).

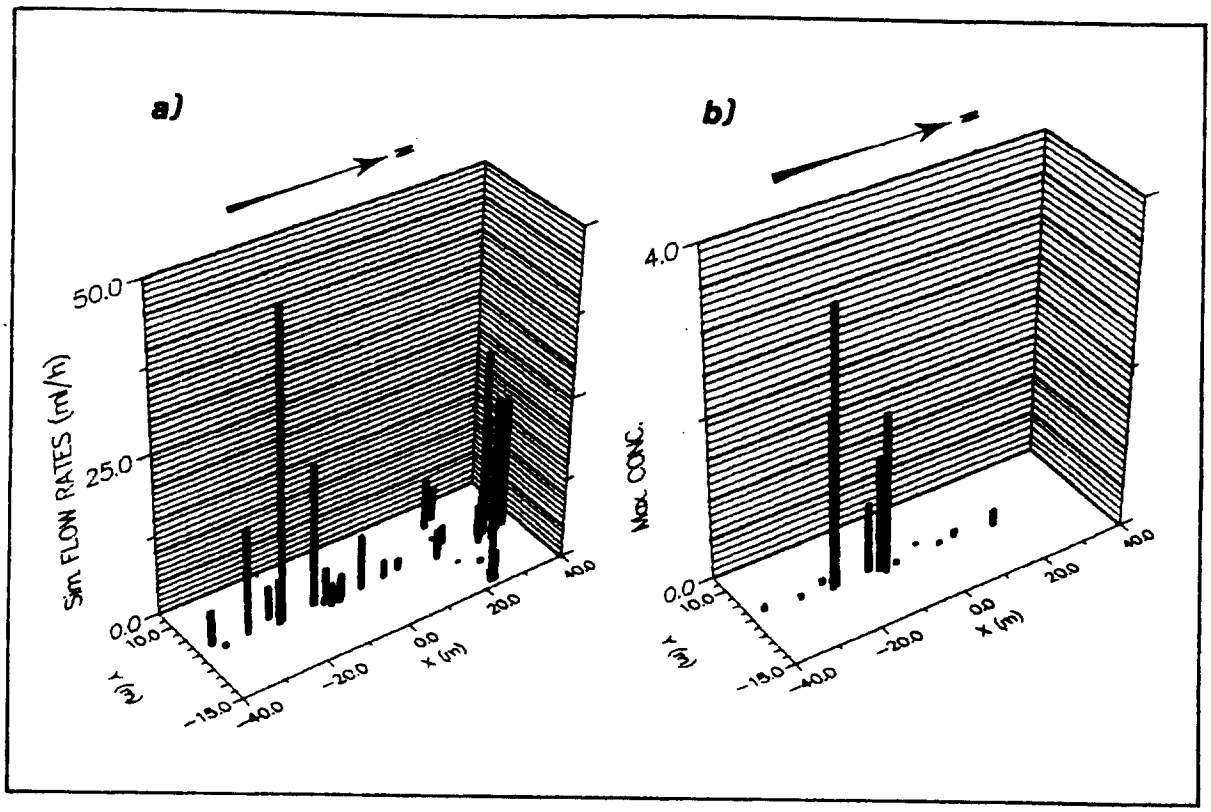

Figure 3.19 Spatial variability of simulated inflow rates (a) and maximum concentrations (b) for one realization. Elbenyl Case. SDM model. (BRGM/ITASCA/ANDRA)

4 The WIPP-2 Test Case

4.1 Introduction

The WIPP-2 test case is based on data from the site investigations carried out at the Waste Isolation Pilot Plant (WIPP) in New Mexico, USA (see Figure 4.1). The site has been chosen as a potential location for a repository for the disposal of radioactive waste, and extensive investigations have been carried out in the region of the site. (Data are available from more than 60 boreholes at 41 locations.) The site investigations mainly focused on data relating to groundwater flow and transport in the Culebra Dolomite. This is a fairly thin, laterally extensive formation, which is considered to form the main pathway for potential transport of radionuclides off the site by groundwater, if there was an accidental borehole intrusion into the repository itself.

The data from the site investigations were made available to the INTRAVAL project for use within the project as the basis of a test case. This provided a very valuable opportunity for the INTRAVAL participants to explore the issues involved in validation of field-scale models of groundwater flow and transport using the sort of data that would result from a typical investigation of a repository site.

The WIPP-2 test case was studied within INTRAVAL by five project teams:
(i) AEA Technology, UK on behalf of UK Nirex Ltd (AEA);
(ii) Universidad Politécnica de Valencia, Spain (UPV);
(iii) Atomic Energy Control Board of Canada (AECB);
(iv) Bundesanstalt für Geowissenschaften und Rohstoffe, Germany (BGR);
(v) Sandia National Laboratory, USA (SNL)

The studies of the project teams are outlined below (see subsections 4.4 and 4.5). More detail on some of the studies is given in project team reports [*Cliffe, Jackson and Impey, 1995; Metcalfe, 1993; Kröhn and Schelkes, 1995*]. The studies addressed:
(i) the issues involved in treating the heterogeneity of the transmissivity of the Culebra Dolomite;
(ii) the choice of conceptual model;
(iii) the possible utility of bounding calculations.

During INTRAVAL, the project teams were able to interact with the WIPP project itself. Presentations on the work being undertaken within the WIPP project were made to the INTRAVAL participants. The INTRAVAL participants were given the opportunity to comment on proposals for a new set of experiments at the site (see subsection 4.6). Presentations of the work undertaken within INTRAVAL were made to the WIPP Geostatistics eXpert Group (GXG), which is addressing the treatment of the heterogeneity of the transmissivity of the Culebra Dolomite for the WIPP project itself.

4.2 Data

A very large amount of information relating to the WIPP site has been collected during the site investigations. It was not practical, or necessary, to distribute all of this to the INTRAVAL participants. Instead, at the start of Phase 2, a brief report that outlined the main features of the hydrogeology of the WIPP site and gave a list of available reports was distributed. Specific reports were then supplied on request to those project teams that tackled the test case. Most of the data used in the INTRAVAL studies are given in *LaVenue et al.* [*1990*], which presents the results of deterministic modelling of flow in the Culebra Dolomite, and in *Cauffman et al.* [*1990*].

The major features of the geology and hydrogeology of the WIPP site are outlined below.

4.2.1 Geology

The WIPP site is in south east New Mexico, USA (see Figure 4.1). The topography of the region is shown in Figure 4.2. The site is in the geologic region known as the Delaware Basin. The stratigraphy of the rocks near the site is shown in Figure 4.3. The proposed WIPP repository location is in the Salado Formation, which is composed of thick beds of halite interbedded with anhydrite, polyhalite, dolomite and clay. The Salado Formation is overlain by the Rustler Formation, which has been divided into five members based on lithology:

(i) an unnamed lower member composed of massive siltstone overlain by beds of halite, siltstone and anhydrite;
(ii) the Culebra Dolomite Member;
(iii) the Tamarisk Member composed of two zones of massive to bedded anhydrite separated by a sequence of halite and siltstone;
(iv) the Magenta Dolomite Member;
(v) the Forty-Niner Member composed of two anhydrite zones separated by a silty-halite unit.

The Rustler Formation is overlain by the Upper Permian Dewey Lake Red Beds, a series of interbedded siltstones and sandstones, with prevalent vertical fractures that are generally filled with gypsum. In the eastern portion of the WIPP site, the Dewey Lake Red Beds are unconformably overlain by the Dockum Group, a Triassic clastic sequence deposited in a transitional complex of fluvial, deltaic and lacustrine environments. Overlying the Dockum Group, where present, and the Dewey Lake Red Beds is a sequence of poorly sorted continental deposits of Quaternary age, which are overlain by Holocene surficial deposits.

The Culebra Dolomite is considered to be the most transmissive hydrogeological unit in the area. It is a relatively thin layer, about 8m thick, that extends for many kilometres. It is highly fractured. It is generally considered that the fracturing is associated with halite dissolution within the upper Salado Formation and the Rustler formation, which led to displacement and fracturing of the overlying rocks. The typical spacing observed between the fractures in the Culebra Dolomite is about 10cm, although the spacing between fractures carrying flow has been inferred from tracer tests to be about 50cm. It was considered that the degree of fracturing was such that

a continuum porous-medium treatment of groundwater flow in the Culebra Dolomite would be a very good representation on the scale of interest of kilometres.

4.2.2 Hydrogeological data

The studies undertaken within INTRAVAL mainly addressed the hydrogeology of the Culebra Dolomite. The available information included transmissivities, steady-state heads and groundwater salinity, which are discussed below. Other data were available, including the transient responses of the heads at various boreholes to numerous well tests and to the construction of various shafts, and the inflows to the shafts during construction. The results of convergent-flow tracer tests at H-3, H-4, H-6 and H-11, and dipole tracer tests at H-2 and H-6 were also available. (The positions of these wells are given in Table 4.1.)

4.2.2.1 Transmissivity

The transmissivity of the Culebra Dolomite has been measured at 41 different locations (shown on Figure 4.2). *LaVenue et al.* [*1990*] reviewed the data and produced a list of recommended values, which are given in Table 4.1. For convenience in visualising the data, Figure 4.4 shows the distribution of transmissivity obtained by interpolating the data (by kriging using a linear generalised covariance function (see *Journel and Huijbregts* [*1978*]). This Figure is only presented as an aid to visualisation and is expected only approximately to represent the actual distribution of transmissivity within the Culebra. The transmissivity exhibits considerable variability. The values in Table 4.1 cover a range of nearly seven and a half orders of magnitude. Over the whole region, the data appear to exhibit a pronounced trend with high values to the west and low values to the east. This seems to be correlated with halite dissolution, with high transmissivities occurring in regions where halite is not present in the Rustler Formation. However, the trend in the data appears to be reversed in the immediate vicinity of the site.

*Table 4.1 Recommended measured values of transmissivity for the Culebra Dolomite (from LaVenue et al. [1990]). The coordinates are given in the Universal Transverse Mercator system [Gonzales, 1989]. The quoted uncertainty corresponds to the estimated standard deviation in the logarithm to base 10 of the transmissivity. (Wells marked * lie outside the domain used in the modelling undertaken by LaVenue et al. [1990], and in the modelling undertaken by the AEA, UPV and AECB project teams, which is reported here.)*

Well name	Coordinates (m)		Transmissivity (m^2s^{-1})	Uncertainty
H-1	613423	3581684	$9.4\ 10^{-7}$	0.50
H-2	612660	3581652	$6.3\ 10^{-7}$	0.25
H-3	613714	3580892	$2.5\ 10^{-6}$	0.25
H-4	612398	3578484	$1.0\ 10^{-6}$	0.25
H-5	616888	3584793	$9.7\ 10^{-8}$	0.25
H-6	610595	3583991	$3.6\ 10^{-5}$	0.25
H-7	608106	3574644	$1.5\ 10^{-3}$	0.25
H-8*	608668	3563553	$8.8\ 10^{-6}$	0.25
H-9	613974	3568252	$1.3\ 10^{-4}$	0.25
H-10	622967	3572458	$7.5\ 10^{-8}$	0.50
H-11	615341	3579124	$3.1\ 10^{-5}$	0.25
H-12	617023	3575452	$1.9\ 10^{-7}$	0.50
H-14	612341	3580354	$3.3\ 10^{-7}$	0.50
H-15	615315	3581859	$1.3\ 10^{-7}$	0.50
H-16	613369	3582212	$7.7\ 10^{-7}$	0.50
H-17	615718	3577513	$2.3\ 10^{-7}$	0.50
H-18	612264	3583166	$1.7\ 10^{-6}$	0.25
DOE-1	615203	3580333	$1.2\ 10^{-5}$	0.25
DOE-2	613683	3585294	$9.6\ 10^{-5}$	0.25
P-14	609084	3581976	$2.8\ 10^{-4}$	0.41
P-15	610624	3578747	$9.2\ 10^{-8}$	0.50
P-17	613926	3577466	$1.1\ 10^{-6}$	0.50
P-18	618367	3580350	$7.5\ 10^{-11}$	0.50
WIPP-12	613710	3583524	$1.1\ 10^{-7}$	0.50
WIPP-13	612644	3584247	$7.4\ 10^{-5}$	0.50
WIPP-18	613735	3583179	$3.2\ 10^{-7}$	0.50
WIPP-19	613739	3582782	$6.5\ 10^{-7}$	0.50
WIPP-21	613743	3582319	$2.7\ 10^{-7}$	0.50
WIPP-22	613739	3582653	$4.0\ 10^{-7}$	0.50
WIPP-25	606385	3584028	$2.9\ 10^{-4}$	0.25
WIPP-26	604014	3581162	$1.2\ 10^{-3}$	0.25
WIPP-27	604426	3593079	$4.3\ 10^{-4}$	0.25
WIPP-28	611266	359680	$2.1\ 10^{-5}$	0.25
WIPP-29*	596981	3578694	$1.1\ 10^{-3}$	0.25
WIPP-30	613721	3589701	$2.5\ 10^{-7}$	0.50
ERDA-9	613696	3581958	$5.1\ 10^{-7}$	0.50
CB-1	613191	3578049	$3.0\ 10^{-7}$	0.50
ENGLE	614953	3567454	$4.6\ 10^{-5}$	0.25
USGS-1	606462	3569459	$5.5\ 10^{-4}$	0.25
D-268	608702	3578877	$2.0\ 10^{-6}$	0.50
AEC-7	621126	3589381	$2.8\ 10^{-7}$	0.50

The matrix porosity of the Culebra Dolomite shows considerably less variability than the transmissivity, and lies between 0.03 and 0.33, with a central value of about 0.16.

4.2.2.2 Steady-state heads

LaVenue et al. [1990] also reviewed the measurements of groundwater head in the Culebra Dolomite, and produced a list of recommended values of steady-state equivalent freshwater heads at 36 locations. (The equivalent freshwater head corresponds to the elevation of a column of fresh water, with a density of $1 gm/cm^3$, that would give rise to the observed pressure in the groundwater in the Culebra Dolomite. Its determination requires the average fluid density in a borehole as well as the depth to the water table.) The values recommended by *LaVenue et al. [1990]* are given in Table 4.2. For convenience in visualising the data, Figure 4.5 shows the distribution of head obtained by interpolating the data (by kriging). This Figure is only presented as an aid to visualisation, and is expected only approximately to represent the actual distribution of head in the Culebra. The general pattern is that the head is high to the north and decreases to the south, corresponding to a general flow from north to south, neglecting the effects of salinity variations.

*Table 4.2 Recommended measured values of equivalent freshwater head in the Culebra Dolomite (from LaVenue et al. [1990]). The coordinates are given in the Universal Transverse Mercator system [Gonzales, 1989]. (Wells marked * lie outside the domain used in the modelling undertaken by LaVenue et al. [1990] and in the modelling undertaken by the AEA, UPV and AECB project teams reported here.)*

Well name	Coordinates (m)		Freshwater head (m)	Uncertainty (m)
H-1	613423	3581684	923.3	+2.0/-2.0
H-2	612660	3581652	923.1	+1.8/-0.1
H-3	613714	3580892	917.1	+1.9/-0.1
H-4	612398	3578484	912.8	+0.6/-0.6
H-5	616888	3584793	934.0	+1.4/-1.4
H-6	610595	3583991	932.6	+1.0/-1.0
H-7	608106	3574644	912.5	+0.5/-0.1
H-8*	608668	3563553	912.1	+0.6/-0.1
H-9	613974	3568252	907.6	+1.2/-0.1
H-10	622967	3572458	921.4	+2.2/-2.2
H-11	615341	3579124	913.1	+1.5/-1.0
H-12	617023	3575452	913.7	+1.2/-1.3
H-14	612341	3580354	915.2	+0.7/-0.1
H-15	615315	3581859	915.7	+2.8/-0.1
H-16	613369	3582212	-	-
H-17	615718	3577513	911.0	+0.9/-0.9
H-18	612264	3583166	932.1	+1.5/-1.1
DOE-1	615203	3580333	914.2	+2.6/-2.2
DOE-2	613683	3585294	935.3	+1.5/-1.5
P-14	609084	3581976	926.9	+0.9/-0.9
P-15	610624	3578747	916.8	+0.8/-0.8
P-17	613926	3577466	911.6	+0.7/-0.7
P-18	618367	3580350	-	-
WIPP-12	613710	3583524	931.5	+1.3/-0.1
WIPP-13	612644	3584247	934.0	+1.2/-1.3
WIPP-18	613735	3583179	930.0	+1.2/-1.2
WIPP-19	613739	3582782	-	-
WIPP-21	613743	3582319	-	-
WIPP-22	613739	3582653	-	-
WIPP-25	606385	3584028	928.7	+1.0/-1.0
WIPP-26	604014	3581162	919.3	+0.4/-0.1
WIPP-27	604426	3593079	938.1	+0.7/-0.7
WIPP-28	611266	3594680	937.2	+0.9/-1.2
WIPP-29*	596981	3578694	905.3	+0.3/-0.2
WIPP-30	613721	3589701	935.3	+0.9/-1.3
ERDA-9	613696	3581958	-	-
CB-1	613191	3578049	911.6	+0.7/-0.6
ENGLE	614953	3567454	-	-
USGS-1	606462	3569459	909.7	+0.4/-0.1
USGS-4	605841	3569887	909.7	+0.1/-0.1
USGS-8	605879	3569888	911.1	+0.1/-0.1
D-268	608702	3578877	915.0	+0.4/-0.1
AEC-7	621126	3589381	931.6	+2.3/-2.3

4.2.2.3 Formation fluid density

LaVenue et al. [1990] also reviewed the available data for the formation fluid density and produced a list of recommended values at 31 locations. The recommended values are listed in Table 4.3. For the purpose of visualising the data, Figure 4.6 shows the distribution of density obtained by interpolating the data (by kriging). This Figure is only presented as an aid to visualisation and is expected only approximately to represent the actual distribution of formation fluid density in the Culebra.

*Table 4.3 Recommended measured values of formation fluid density in the Culebra Dolomite (from LaVenue et al. [1990]). The coordinates are given in the Universal Transverse Mercator system [Gonzales, 1989]. (Wells marked * lie outside the domain used in the modelling undertaken by LaVenue et al. [1990] and in the modelling undertaken by the AEA, UPV and AECB project teams reported here.)*

Well name	Coordinates (m)		Formation fluid density (g/cm^3)
H-1	613423	3581684	1.022
H-2	612660	3581652	1.006
H-3	613714	3580892	1.035
H-4	612398	3578484	1.014
H-5	616888	3584793	1.102
H-6	610595	3583991	1.038
H-7b	608106	3574644	0.999
H-8b*	608668	3563553	1.000
H-9b	613974	3568252	1.000
H-10b	622967	3572458	1.047
H-11	615341	3579124	1.078
H-12	617023	3575452	1.095
H-14	612341	3580354	1.010
H-15	615315	3581859	1.154
H-16	613369	3582212	-
H-17	615718	3577513	1.100
H-18	612264	3583166	1.017
DOE-1	615203	3580333	1.088
DOE-2	613683	3585294	1.041
P-14	609084	3581976	1.018
P-15	610624	3578747	1.015
P-17	613926	3577466	1.061
P-18	618367	3580350	-
WIPP-12	613710	3583524	-
WIPP-13	612644	3584247	1.046
WIPP-18	613735	3583179	-
WIPP-19	613739	3582782	1.059
WIPP-21	613743	3582319	-
WIPP-22	613739	3582653	-
WIPP-25	606385	3584028	1.009
WIPP-26	604014	3581162	1.009
WIPP-27	604426	3593079	-
WIPP-28	611266	3594680	1.032
WIPP-29*	596981	3578694	-
WIPP-30	613721	3589701	1.018
ERDA-9	613696	3581958	-
CB-1	613191	3578049	-
ENGLE	614953	3567454	1.001
USGS-1	606462	3569459	1.000
USGS-4	605841	3569887	1.000
USGS-8	605879	3569888	1.000
D-268	608702	3578877	-
AEC-7	621126	3589381	-

4.3 Issues

This test case provided an opportunity for the INTRAVAL participants to address many important issues relating to groundwater flow and transport models for use in repository performance assessments on the basis of real, rather than synthetic, data. Modelling issues that could have been considered are:

(i) the treatment of heterogeneity in transmissivity;
(ii) how to condition stochastic models on head data, that is how to ensure that the calculated head for each realization matches the measured heads;
(iii) quantification of the uncertainty in travel time resulting from heterogeneity;
(iv) the use of different conceptual models;
(v) the use of three-dimensional or two dimensional models;
(vi) the effects of density variations due to variations in salinity;
(vii) what the appropriate boundary conditions are, and the effects of the boundary conditions;
(viii) the use of geologic information;
(ix) the use of geochemical information;
(x) the identification of processes and parameters critical to repository performance;
(xi) the determination of the extent to which processes and parameters need to be characterized to demonstrate safety;

and one specific validation issue that could have been considered is the validation of stochastic models. Of course, not all of these issues could be explored in full within the limits of budget and time imposed on the INTRAVAL project teams. Some of the issues are discussed in more detail below.

4.3.1 Stochastic models

One of the most important aspects of the test case was the impetus it provided towards the study within INTRAVAL of stochastic models for the treatment of heterogeneity. As discussed in subsection 4.2.2.1, the transmissivity of the Culebra Dolomite varies considerably from point to point. One effect of heterogeneity that is of particular importance in a performance assessment for a repository is that it leads to uncertainty in quantities of interest, such as the groundwater travel time from a specified point. The uncertainty arises because of ignorance as to the precise variation of the hydrogeological properties between the points at which they have been measured.

At present the generally-agreed approach to dealing explicitly with heterogeneity is to use stochastic models [*de Marsily, 1985*]. The basic idea of these is that the spatial variation of the properties of interest, which results from the vagaries of the natural process that have acted on the rocks over the millions of years since their formation, can be effectively treated as random. (Of course, the heterogeneity is not really random, but it can be treated as if it was.) Each hydrogeological property (for example transmissivity) is regarded as one realization of a random spatial process from an ensemble of such realizations that have a statistical distribution deduced from the observations.

The uncertainties in the quantities of interest are then determined from the range of behaviour across the ensemble of realizations. In practice this is determined numerically by Monte-Carlo techniques. Many realizations are generated numerically by some suitable technique (for example, the Turning Bands method [*Mantoglou and Wilson, 1982*]), the quantities of interest are computed (numerically) for each realization, and then suitable measures of the associated uncertainties, such as the mean and variance, are computed.

Several issues arise in this, namely:

(i) What sort of stochastic model should be used? In particular, are Gaussian models, in which the properties are treated as (or as derived from) multivariate normal distributions, adequate, or should non-Gaussian models be considered? Gaussian models have several practical advantages, but effectively imply that regions with higher (or lower) than average transmissivities are not connected over long distances, which may not be a good representation of reality;

(ii) How should the parameters of the statistical model be estimated?

(iii) How should the realizations be generated numerically?

(iv) How can data be taken into account best? In particular what is the best way to use data on quantities such as the groundwater head that depend on the underlying (stochastic) properties such as transmissivity, but are not simply related to the underlying quantities?

(v) How can stochastic models be validated?

(vi) How well does the transmissivity field need to be characterized in order to demonstrate the safety of a proposed disposal facility?

(vii) What are the limits on our ability to characterize the transmissivity field?

These issues are discussed further in the summaries of the studies of the various project teams given below.

It is perhaps worth noting that, in some cases, it may not be necessary to undertake calculations in which the effects of heterogeneity are explicitly considered, because it may be possible, for example, to demonstrate that a proposed disposal facility is safe using bounding 'worst-case' calculations.

4.3.2 Conceptual models

Other important issues are those relating to the choice of conceptual model. In particular

(i) Is a two-dimensional model of groundwater flow in the Culebra Dolomite adequate, or should a three-dimensional model be used, or might an intermediate model that took account of leakage between the Culebra and overlying rocks be adequate? The groundwater flow system is three-dimensional in nature. However, two-dimensional models require fewer computational resources than three-dimensional models that represent the same level of detail, and may represent the system adequately.

(ii) Is a steady-state model adequate, or should a transient model be used? The groundwater flow system will change with time as a result of, for example, changing climate, which will alter the recharge, or as a result of the coupling of the groundwater flow with

transport of salt. However, a steady-state model may represent adequately those aspects of the flow of interest.

(iii) Is a continuum porous-medium model adequate, or should fracture-network models be used?

(iv) Is a fresh-water model adequate or should a model that takes account of coupled transport of salinity by groundwater and the effect of density variations on the groundwater flow be used?

(v) What is the appropriate domain to represent the system?

(vi) What are appropriate initial and boundary conditions? If transient models are used, how do the boundary conditions change with time?

(vii) What are the inaccuracies introduced by the various possible approximations indicated above?

4.4 Methods and Models

In this section the methods used by the various project teams to study the test case are outlined. All the models used were continuum porous-medium models. First a brief overview of stochastic modelling is presented, since much of the work on this test case addressed issues relating to stochastic models.

4.4.1 Stochastic models

In the stochastic models used by the project teams the logarithm Z of the transmissivity T was taken as the underlying random process. Both the AEA and UPV project teams used Gaussian models; in addition, the UPV project team considered the adequacy of Gaussian models, although they did not undertake any actual calculations for such models. In a Gaussian model Z is taken to be a Gaussian process, that is the joint probability density function for the values of Z at any set of points is a multivariate normal distribution. The process is characterized by its first- and second-order moments: the mean and the variogram. The mean is given by

$$m(\mathbf{x}) = E[Z(\mathbf{x})] ,$$

where

$\mathbf{x}$ is position,

$E[...]$ denotes the expectation (average over the ensemble);

and the variogram is given by

$$\gamma(\mathbf{x},\mathbf{y}) = 1/2 \ \mathrm{var}((Z(\mathbf{x}) - Z(\mathbf{y}))) ,$$

where var(...) denotes the variance.

If the variance

$$\sigma^2(\mathbf{x}) = E[(Z(\mathbf{x}) - m(\mathbf{x}))^2]$$

of the field exists (and is finite) then the variogram is related to the covariance

$$C(\mathbf{x},\mathbf{y}) = E[(Z(\mathbf{x}) - m(\mathbf{x}))(Z(\mathbf{y}) - m(\mathbf{y}))]$$

by

$$\gamma(\mathbf{x},\mathbf{y}) = 1/2(\sigma^2(\mathbf{x}) + \sigma^2(\mathbf{y})) - C(\mathbf{x},\mathbf{y}) .$$

(The variogram is defined even if the variance does not exist).

In order to use stochastic models in practice, and in particular in order to infer the parameters of the stochastic model from the data it is necessary to make an assumption that relates the statistical properties of Z (over the ensemble) at different points. One assumption that is widely used is the intrinsic hypothesis that the mean exists and is independent of position, and that the variogram exists and is independent of position. It is also possible to use more general assumptions, for example that there is a trend (or drift) of a certain form, that is the mean $m(\mathbf{x})$ has a certain functional form (see subsection 4.4.2).

Once such an assumption has been made, the variogram can then be inferred from the statistics of the data. Various methods can be used. The simplest is to fit (by eye or using automated methods such as least-squares fitting) a function of a suitable form to the experimental variogram, which is obtained as follows for an isotropic stochastic model. The pairs of observations are grouped into classes based on their separation, and the average value of the square of the difference in the measured values computed for each class. The experimental variogram is the graph of these averages against the average separation for each class. If the stochastic model is not isotropic then the set of possible orientations of the separation vectors is subdivided into several angle classes, and a directional variogram is computed for each class by considering only those pairs of points whose separation lies in the angle class (see subsection 4.4.3). Methods other than fitting to the experimental variogram, such as maximum-likelihood estimation (see subsection 4.4.2), can also be used to deduce the parameters of the variogram.

Once the underlying stochastic model has been estimated, realizations of fields with the appropriate statistics can be generated by various techniques such as the Turning Bands method [*Matheron, 1973; Mantoglou and Wilson, 1982*], or sequential simulation [*Gómez-Hernández and Journel, 1993*]. The Turning Bands method can only be used to generate realizations of a Gaussian model; the sequential simulation method can also be used to generate realizations of a non-Gaussian model. The groundwater flow in each realization can then be calculated numerically by standard finite-element or finite-difference techniques, and then transport through the flow field in each realization can be calculated, for example by particle tracking. The uncertainty in quantities of interest such as the groundwater travel time can then be assessed from the range of behaviour over all the realizations considered.

The geostatistical interpolation technique of kriging [*Journel and Huijbregts, 1978*] plays a very important role in stochastic modelling. In particular the approach used by the AEA project team to condition realizations on transmissivity data [*Journel, 1974*] was based on the use of kriging. Kriging also played an important role in the approach used by the UPV project team to condition

realizations on head data. (Kriging was also used to derive the interpolated fields used in Figures 4.4, 4.5 and 4.6 to aid in visualisation of the experimental data).

The kriging interpolate is simply the Best Linear Unbiased Estimator (BLUE), that is the estimate at a point $\mathbf{x}_0$ is of the form

$$Z_0^* = \sum \lambda_i Z_i ,$$

where Z_i are the measured values at the measurement points $\mathbf{x}_i$, and the weights λ_i are chosen so that the estimate is unbiased and has minimum variance. These requirements lead to the conditions

$$\sum \lambda_i = 1 ,$$
$$\sum \lambda_j \gamma(\mathbf{x}_i - \mathbf{x}_j) + \mu = \gamma(\mathbf{x}_i - \mathbf{x}_0) ,$$

where μ is a Lagrange multiplier.

These are the equations for ordinary kriging (see [*Journel and Huijbregts, 1978*]). The basic technique can be modified in various ways. For example, other forms of kriging can be derived depending on the assumptions made about the mean (see [*Journel and Huijbregts, 1978*]), the interpolation may only use measurements within a restricted region about the interpolation point, and the technique can be extended to deal with several correlated variables (the technique of co-kriging).

4.4.2 The AEA approach and models

The AEA project team considered four different stochastic models. All the models were isotropic. The first model was a stationary model with a constant mean m and an exponential covariance

$$\omega \exp(-r/\lambda) ,$$

where
ω is the variance,
λ is a length scale,
r is separation ($r = |\mathbf{x} - \mathbf{y}|$ in the notation of subsection 4.4.1).

This covariance corresponds to a variogram

$$\gamma(r) = \omega \, (1 - e^{-r/\lambda}) .$$

The second model considered by the project team was a stationary model with a truncated power-law (fractal) variogram

$$\gamma(r) = \min(\alpha \, r^{\beta} , \omega) ;$$

the third model was a stationary model with a variogram that was pure nugget (that is, constant for non-zero separations, which corresponds to a field that is completely uncorrelated from point to point, at least on the scales considered); and the fourth model was a model with an exponential covariance and a linear drift (or trend)

$$m(\mathbf{x}) = a + b_x x + b_y y \ ,$$

where a, b_x and b_y are constants, and x and y are spatial coordinates.

The project team explored various ways of deriving the parameters of the stochastic models from the data. First the approach of computing the experimental variogram and fitting a suitable analytical form to it was used. Fits by eye and automated methods using least-squares were tried. Confidence intervals for the parameters obtained from the least squares method were also estimated by linearizing about the best fit.

A maximum-likelihood method was also used for estimating the parameters of the stochastic model. The parameters were chosen to maximise the likelihood L of the measured values given the values of the parameters. For a Gaussian model, L is given by

$$L = \frac{1}{(2\pi)^{n/2}|\mathbf{C}|^{1/2}} \exp\left(-\frac{1}{2}(\mathbf{Z}_m - \overline{\mathbf{Z}})^T \mathbf{C}^{-1} (\mathbf{Z}_m - \overline{\mathbf{Z}})\right)$$

where

C is the covariance matrix between the measurement points,
|C| is the determinant of the covariance matrix,
$\mathbf{Z}_m$ is the vector of measured values of Z, and
$\overline{\mathbf{Z}}$ is the vector of the values of the mean at the n measurement points.

This approach was used to estimate the parameters (m, ω and λ) for a stationary model with constant mean m and an exponential covariance, and to estimate the parameters (a, b_x, b_y, ω and λ) for the model with a linear trend and an exponential covariance.

For the model with an exponential covariance, the project team also undertook a Monte-Carlo study of the bias in the automated parameter-estimation methods considered. Values were selected for each parameter, many (10000) realizations of the logarithm of the transmissivity field were generated for these parameters, the realizations were sampled at the measurement points (corresponding to the measurement points at the WIPP site) and the parameters estimated for each realization using the various methods. In this way confidence intervals could be determined for the estimated parameters, given that the actual parameters of the underlying stochastic model for the logarithm of the transmissivity had the selected values. The analysis was then repeated for different values of the parameters. In this way, confidence intervals for the parameters of the underlying stochastic model as functions of the estimated parameters were determined.

The project team undertook a Monte-Carlo analysis of the uncertainties in quantities relevant to repository performance assessments, such as the head at a particular point, the Darcy velocity at a particular point, the travel time along a pathline from a particular point to the boundary of the domain, and the position at which the pathline left the domain. They generated the realizations using the Turning Bands method [*Matheron, 1973; Mantoglou and Wilson, 1982*]. Care was taken to ensure that the parameters of the method were chosen to ensure that the generated fields were good approximations to those intended and that problems such as striping [*Tompson et al., 1989*] were avoided. This meant that many lines had to be used (50) and a fine discretisation had to be used on each line. Typically 300 realizations were generated for each case studied.

The realizations were conditioned on measurements of transmissivity using a technique [*Journel, 1974*] based on the geostatistical interpolation technique of kriging (see subsection 4.4.1). Each realization was conditioned by adding a field obtained by kriging the differences between the measured values of the logarithm of transmissivity and the values in the realization. They considered cases in which the realizations were conditioned on varying numbers of measurements from 39 (the total number of measurements) to 0.

Steady-state groundwater flow in each realization was calculated using the finite-element groundwater flow and transport program NAMMU [*Hartley and Jackson, 1993*]. (They only considered freshwater flow.) The domain modelled was the same as that used in the original study of *LaVenue et al.* [*1990*] (see Figure 4.2). The domain was discretised into a 40x60 grid of bi-quadratic quadrilateral finite elements. Transport through the calculated flow field for each realization was then calculated by particle tracking. The project team examined the uncertainties in the pathlines, travel time, head and Darcy velocity that resulted from the uncertainties in the parameters.

The project team was particularly interested in studying techniques for validating stochastic models. They used the framework of statistical hypothesis-testing techniques. A suitable statistic was defined, that would be expected to have a small value if the model was correct. The value of the statistic was then calculated, and if this value was sufficiently large that it could not reasonably be expected to arise by chance, the model was rejected. The project team used the χ^2-test and Kolmogorov-Smirnov test (KS-test) for normality to assess the pure nugget model (for which the data are considered to be uncorrelated). In order to use the tests to assess whether or not the other models were possible explanations of the data, it was necessary to take account of the correlations between the data. This was done by calculating suitable linear combinations of the data that would be effectively independent samples from a unit normal distribution, provided that the model was correct. These combinations were determined by diagonalising the correlation matrix between the measurement points. Then the χ^2-test and the KS-test for normality could be applied.

In most of their work the realizations were conditioned only on the measurements of transmissivity, and the available head measurements were used only to check the model. The project team also explored the use of the following technique for conditioning on measurements of steady-state groundwater heads. It can be shown that, provided the differences between measured and computed heads are small and the variance of the logarithm of the transmissivity field is small, the realizations can be conditioned on heads as well as transmissivities using a

technique based on co-kriging. Each realization is conditioned by adding a field obtained by co-kriging the differences between the measured values of head and the logarithm of transmissivity and their values in the realization. Effectively this expresses each conditioned realization as the sum of an unconditioned realization and a linear combination of basis functions, each corresponding to a measurement.

However, this approach requires the cross covariance between the logarithm of the transmissivity and the head. The project team suggested that the required cross-covariance could be calculated by Monte-Carlo techniques. A large number of realizations are generated, the flow calculated for each realization and then the covariances estimated as an average over all the realizations generated.

The project team suggested that the technique could be extended to deal with the non-linear case of large variance. The basis functions are computed as in the linear case. Then unconditioned realizations are generated, and conditioned by adding a suitable linear combination of the basis functions. The linear combinations are chosen so that the resulting realizations satisfy both the flow equations and the measurement equations. These conditions form a coupled non-linear system. Provided that this system can be solved, then from the way that they were constructed, the generated realizations clearly match the measured transmissivities and lead to head fields that match the measured heads. However, the generated realizations may not have the same covariance as that of the transmissivity measurements.

4.4.3 The UPV approach and models

The UPV project team also undertook studies of stochastic models. They began by undertaking an extensive exploratory data analysis, including an attempt to correlate the variability in transmissivity with geology. The project team also undertook statistical testing to see whether a univariate Gaussian model is acceptable. The raw data are correlated so the project team declustered the data using declustering weights proportional to the kriging weights for estimation of the average over the entire domain. Initial estimates of the experimental variograms were used in this. The KS-test was then used to check for normality. They considered the anisotropy of the variogram, computing the experimental variograms for different angle classes. Indicator variograms were computed for several thresholds.

The project team generated realizations using sequential (Gaussian) simulation [*Gómez-Hernández and Journel, 1993*], and evaluated the uncertainties in quantities such as hydraulic head, the travel time along pathlines and the position at which pathlines left the domain. In their initial simulations, the realizations were conditioned only on the measured values of transmissivity. The programs MODFLOW [*McDonald and Harbaugh, 1988*] and MODPATH were used respectively to compute constant-density groundwater flow and particle paths in each realization. The initial simulations did not give a very good match to the observed heads so the model was improved to take into account the effects of density variations due to variations in salinity, uncertainties in the boundary heads, and the observed heads.

The project team used the following method for conditioning the realizations on the measured heads. The basic idea of the method is to compute a modification to the transmissivity field that leads to an improved match to the observed heads. The modification is parameterised in terms of ΔZ_j, the modifications to the values of the logarithm of transmissivity at J selected points, with the modification at other points in the grid being obtained by interpolating from ΔZ_j using kriging (see subsection 4.4.1).

The values of ΔZ_j are obtained as follows. The finite-element or finite-difference numerical equations for the equivalent freshwater head, for a specified variation in groundwater density, can be expressed as

$$\mathbf{T.H = Q} ,$$

where

T is the transmissivity matrix,
H is the vector of nodal head values,
Q is the vector of sinks and sources, which includes the effects of boundary conditions.

By expanding these equations about the original transmissivity matrix T_0 and the corresponding head vector $\mathbf{H}_0$ a linear approximation

$$\mathbf{H} = \mathbf{H}_0 + \sum_{j=1}^{J} \frac{\partial \mathbf{H}}{\partial \Delta Z_j} \Delta Z_j$$

to the modified head vector as a function of ΔZ_j can be derived, where

$$\frac{\partial \mathbf{H}}{\partial \Delta Z_j} = T_0^{-1} \left(\frac{\partial \mathbf{Q}}{\partial \Delta Z_j} - \frac{\partial T}{\partial \Delta Z_j} \mathbf{H}_0 \right)$$

The right hand side of this equation is computed essentially by solving a flow problem for a modified source term. Variable-density flow can be treated in the same way by linearizing about the initial density distribution. Quadratic programming is then used to determine the values of ΔZ_j that minimise a weighted sum of the squares of the differences between measured and calculated heads. In order to stabilise the process, the minimisation is constrained so that the changes ΔZ_j are smaller than two kriging standard deviations of the kriged estimate at the corresponding point. After the minimization has been completed, the calculated heads are compared with the measured ones. If they do not match well, then the whole process is repeated using the updated heads as the new initial field, and so on.

The uncertainties in the boundary conditions can be dealt with in a similar manner. A modification to the head on the boundary is parameterised in terms of selected values. The change in head is expressed as linear combination of these parameters by linearising the flow equation. The values of the parameters are determined by including them in the minimisation procedure. This leads to heads on the boundary that give a better match to measured heads.
The project team has also extended the approach to handle transient data.

4.4.4 The AECB approach and models

In order to build confidence in the results of an assessment, the AECB advocates the use of a variety of conceptual models and approaches for demonstrating safety, including relatively simple scoping or bounding calculations and sensitivity studies. Validation of detailed models is involved and time-consuming. Initial scoping and bounding calculations can highlight the most important processes and parameters and so help to focus more detailed studies, and may even adequately address some aspects of the problem, so avoiding the need for detailed calculations.

The AECB project team applied this methodology to the WIPP-2 test case. The groundwater densities south of the site (which is the general direction of groundwater flow paths from the site) are rather uncertain. Figure 4.6 shows the limited number of data points in this region. Furthermore, groundwater densities could change with time as the regional flow system continues to evolve. Previous work [*Davies, 1989*] indicated that groundwater density has a large effect on the groundwater flow in the area on interest. The project team undertook bounding calculations to examine the effects of variable fluid density on the groundwater flow south of the site, to try to determine if the uncertainties in the fluid density were important for the performance of a repository at the WIPP site.

The project team took the calibrated model obtained by *LaVenue et al.* [*1990*] as a base case. In this model, the transmissivity distribution was obtained by calibrating against the transient head data, and the distribution of salinity was obtained by interpolating between the measurements using kriging. They compared the groundwater flow and head calculated for this model with those calculated using two variants that were considered to represent bounding distributions for the fluid density:

(i) a distribution obtained by increasing the salinity by 50% everywhere, and
(ii) freshwater everywhere.

They used the SWIFT finite-difference program for the calculations. The model was two-dimensional and comprised 1344 grid blocks. As a preliminary verification step they compared the results for their base case with those obtained by *LaVenue et al.* [*1990*]. This was done because, although they and LaVenue et al. both used SWIFT, the versions differed slightly.

4.4.5 The BGR approach and models

The BGR project team addressed issues relating to the choice of conceptual model. The AEA, UPV and AECB project teams considered flow in two-dimensional areal models of the Culebra Dolomite. Underlying this sort of model is the assumption that the permeabilities of the units above and below the Culebra Dolomite are sufficiently small that vertical flow can be neglected. The BGR project team considered an alternative conceptual model in which all the units above the Salado were represented, and vertical flow between the units modelled, as well as flow within the units. They modelled the entire regional flow system, taking the limits of the domain at assumed water divides, and assuming that the water table was close to the ground surface. This avoids some of the difficulties associated with the choice of boundary conditions in the two-dimensional areal models. Decisions about these boundary conditions are replaced by

assumptions, which may be easier to justify, about the location of the water divides and the position of the water table. In the resulting model groundwater inflows and outflows are only possible at the upper boundary which represents the land surface.

In principle, such a model is three-dimensional. However, for the conditions of the site a reasonable approximation to the full three-dimensional model is given by a two-dimensional vertical cross-section model running from the regional high point of the Divide to Nash Draw (see Figure 4.7). This line runs parallel to the steepest surface gradient, and is normal to the margins of halite beds in the Rustler Formation, which represent a potential source of salinity. source of salinity. The line runs from east to west through the southernmost part of the WIPP site (see Figure 4.7).

All available relevant data were incorporated in the BGR model, but nevertheless many parameters had to be estimated, which was done in a manner consistent with the geological setting where possible. The project team used vertically-averaged values of the permeability and porosity for each of the five members of the Rustler Formation other than the unnamed lower member, which means that vertical heterogeneity within these members was not explicitly taken into account. Upper and lower parts of the unnamed lower member were distinguished, corresponding to the two different halite beds in this layer. The groundwater in the halite beds was assumed to be saturated brine.

The finite-element program ROCKFLOW [*Kröhn, 1987*] was used for the calculations. Various preliminary simulations with simplified models were undertaken to investigate the effects of discretization, density variations and permeability contrasts, prior to setting up a physically and numerically realistic model. The model used is shown in Figure 4.8. Density-dependent groundwater flow was then simulated until a steady state was reached. The plausibility of the solution was checked by comparing the computed density distribution with measurements. More information on the regional flow system was obtained by tracking back pathlines through the Culebra Dolomite. Groundwater inflow rates were also calculated.

4.4.6 The SNL approach and models

Like the BGR project team, the SNL project team also explored the use of different conceptual models [*Corbet and Wallace, 1993*]. In particular, they used a three-dimensional regional model to study the importance of vertical flow between the Culebra Dolomite and the overlying units, and to examine the impact of climate change on the flow system. The model represented all the rocks above the Salado, and extended laterally to locations that were believed to correspond to groundwater divides for the entire time simulated. The location of the region modelled is shown in Figure 4.9. Ten stratigraphic units were represented by fifteen model layers. Each stratigraphic layer was taken to be homogeneous, with a hydraulic conductivity representative of the dominant rock type in that layer.

The finite-difference program MODFLOW [*McDonald and Harbaugh, 1988*] was used for the calculations. The program was modified to allow seepage faces to develop where appropriate.

Simulations were undertaken for a period of 41000 years. The initial condition was taken to be the steady-state flow corresponding to the water table at the land surface. This was taken to be representative of the wetter conditions that prevailed in the region at the end of the Pleistocene. For the first 21000 years simulated, infiltration was taken to be zero, representing a dry period. The final 20000 years simulated was taken to correspond to a somewhat wetter period with a maximum potential infiltration of 0.5mm/year. (This is less than 0.2% of the present-day annual rainfall, representing the fact that most rainfall is lost to surface runoff or evapotranspiration.)

4.5 Modelling Results

4.5.1 AEA

The AEA project team compared different methods for estimating the parameters of the stochastic model, once the form of the variogram had been determined (which they felt should take into account geological information). For parameter-estimation methods based on fitting to the experimental variogram, they considered that automated methods based on least-squares fitting were to be preferred to fitting by eye. The least-squares methods had the benefit of providing a quantitative measure (R^2) of the quality of the fit. However, all methods based on fitting to the experimental variogram had the disadvantage of requiring a choice of classes in the calculation of the experimental variogram. This choice was fairly arbitrary and had a noticeable effect on the estimated parameters. The project team concluded that the best method for determining the parameters was the use of maximum likelihood. This method had the advantage of not requiring an arbitrary choice of classes, and led to estimates of the parameters with narrower confidence intervals than those resulting from fitting to the experimental variogram.

The parameters for the exponential model obtained by least-squares fitting to the experimental variogram for one set of classes were

$$m = -4.929 \, , \, \omega = 4.599 \, , \, \lambda = 10.51 \text{ km} \, .$$

The 90% confidence region estimated by linearization about the estimated parameters is an ellipse with major axis from $\omega = 2.925$, $\lambda = 4.81$ to $\omega = 6.273$, $\lambda = 16.21$ and minor axis from $\omega = 4.26$, $\lambda = 11.03$ to $\omega = 4.93$, $\lambda = 10.00$. Using the maximum-likelihood approach the values of ω and λ obtained for the exponential model model were

$$\omega = 4.306 \, , \, \lambda = 8.59 \text{ km} \, .$$

As can be seen the two methods of estimating the parameters lead to similar results. The maximum-likelihood method gives a slightly smaller correlation length (λ). The parameters obtained for the power-law model by fitting to the experimental variogram were

$$m = -5.437 \, , \, \alpha = 0.0257 \, , \, \beta = 0.6919 \, .$$

The parameters obtained by maximum-likelihood estimation for the model with a linear trend and an exponential covariance were

$a = -1.99$, $b_x = -2.7\ 10^{-4}$, $b_y = -3.6\ 10^{-5}$, $\omega = 1.253$, $\lambda = 2.00$km .

Results from their Monte-Carlo study of the bias in the parameters as estimated by the different methods are illustrated by Figure 4.10. This shows the mean value of the estimates of λ as a function of the actual λ, which is known in the circumstances of the study, and the one-standard deviation range about the mean value. The study showed that:

(i) the confidence intervals for the maximum-likelihood method were about half those for least-squares fitting to the experimental variogram;

(ii) both methods had significant biases. For the maximum-likelihood method the bias increased with the correlation length;

(iii) the confidence intervals estimated by linearization about the least-squares best-fit were much smaller than the true confidence intervals, and indeed that if the correlation length was comparable to (or greater than) the size of the domain under consideration, then it was not possible to estimate an upper limit to the correlation length from the data.

The results of the Monte-Carlo uncertainty analysis undertaken by the project team are illustrated in Figures 4.11 to 4.13. Figure 4.11 shows three of the conditioned realizations for the case of a constant mean and an exponential covariance with the parameters obtained using maximum-likelihood. The Figure also shows the field obtained by interpolating the measurements using kriging with the same variogram. Figure 4.12 shows the corresponding head fields. Figure 4.13 shows the pathlines starting at the location of borehole H-1 (near the centre of the WIPP site) for 300 realizations, and the pathline in the kriged field. Figure 4.14 shows the probability density function and cumulative distribution function for the travel time from H-1 to the boundary of the domain considered.

Figure 4.13 also illustrates the effect of the number of measurements on the uncertainty. As can be seen the uncertainty is greater if there are fewer measurements available for conditioning with. Compared to the case in which all 39 transmissivity measurements were used to condition the realizations, the uncertainty is about 5 times greater if no measurements are available. It should be noted that in these calculations the statistical model deduced from all 39 measurements was used. The uncertainties would be greater if the stochastic model had to be deduced from fewer data than the available 39 measurements, as would be the case in practice if fewer data were available. In general it was expected that it would depend on the site whether conditioning on transmissivity data led to significant reductions in uncertainty. This reduction was expected if the correlation length was comparable to the spacing between the measurements.

The uncertainties after conditioning were very similar for all the models, even though the model with a trend has much less variability about the trend than the exponential model for example. The project team suggested that this might be because the correlation length for the model with a trend was much smaller than the correlation length for the other models, which was comparable with the domain size. Therefore, although the uncertainty before conditioning was considerably smaller for the model with a trend, conditioning on measured values of transmissivity had much less effect for this model, as fewer data affected the value at a given point.

The statistical tests carried out by the project team led them to conclude that the pure nugget model was unlikely to be an explanation of the data, but the models with an exponential covariance and a power-law covariance were acceptable. This does not mean that the models are the best models or that further investigation might not lead to the rejection of the models. The tests also showed that the model with a linear trend and an exponential covariance was unlikely to be an explanation of the data. It should be emphasised that this does not mean that all models with a trend would be rejected, but only that the model considered, with a linear trend and an exponential covariance is unlikely to be an explanation of the data.

Although the exponential model and the power-law model could not be ruled out by the analysis of the transmissivity distribution, when the heads were considered it was concluded that the models were unlikely to be acceptable. Although the measured heads were generally within one standard deviation of the predicted mean over all realizations, when correlations were taken into account the measured heads were considered to be unlikely to arise as a sample from the ensemble of realizations. It was noted that, although the discrepancies might have arisen because the statistical model was not appropriate, they might also have arisen because the calculations were for freshwater flow only or because inappropriate boundary conditions were used. (The prescribed boundary heads were obtained by *LaVenue et al.* [*1990*] by extrapolating from measured heads, using kriging.)

The project team noted that it was to be expected that more than one stochastic model might be adequate explanations of the data.

The project team pointed out that if all the data including the steady-state head data and the transient responses are used to condition the models, then there are no data to check the models against, and the only checks that can be applied to the models are internal consistency checks.

4.5.2 UPV

From their initial analysis of the transmissivity data, the UPV project team concluded that there is an overall East to West trend in the transmissivity with decreasing values towards the East, which may be explained by halite dissolution in the upper Salado Formation and the Rustler Formation. The project team also noted that the raw data have a bimodal distribution, with a clear break at Z = -5.5 (see Figure 4.15), which might also be explained by dissolution. The declustered data were found to just pass the KS-test for normality at a significance level of 0.05 (see Figure 4.16).

The project team considered that manual fitting of the variograms, with analysis of the scattergrams for all relevant lags to detect anomalies, is better than automatic fitting. The variogram computed for the uniform transform of the data confirmed that the data were best represented by an anisotropic model with principal axes North-South and East-West. Figure 4.17 shows the experimental variograms in the North-South and East-West directions respectively (that is, the variograms for separations restricted to angles of 45° about the y and x axes respectively). The zonal anisotropy shown is consistent with geological understanding of the Culebra (see subsection 4.2.1). The indicator variograms did not show any clear structure

and so the project team decided to use a Gaussian model, although they noted that such a model does not have continuity of extreme values.

The variogram in the East-West direction was fitted by a spherical model with range 4000m and sill 1.6. The variogram in the North-South direction was fitted by a linear model with slope 0.005. The overall variogram was chosen to interpolate smoothly between the directional variograms, and be non-negative definite.

The heads computed for the initial set of realizations generated by the project team did not match the observed heads very well, as can be seen from Figure 4.18. This presents a comparison of the measured and observed heads for a single realization. It also shows the improvements to the model obtained by using the optimisation technique outlined in subsection 4.4.3. Figure 4.19 shows the effect of taking into account the variation in groundwater density (for the same realization). As can be seen there is quite a significant change to the head gradients to the East of the site.

One interesting point that emerged from the analysis was that the transmissivity measured at point P-18 seemed to be too low, in that the optimisation tended to increase values in its neighbourhood. P-18 was also singled out by the AEA project team as anomalous on the basis of a simple cross-validation test in which the measured value at each point was compared with the value obtained by kriging from all the other measurements. It should be noted that there are two measurements of the transmissivity at P-18, which differ by several orders of magnitude, and *LaVenue et al.* [*1990*] decided that the lower value was better.

Although the UPV project team only undertook calculations for a Gaussian model, they stressed the need to consider non-Gaussian models. For Gaussian models, regions of higher (or lower) than average transmissivity are not connected over distances long compared to the correlation scale. In a performance assessment for a repository for radioactive waste, it is important to consider models in which high-transmissivity regions can be connected over long distances, as these regions may form fast flow paths from the repository and lead to the main radiological consequences. The project team discussed methods such as indicator simulation for generating realizations of non-Gaussian models. They intend to consider such models in the future.

4.5.3 AECB

The AECB project team performed bounding calculations to assess the importance of uncertainties in the groundwater density in a performance assessment of the WIPP site. They compared the head and flow fields for a base-case distribution of salinity obtained by interpolating from measurements [*LaVenue et al., 1990*] with head and flow fields computed for two different distributions of salinity: freshwater everywhere, and the salinity increased by 50% everywhere.

In their preliminary verification step, the project team found some differences between the results computed using their version of SWIFT and that used by *LaVenue et al.* [*1990*]. The computed heads were generally in very good agreement (within 0.16%), but the computed

velocities differed noticeably (by up to 20%) in regions of low head-gradient. The Darcy velocities are computed within SWIFT from differences in heads, so that in regions of low head-gradient, small differences between the heads calculated by the two versions of the program are effectively magnified. The differences in the magnitude and direction of the computed Darcy velocity in the region of interest in the immediate vicinity of the site and to the south (the region that path lines from the centre of the site traverse) were only a few percent. Therefore, the project team concluded that the differences between the results calculated using the two versions of SWIFT were not significant for present purposes, namely comparing flow paths from the centre of the site for the purposes of a repository performance assessment.

The project team then compared the results from the base case with those calculated for the two variant bounding calculations. Figure 4.20 shows the difference between the Darcy flux in the base case and that in the variant with freshwater everywhere. As shown in Figure 4.20(a), in the immediate vicinity of the WIPP site the difference in the direction of the Darcy velocity in the two cases is generally less than 10°. To the south of the site, the difference in the direction of the Darcy velocity is up to 70°. In this region, the flow in the base case was generally directed to the south or south-east, whereas in the variant with freshwater everywhere, the flow is directed in a more westerly direction towards the Nash Draw, as expected. The maximum difference in the magnitude of the Darcy flux in the region to the south of the site is about 50%, which is small compared to the uncertainties in the transmissivity field.

Figure 4.21 presents a comparison of the head calculated for the variant with freshwater everywhere with that calculated for the base case. The pathlines from the centre of the site in the two cases are also shown. As can be seen, the groundwater flow path from the centre of the site in the variant does not differ significantly from that in the base case. In both cases the path runs through the high-transmissivity channel postulated by *LaVenue et al.* [*1990*]. This is consistent with the changes to the direction of the Darcy flux discussed above, because the largest changes occur on either side of the postulated high-transmissivity channel.

In the case in which the salinity was increased by 50% everywhere, the difference in the direction of the Darcy velocity was generally less than about 10°, except for a small region near the northern boundary of the site. The flow path from the centre of the site therefore followed a very similar path to that in the base case (see Figure 4.21(b)).

Overall the project team concluded that the uncertainties in the salinity (and hence groundwater density) did not significantly affect the flow paths in the Culebra Dolomite from the centre of the site, calculated on the basis of the conceptual model of *LaVenue et al.* [*1990*]. These paths, which are the important paths in a performance assessment, followed the high-transmissivity channel postulated by *LaVenue et al.* [*1990*]. This channel provides a preferred route for groundwater flow from the site towards the south because of its high transmissivity relative to the rocks on either side of it. The project team concluded that the flow paths were controlled by the transmissivity distribution, and they suggested that field studies to further characterize the high-transmissivity channel should be an important part of future site investigations.

4.5.4 BGR

The results of the preliminary modelling undertaken by BGR to assist in the development of a reasonable model showed that:

(i) element aspect ratios should not exceed 100;

(ii) horizontal pressure gradients were generated at the margins of the halite, which were assumed to be sharp and vertical. These pressure gradients lead to convection cells, which needed a finer grid to resolve at the end of the lower halite bed in the unnamed lower member;

(iii) the use of a realistic permeability distribution led to an erratic velocity distribution because of the high permeability contrasts between different layers. The differences in permeability were therefore smoothed so that the contrasts did not exceed two orders of magnitude;

(iv) the combination of the fixed-pressure boundary condition at the top of the model, which was taken to be the water table, together with a top surface determined by linear interpolation between measured elevations at several locations led to an unrealistic flow field near changes in surface slope. This problem was resolved by modifying the top-surface boundary condition.

Once a reasonable model had been set up, a transient flow simulation was performed. It was found that steady-state conditions were only approached very slowly. Figure 4.22 illustrates the flow field at four million years, which was taken to be close to steady state. Infiltration occurs over almost all of the top boundary of the model. The infiltration rate was found to be mostly less than 60mm per year, which is consistent with inferred palaeo-precipitation rates. The infiltration represents about 10% of the inferred precipitation rate during the last glacial maximum 20000 years ago [*Swift, 1991*]. The groundwater largely flows round the halite zones in the eastern part of the model. The flow in the Culebra outside the halite zones is several orders of magnitude larger than that in the halite zones.

The salt concentration is loosely related to the halite zones. The salt plume reached the surface in the eastern part of the site, but is quite narrow west of the WIPP site. The steep concentration gradients in the Culebra Dolomite that were recorded in the field are reproduced by the model (see Figure 4.23); and the model has nearly fresh water in the Magenta Dolomite at the position at which this was measured.

Interpretations of groundwater chemistry suggest that the water in the Culebra in the WIPP area may be greater than 12000 years old [*Lambert and Harvey, 1987, Siegel et al., 1991*]. This estimate was compared with groundwater ages estimated by tracking back along pathlines through the WIPP site (see Figure 4.24), which gave ages of 29000 years for the groundwater on the Western boundary of the WIPP site and 22 million years for the groundwater on the Eastern boundary. (These travel times do not take account of dispersion and so only provide an indication of groundwater age.)

These results suggest that the model is reasonable. It should be noted that the model was not fully calibrated. The permeabilities used were based on a first estimate of realistic parameters.

Overall the model shows that transport of salt in the eastern part of the region is dominated by diffusion and the flow velocities are very low. The salt plume does not spread west of the halite zones into the dolomites. Density effects have only a minor effect on the flow field, as confirmed by further investigations. The main factor affecting the flow field is the distribution of permeability, with its large heterogeneities.

The most important result of the study is that significant vertical leakage occurs into the Culebra Dolomite. Figure 4.25(a) shows the vertical flux through the Tamarisk Member, and Figure 4.25(b) shows the horizontal flux in the Culebra Dolomite. The calculated infiltration rates at the WIPP site and to the east of it are low (less than 1mm per year) which suggests that very little precipitation is needed to maintain the vertical leakage into the Culebra Dolomite.

4.5.5 SNL

The results of the modelling [*Corbet and Wallace, 1993*] undertaken by the SNL project team are illustrated in Figures 4.26. Figure 4.26(a) shows the initial calculated head distribution in the Culebra. This is a subdued replica of the land-surface topography, even though there are four model layers between the Culebra and the surface with a hydraulic conductivity five orders of magnitude smaller than that of the Culebra.

Figure 4.26(b) shows the calculated head in the Culebra after 21000 years (at the end of the dry period). The head has decreased everywhere, with the greatest decrease in regions of high head. Figure 26(c) shows the head after a further 20000 years during which the infiltration was maintained at 0.5mm per year. As can be seen, even this very low value of infiltration is sufficient to restore heads in the Culebra to levels approaching the initial values.

Figure 4.26(d) shows the distribution of vertical leakage after the first 21000 years. The pattern is similar to the initial one, although in some areas the directions of vertical flow have reversed. The project team also compared the relative magnitude of the horizontal and vertical fluxes into the Culebra in the rectangular region shown in Figure 4.26(d), and found that about 57% of the total flux entering the region is due to vertical flow and about 32% of the outflow is due to vertical flow.

The project team noted that there were large uncertainties in many of the parameters of the model and various simplifying assumptions had been made in their modelling, so that the model should not be taken too literally. Rather the modelling should be considered as helping to improve understanding of regional groundwater flow in the Delaware Basin. The calculations suggest that:

(i) the flow of groundwater in confined units may be strongly influenced by the overlying water table;
(ii) vertical flow through low permeability layers may have an important effect on the flow in relatively permeable layers;
(iii) climate changes may be important.

4.6 Tracer Test

During the course of the INTRAVAL project the participants were given the opportunity to interact with the WIPP project. In particular the INTRAVAL participants were provided with the opportunity to comment on designs for a proposed experiment at the WIPP site, and these comments were taken into account by the experimentalists. It should be stressed that the ultimate responsibility for the design of the the experiment, which was not carried out during the course of INTRAVAL, rested with the WIPP project.

The proposed experiment was intended to examine transport of both reactive and non-reactive tracers in the field over a range of length scales (from 6m to 60m). The objectives of the experiment were:

(i) to address vertical heterogeneity in the Culebra Dolomite;
(ii) to try to demonstrate the significance of rock-matrix diffusion for transport through the Culebra Dolomite;
(iii) to try to distinguish between different possible conceptual models;
(iv) to provide data on in-situ retardation properties;
(v) to obtain core samples to enable comparison of laboratory and field studies of tracer transport;
(vi) to test the appropriateness of transport models, as opposed to simply calibrating the models;
(vii) to study the directional characteristics of flow and transport in the Culebra Dolomite.

The experiment was to be carried out using an assembly of boreholes arranged as shown in Figure 4.27. This allowed for measurement of transport over different distances using different combinations of boreholes for tracer injection and measurement. The possibility of focusing on specific horizons within the Culebra was allowed for. Two possible locations for the test were suggested (the location of the existing H-3 hydropad, or a new location nearly one kilometre north east of this, see Figure 4.28).

It was proposed that there would be three phases to the experiment. In the first phase, a convergent-flow tracer test would be performed by pumping the central well and injecting conservative (non-reactive) tracers at different levels in the other wells. The fastest flow path identified would then be tested again using a second conservative tracer and a much larger chase volume to try to study channelling.

In the second phase of testing another convergent-flow tracer test would be performed, pumping the well identified as lying along the fastest flow path. Conservative tracers would again be injected in all wells, and in addition, reactive tracers would be injected in the three wells nearest the pumping well. The pumping rate would be changed during the test and a second set of conservative tracers would be injected to try to study channelling and velocity-dependent processes such as rock-matrix diffusion. In the third phase it was proposed to perform a dipole tracer test using two of the wells that had not been pumped during the convergent-flow tests. Again, it was proposed to change the pumping rate during the test to try to study channelling and velocity-dependent processes such as rock-matrix diffusion.

It was considered that the proposed experiment would provide valuable information about the transport of both reactive and non-reactive tracers, and begin to address issues of scaling. However, for reasons unconnected with INTRAVAL, the proposed experiment was not actually carried out during the period of INTRAVAL. It is currently scheduled to begin towards the end of 1995.

4.7 Conclusions

This test case provided a very valuable focus for the development and study of stochastic models for the treatment of heterogeneity in hydrogeological properties. Two project teams (AEA and UPV) devoted their efforts to study of such models and their application to the test case. Both project teams developed stochastic models of the transmissivity and quantified the uncertainty in quantities of interest in a repository performance assessment, such as the time to travel a certain distance from the site, or the Darcy velocity at a certain position. The project teams showed that stochastic modelling approaches can be used in practical cases relevant to repository performance assessments. Their work should help to build confidence within the wider scientific community in the application of stochastic groundwater flow models, which is an important part of validation.

The AEA project team examined the uncertainties in the parameters of the stochastic model. They showed that the estimates are biased, and that the confidence intervals may be very large, much larger than confidence intervals estimated by linearization about the estimated parameters. Indeed, they showed that if the correlation length was comparable to, or greater than, the size of the domain investigated it was not possible to determine the correlation length from the measured data. However, this did not have a significant impact on the uncertainties in quantities such as the travel time, provided that the model was conditioned on a reasonable number of transmissivity measurements, because the transmissivity distribution was then strongly controlled by the data.

The project team attempted to quantify the reduction in uncertainty resulting from increased information. They found that the uncertainties were reduced considerably by conditioning on transmissivity data, although this is probably a site-specific conclusion.

The project team also examined the issues involved in validation of stochastic models. They recommended the use of statistical hypothesis-testing techniques. They showed that it was possible using this approach to demonstrate that some models were unlikely to be adequate explanations of the data. The project team noted that it was possible that there might be more than one model that was an adequate explanation of the data.

The project team was developing methods for conditioning on measured heads, and on transient responses. However, they noted that if all the data were used to condition the model, the only checks that could be applied to the model were internal consistency checks.

The UPV project team undertook an extensive exploratory data analysis, including an attempt to correlate the variability in transmissivity with geology. Unlike the AEA project team who

considered that an isotropic model was adequate, the UPV project team considered that there was an overall East to West trend in the data, which was best represented by an anisotropic zonal variogram.

The project team developed a technique for conditioning on heads, which was quite successful.

Although the project team only undertook calculations for Gaussian models, they stressed the need to consider non-Gaussian models. For Gaussian models, regions of higher (or lower) transmissivity than the average are not connected over distances long compared to the correlation length. In a repository performance assessment it is important to consider models in which regions of high transmissivity are connected over long distances, as these may form fast flow paths, which may lead to the main radiological consequences of the repository.

The AECB project team devoted its efforts to examining the impact of uncertainties in the distribution of salinity on a performance assessment. They concluded that the flow paths from the centre of the site were largely controlled by the distribution of transmissivity and that the distribution of salinity only had a small effect.

The BGR and SNL project teams addressed issues relating to the choice of conceptual model. The BGR team developed a two-dimensional vertical cross-section model and the SNL project team developed a three-dimensional model. Both teams showed the importance of vertical flow between the Culebra and the lower permeability units above and below it. The BGR team compared results from their model with inferred groundwater ages, inferred palaeo-precipitation rates and experimental measurements of salinity and found reasonable agreement.

All the project teams stressed the need to take account of information about the geology in setting up the models.

It is desirable to consider alternative models. In particular, it was shown that vertical flow through low permeability formations may affect the flow in much higher permeability confined formations, and that it may be necessary to consider the effects of climate change.

One of the valuable aspects of this test case was that it provided a valuable opportunity for modellers and experimentalists to interact. During the course of the INTRAVAL project the participants were given the opportunity to comment on designs for a proposed experiment at the WIPP site, which was intended to examine transport in the field of both reactive and non-reactive tracers over a range of length scales from 6m to 60m, and their comments were taken into account by the experimentalists. It should be stressed that the ultimate responsibility for the design of the experiment rested with the WIPP project.

The test case provide a valuable opportunity to explore the issues involved in validation of field-scale models of groundwater flow and transport. As can be seen from the above discussion, the different project teams tackled different aspects of the test case. There was some overlap between the issues addressed by AEA and UPV, and between the issues addressed by BGR and SNL, although the approaches used by the different project teams differed in detail. Taken together, the conclusions reached by the project teams were generally consistent, and helped to

build up the picture of flow and transport at the WIPP site. Overall, the work undertaken on this test case should help to build confidence in models of the hydrogeology of the WIPP site.

Acknowledgment

The financial support of Nirex for the work of the author, which was carried out as part of the Nirex Safety Assessment Research Programme, is gratefully acknowledged.

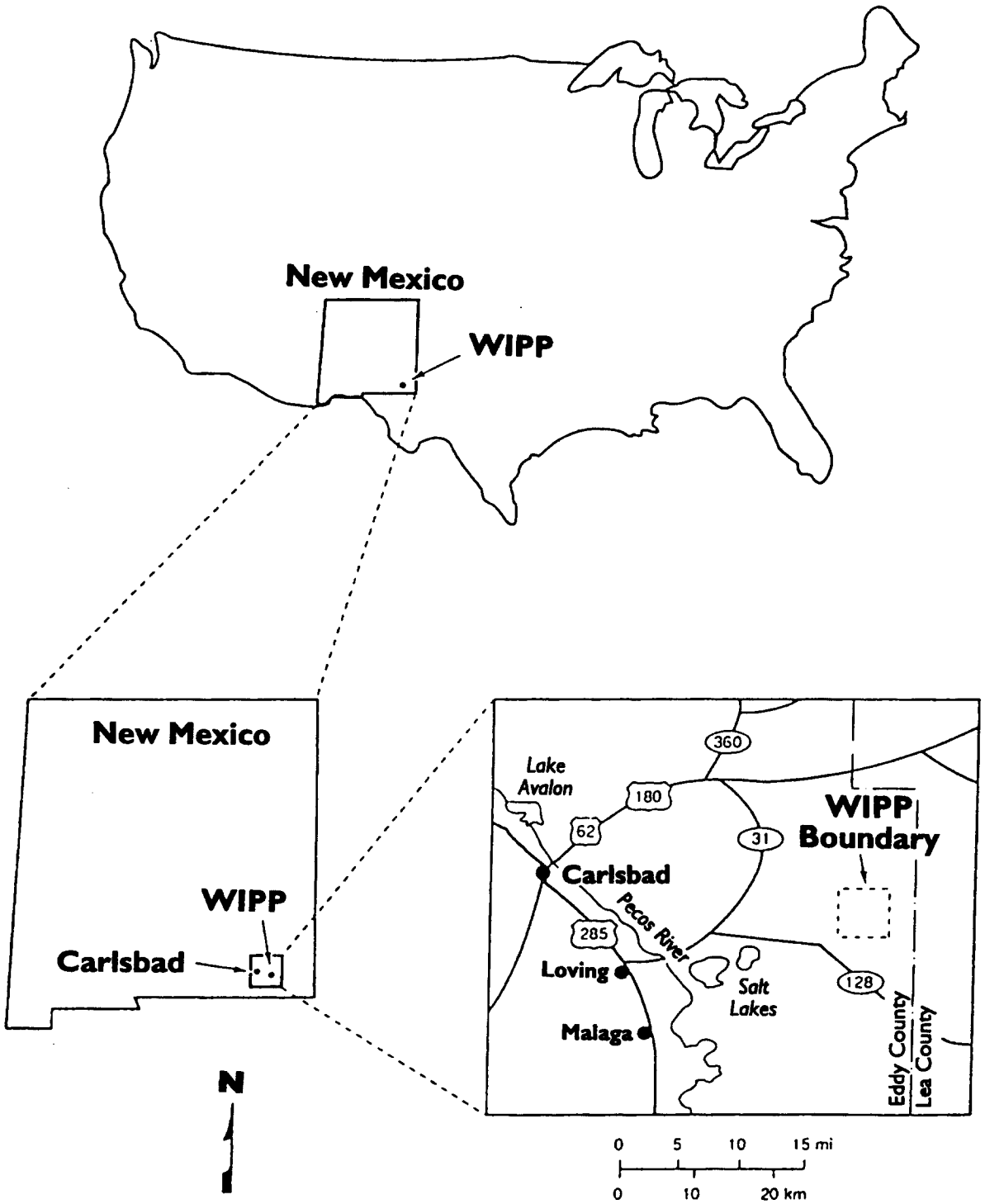

Figure 4.1 The location of the Waste Isolation Pilot Plant in New Mexico, USA.

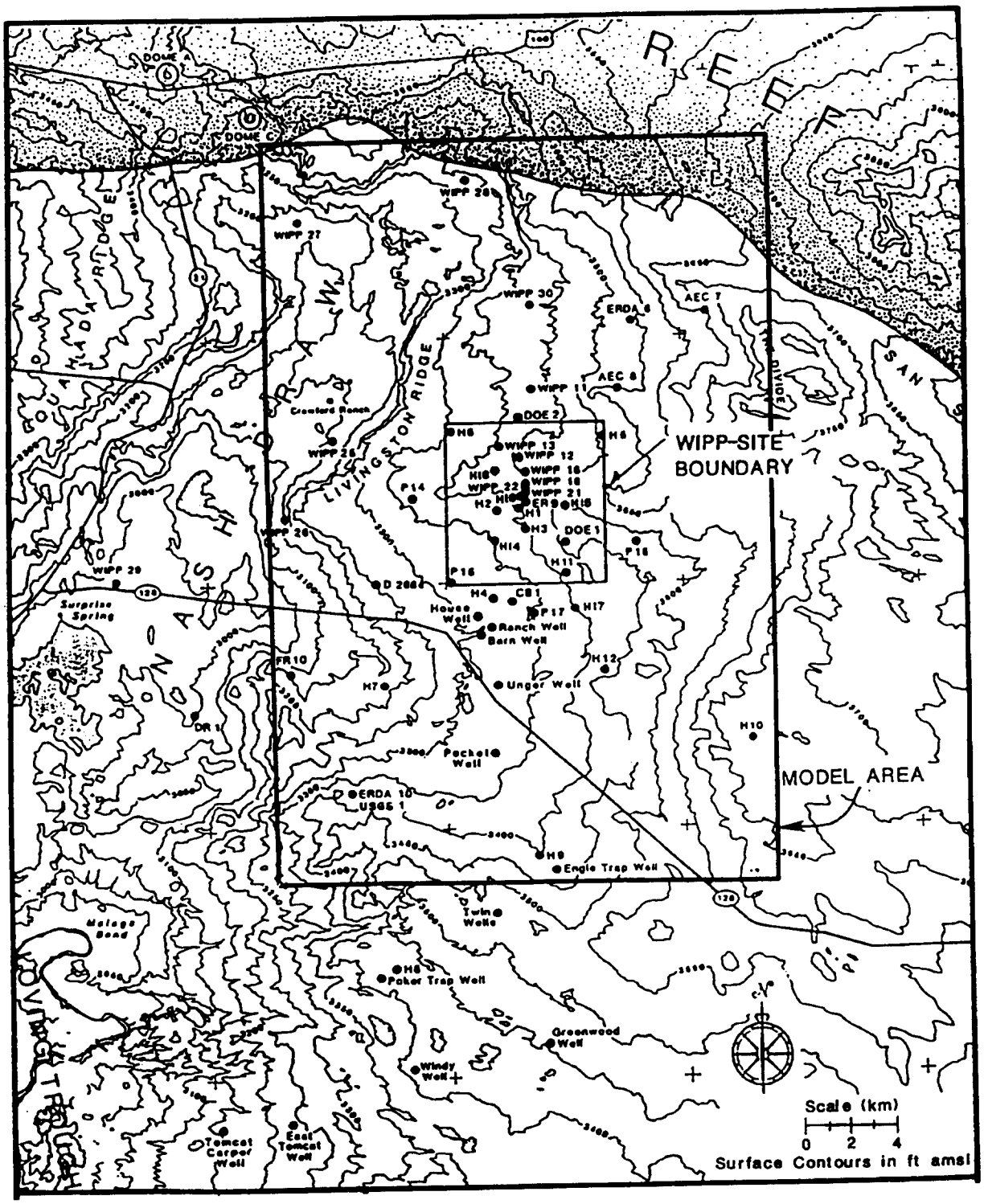

Figure 4.2 The topography in the WIPP region. The nearly square region is the WIPP site itself, and the large rectangle is the region modelled in the original studies of *LaVenue et al.* [*1990*] and in the studies of the AEA, UPV and AECB project teams reported here.

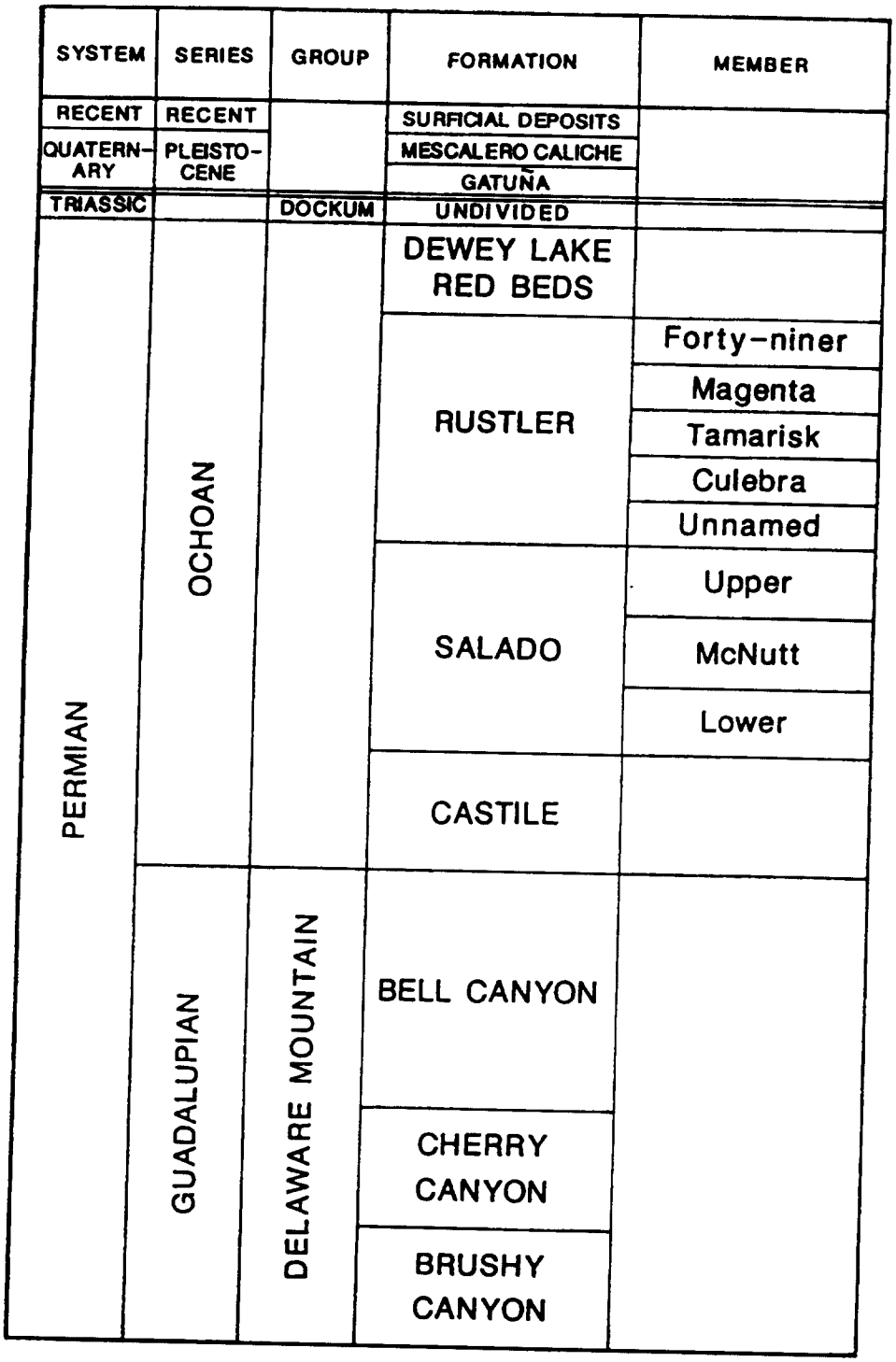

Figure 4.3 The stratigraphy of the rocks in the region of the WIPP site.

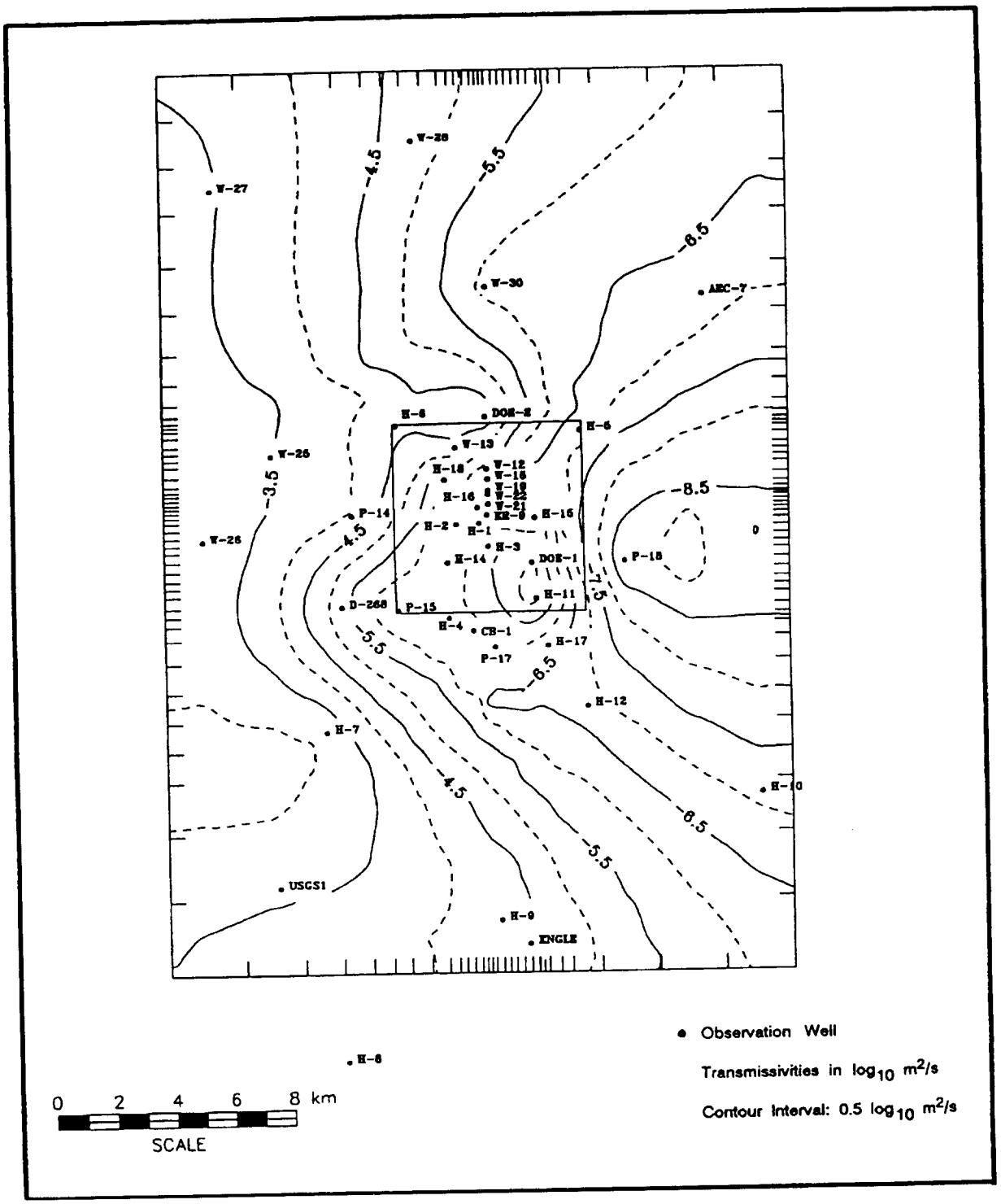

Figure 4.4 The distribution of transmissivity obtained by interpolation between the measured data using kriging (with a linear generalised covariance function). The figure is reproduced from *LaVenue et al. [1990]*.

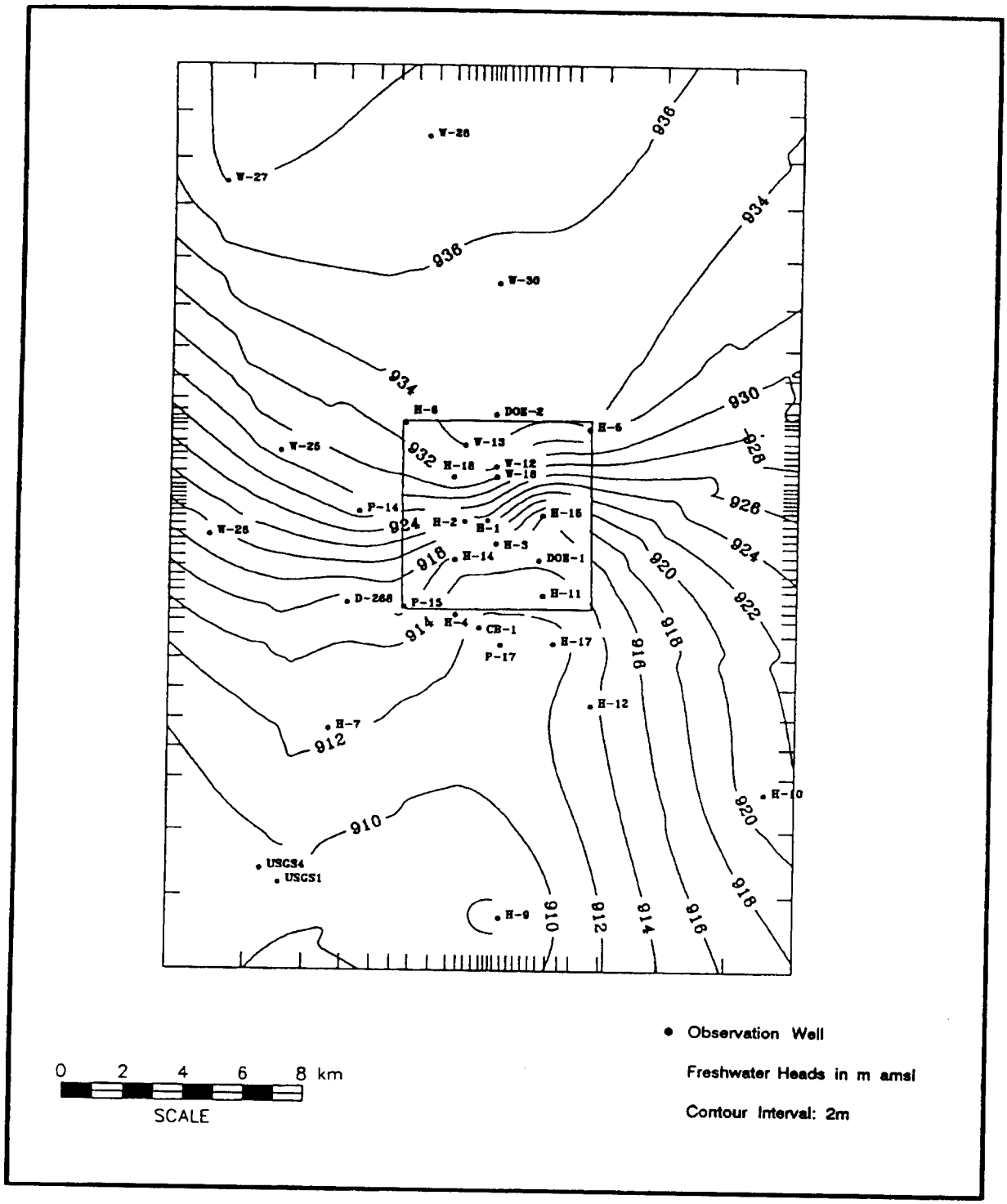

Figure 4.5 The distribution of equivalent freshwater head obtained by interpolation between the measured values using kriging (reproduced from *LaVenue et al.* [*1990*]).

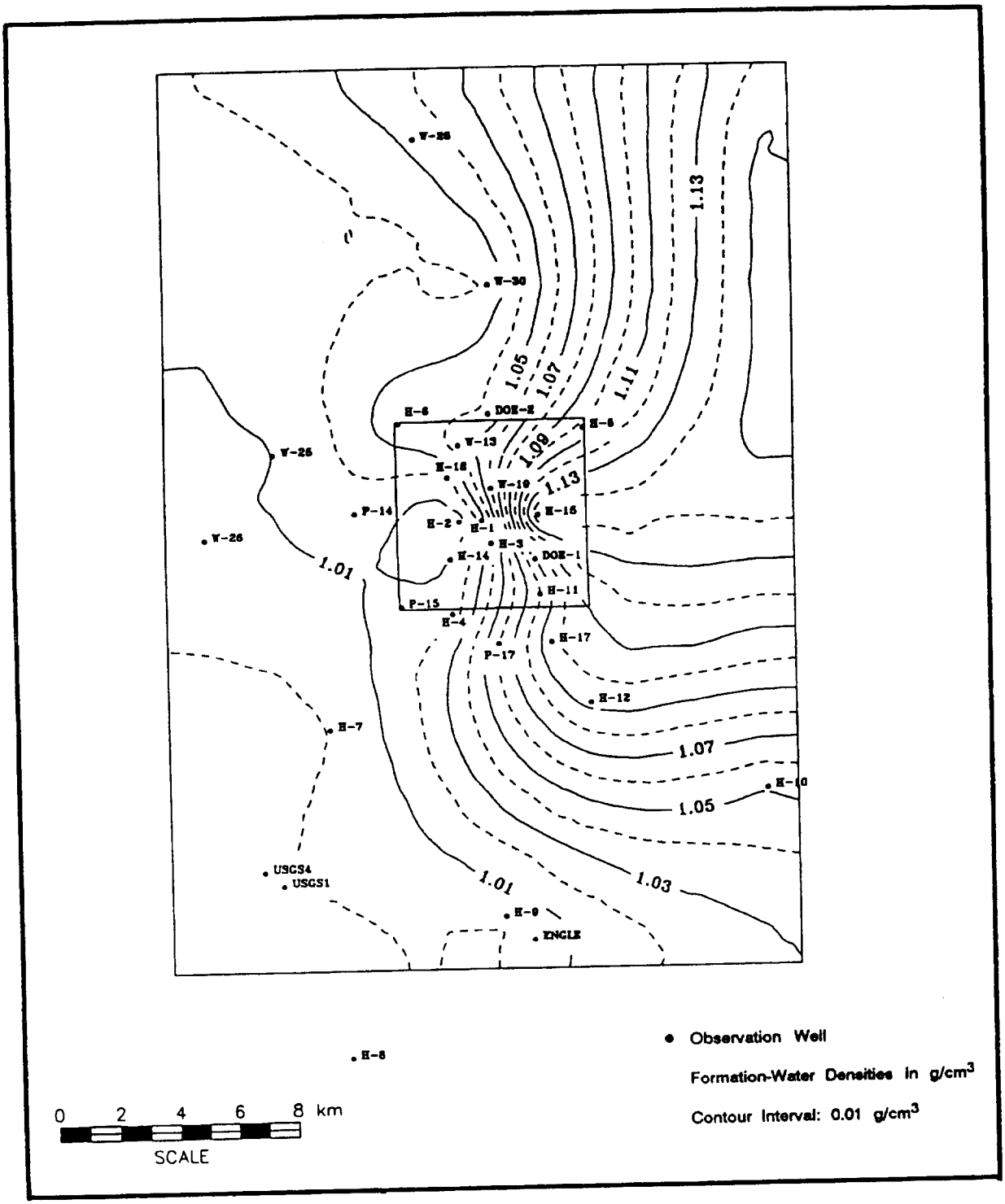

Figure 4.6 The distribution of formation fluid density obtained by interpolation between the measured values using kriging (reproduced from *LaVenue et al. [1990]*).

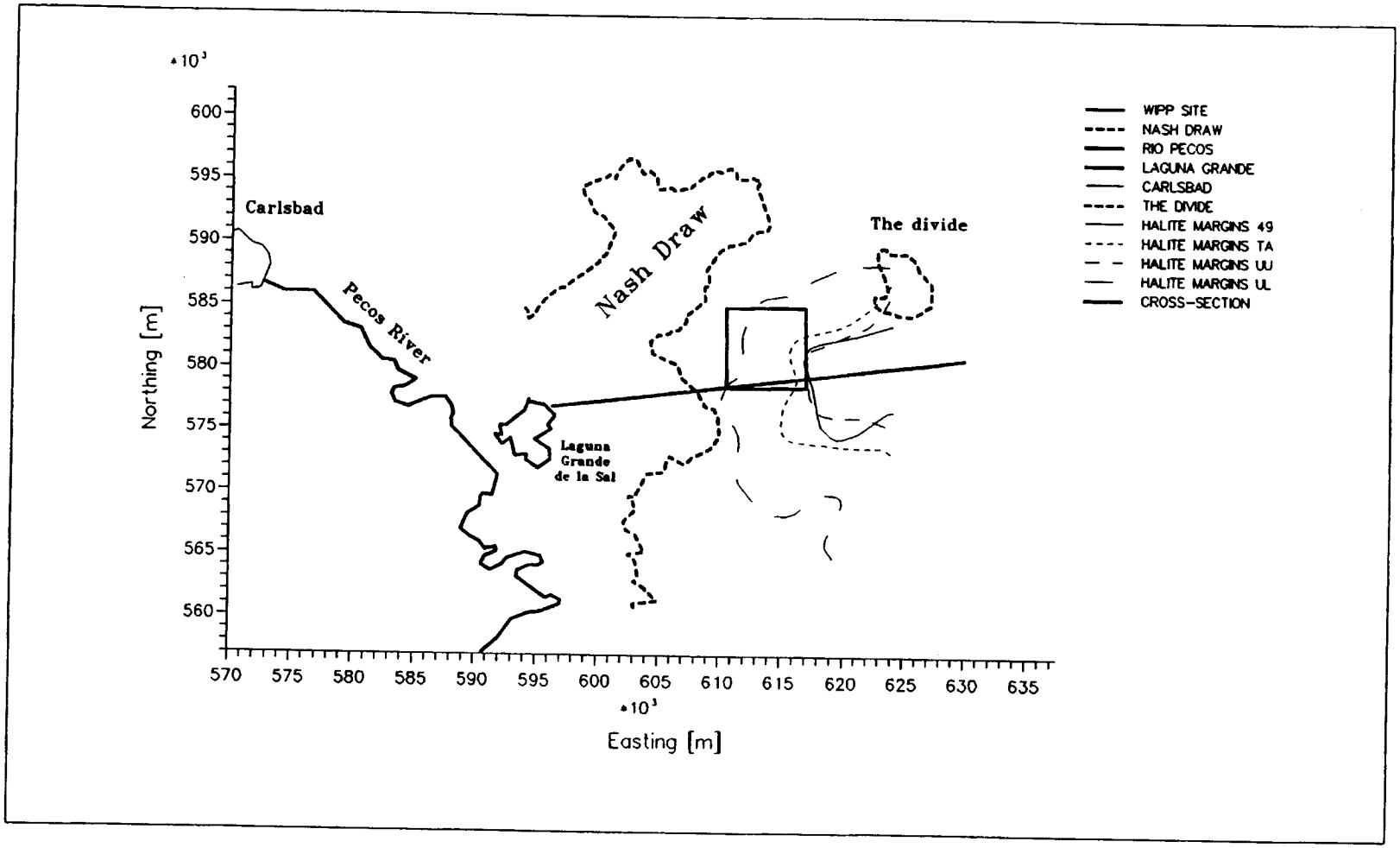

Figure 4.7 The line of the vertical cross section modelled by the BGR project team. (In the legend, 49 denotes the Forty-Niner Member, TA denotes the Tamarisk Member, UU denotes the upper part of the unnamed lower member, and UL denotes the lower part of the unnamed lower member.)

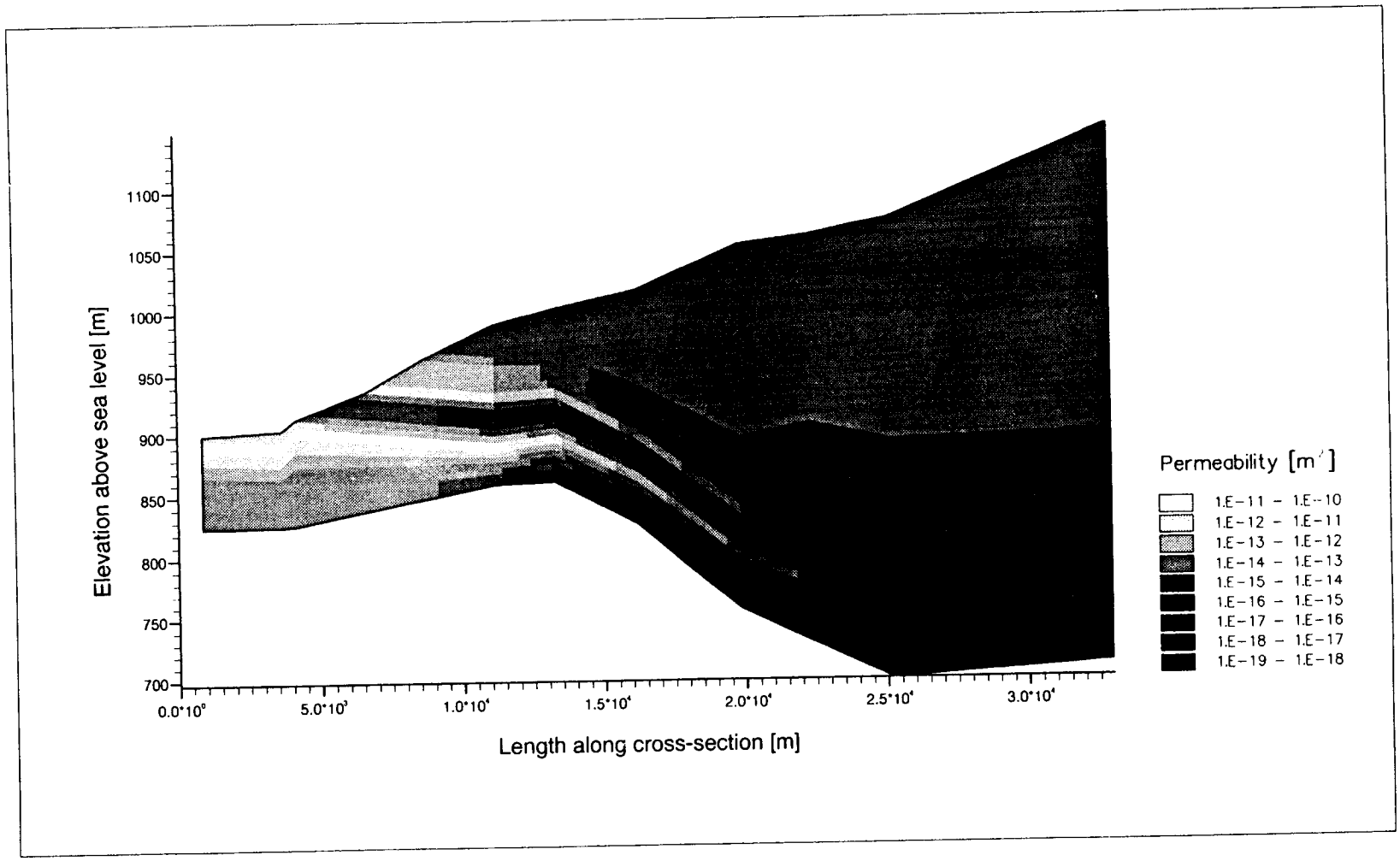

Figure 4.8 The distribution of permeability in the two-dimensional vertical cross section model used by the BGR project team.

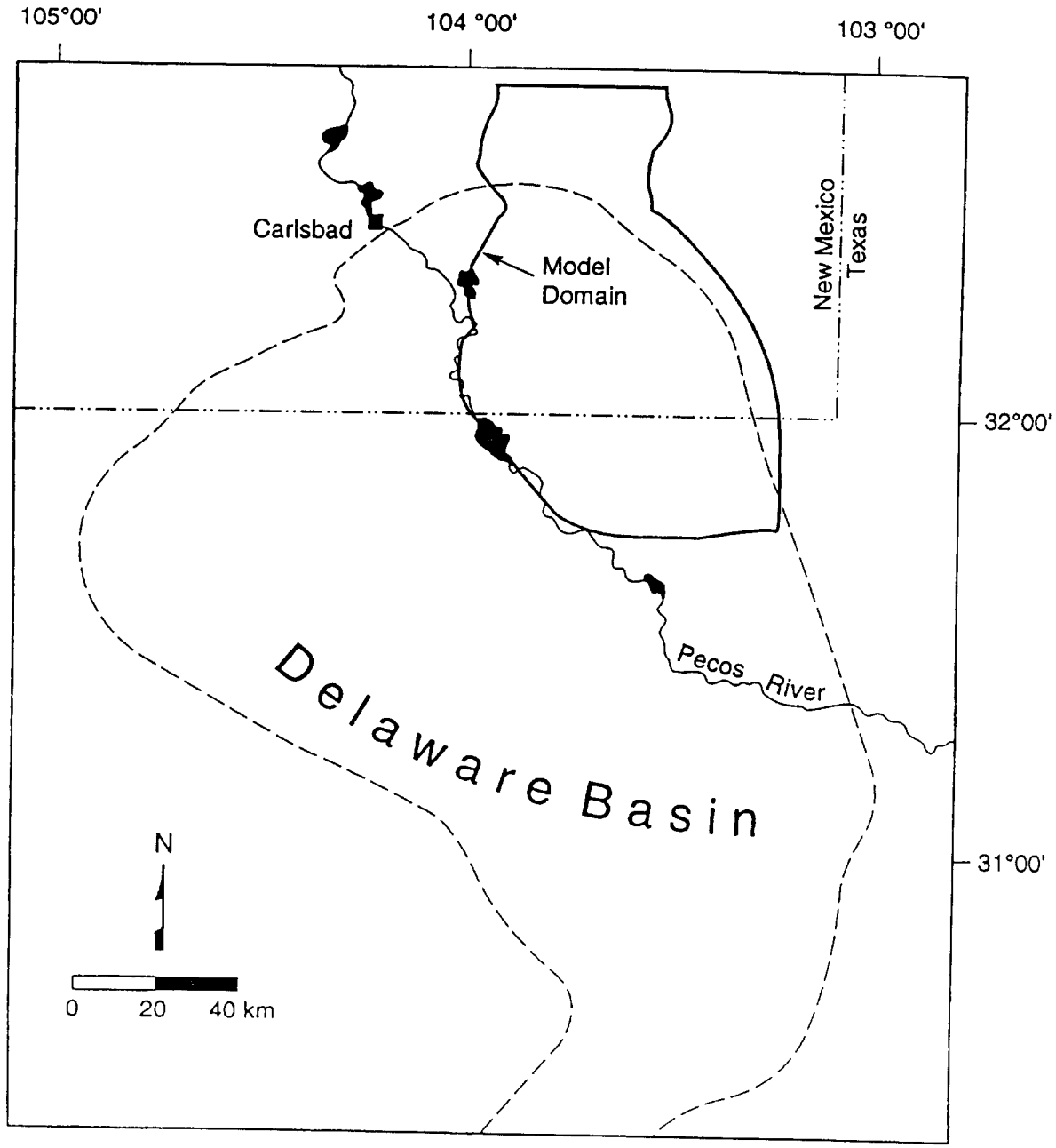

Figure 4.9 The location of the region modelled by the SNL project team. The region modelled comprised all the rocks above the Salado in the indicated area.

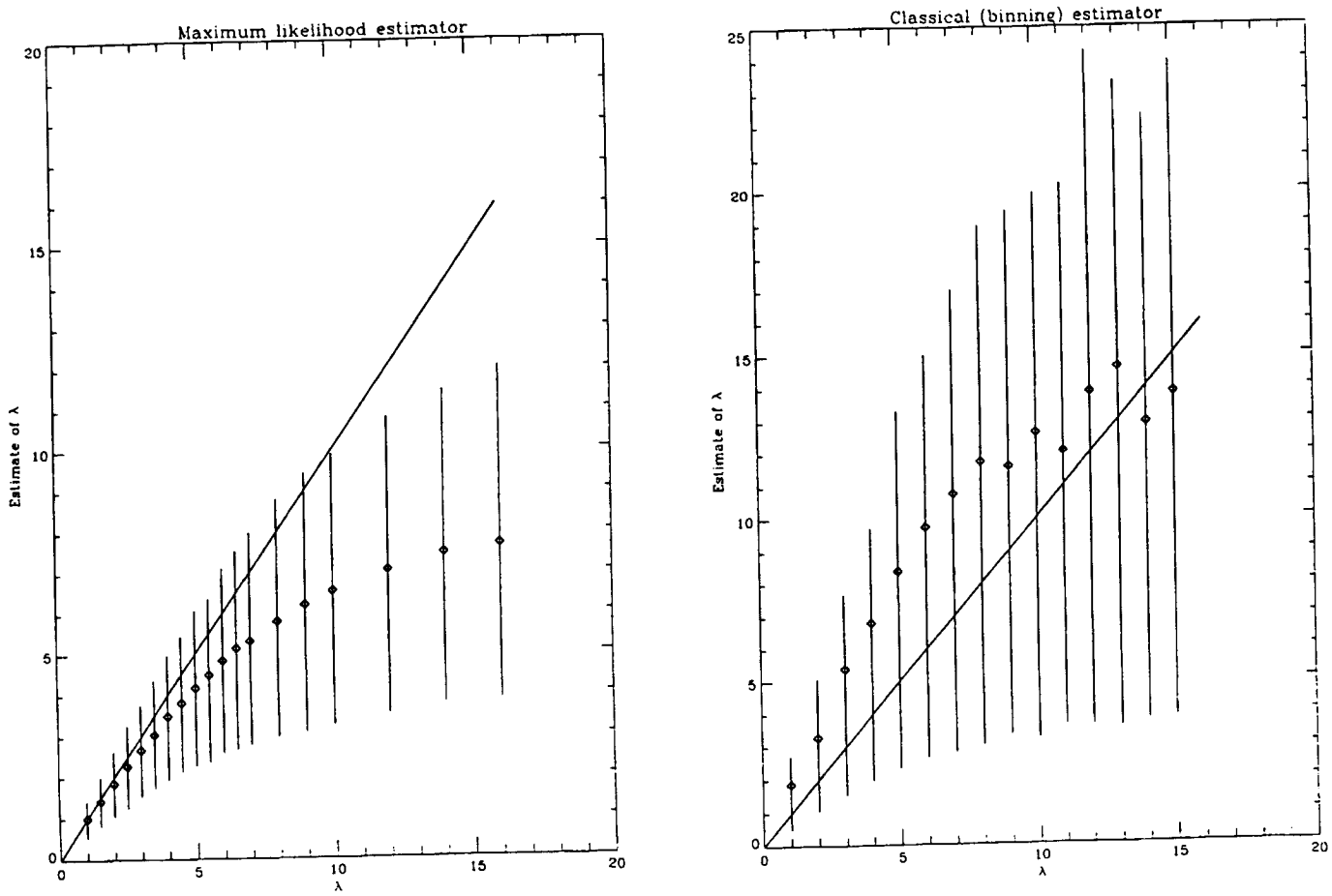

Figure 4.10 The behaviour of the estimators of λ as a function of the actual λ. (a) the maximum likelihood estimator, (b) the estimator obtained by least-squares fitting to the experimental variogram for one particular choice of classes. For each value of λ for which Monte-Carlo simulations were undertaken a diamond is plotted at the mean of the estimated λ, together with a line extending one standard deviation either side of the mean. As can be readily seen from the Figure, the confidence intervals on the underlying λ, considered as a function of the estimated λ are very large.

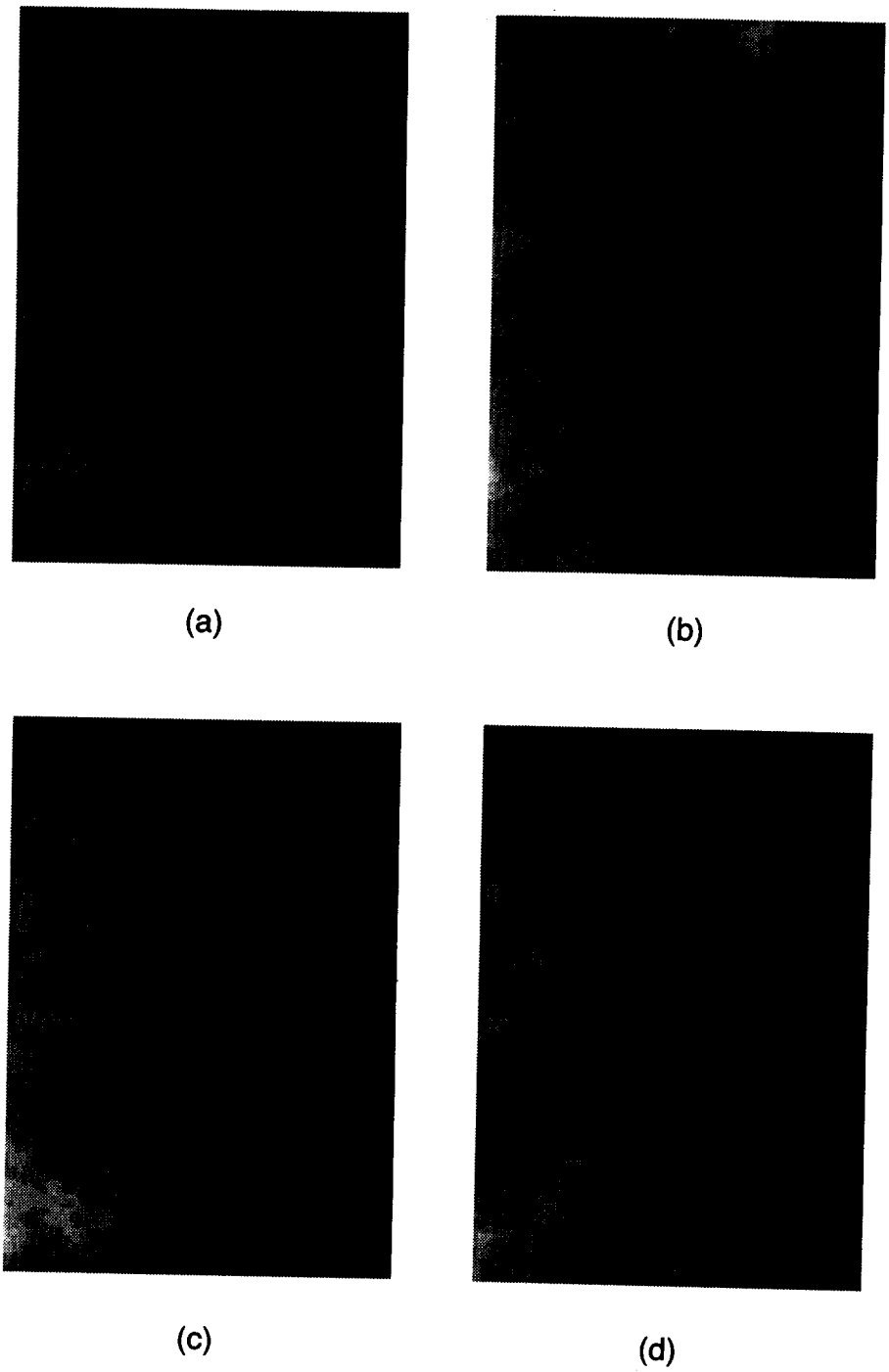

Figure 4.11 Realizations of the transmissivity field obtained by the AEA project team for the stochastic model with a constant mean and an exponential covariance (with parameters estimated by fitting to the experimental variogram). (a) the field obtained by interpolating between the measurements using kriging, (b), (c) and (d) three conditioned realizations. (Light denotes high transmissivity and dark denotes low transmissivity.)

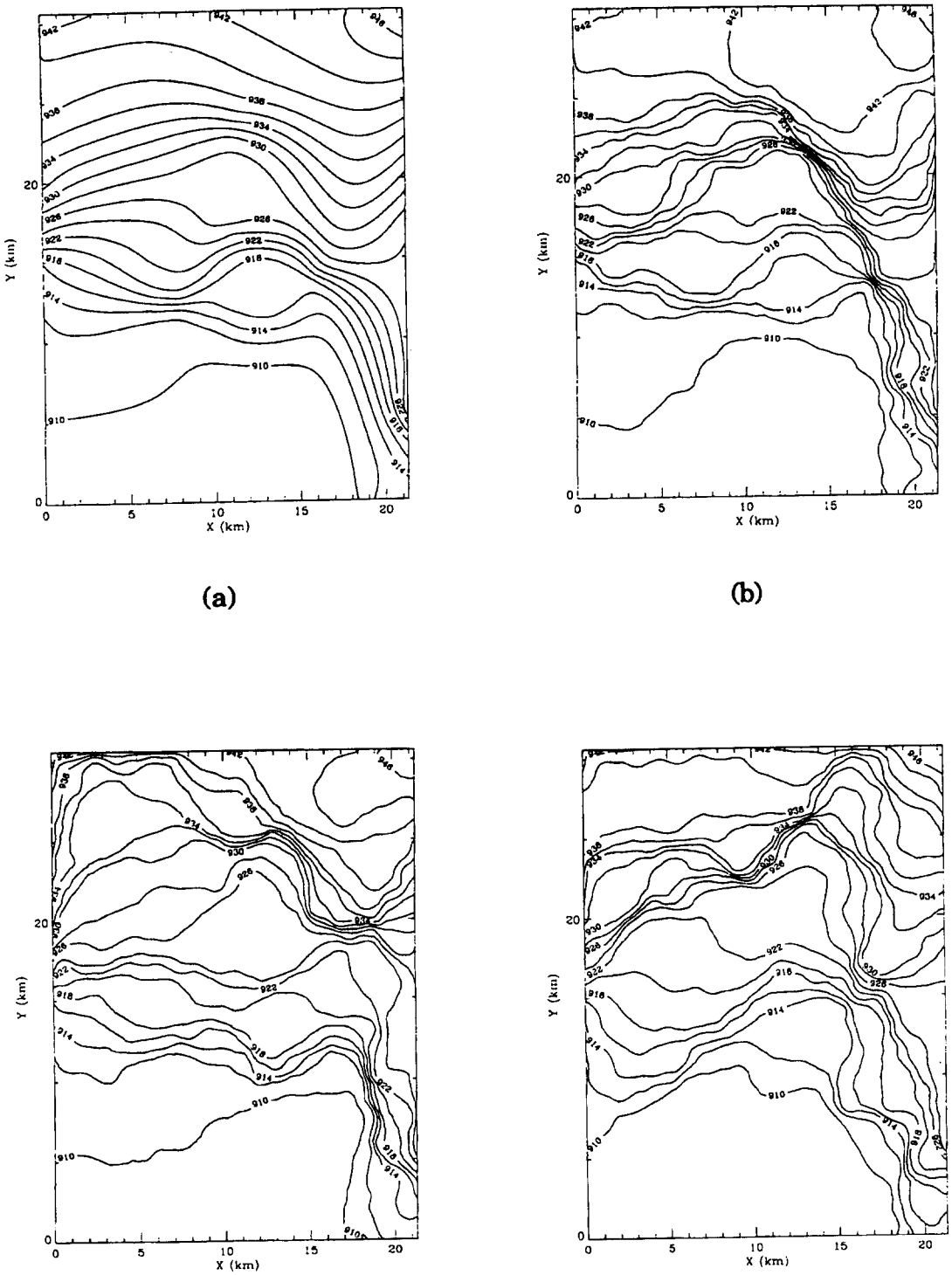

Figure 4.12 The (freshwater) head field computed by the AEA project team for the transmissivity realizations shown in Figure 4.11.

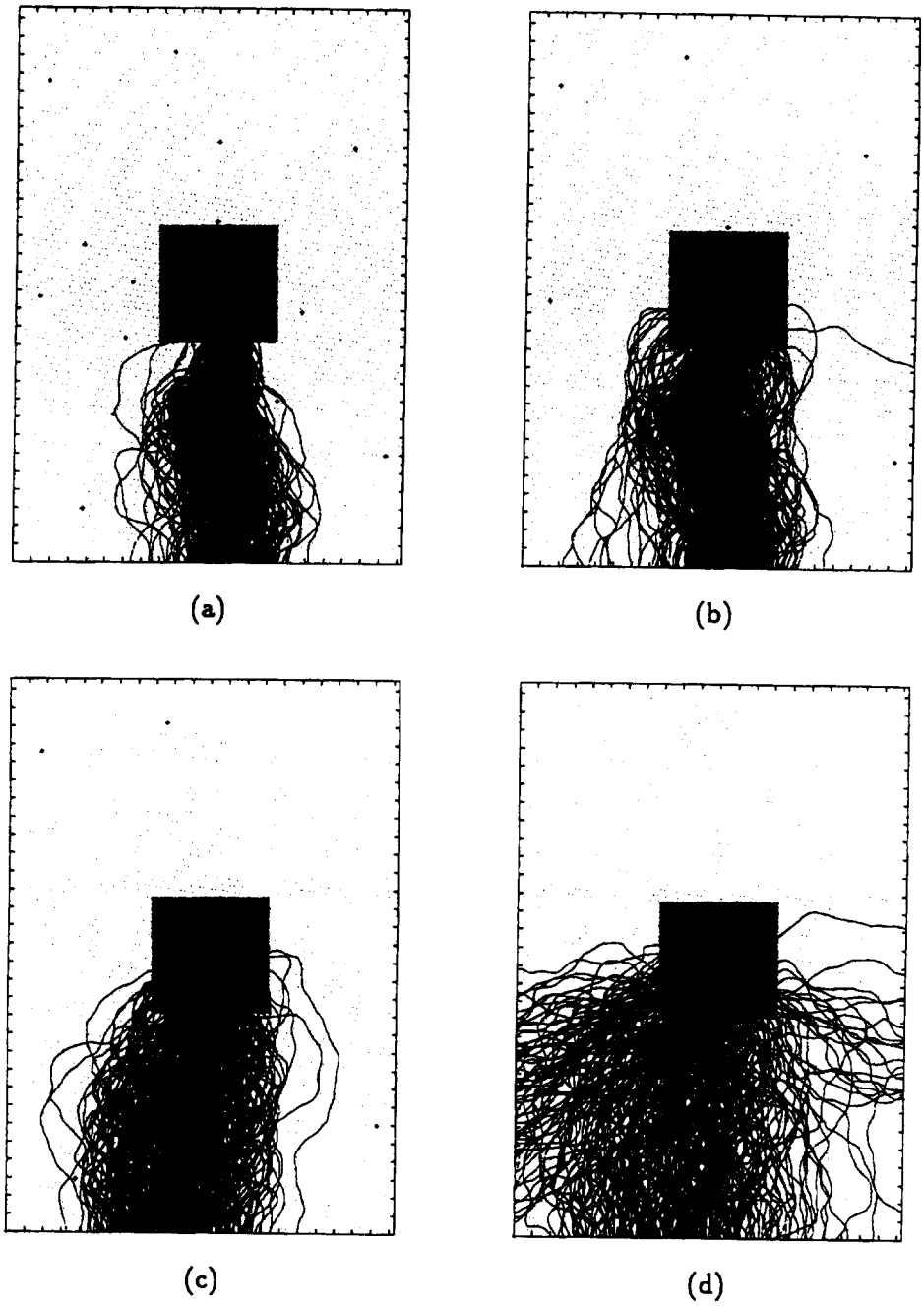

Figure 4.13 Pathlines computed by the AEA project team for 300 realizations of the transmissivity field for the stochastic model with an exponential covariance. (a) realizations conditioned on all 39 transmissivity measurements in the domain modelled, (b) realizations conditioned on 20 transmissivity measurements only, (c) realizations conditioned on 10 transmissivity measurements only, (d) unconditioned realizations. (The ticks around the boundary are spaced at 1km intervals, the central square is the WIPP site itself, and + denotes a borehole at which the measured transmissivity was used to condition the realizations.)

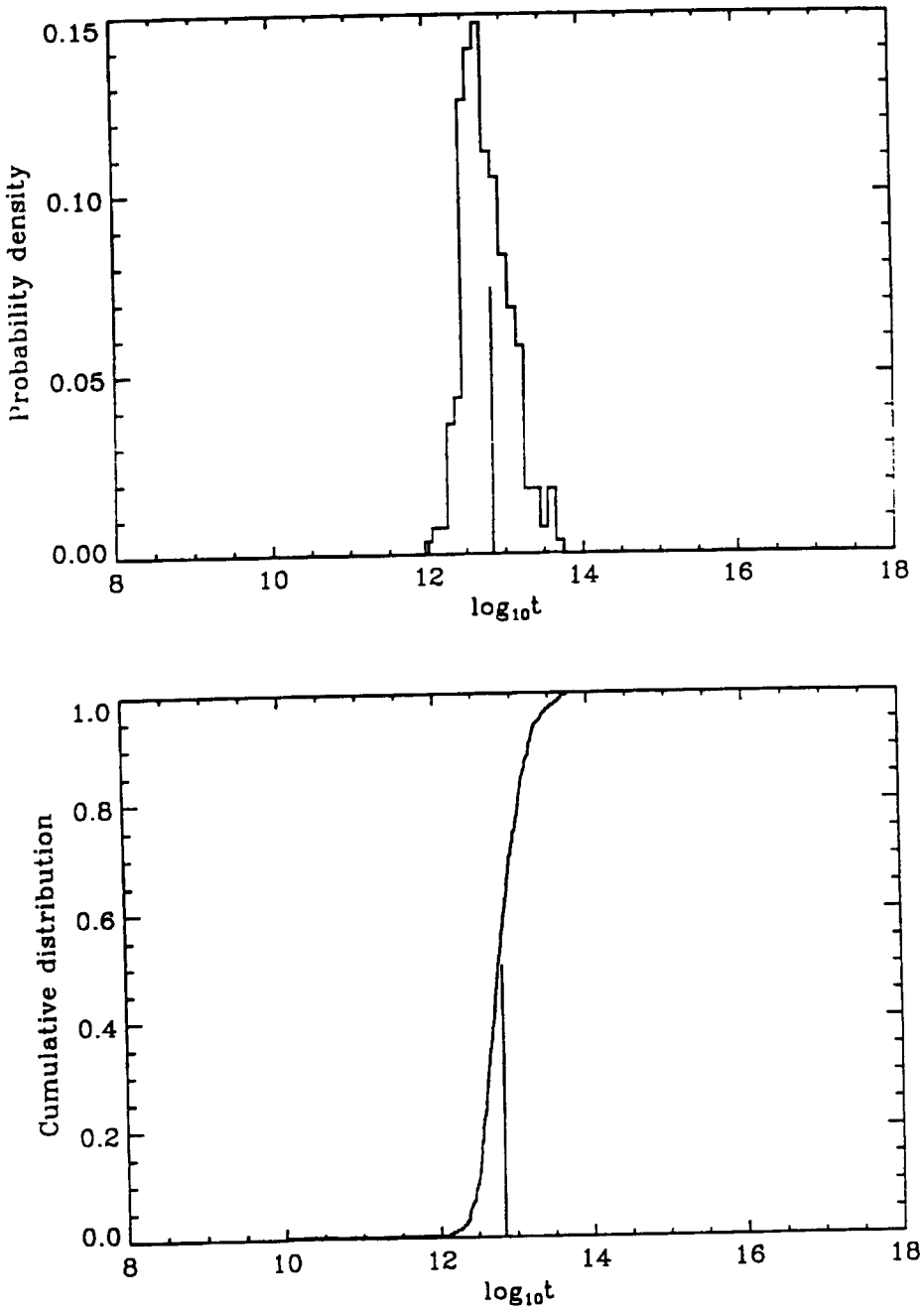

Figure 4.14 The probability density function and cumulative distribution function for the logarithm (to base ten) of the travel time (in seconds) from the location of borehole H-1 to the boundary of the domain modelled as obtained by the AEA project team from results for 300 realizations. The vertical line in each plot is at the travel time in the transmissivity field obtained by interpolating the data using kriging (see Figure 4.11(a)).

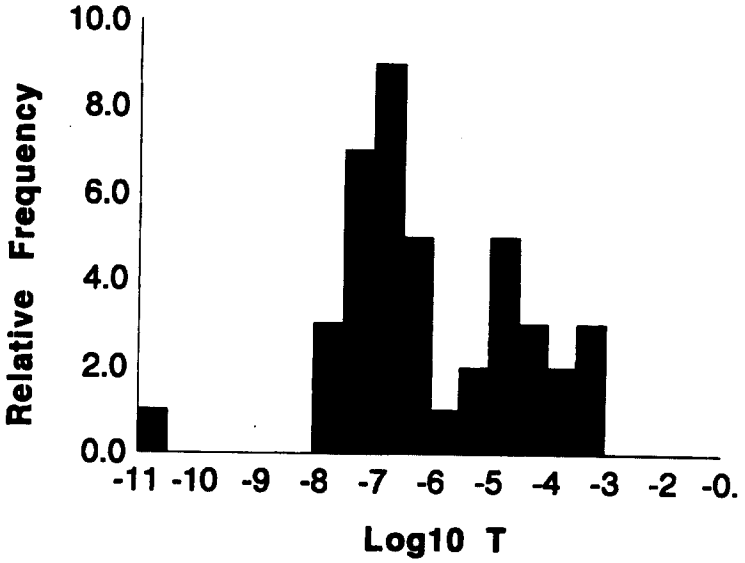

Figure 4.15 Histogram of the raw data for the logarithm (Z) of the transmissivity of the Culebra Dolomite.

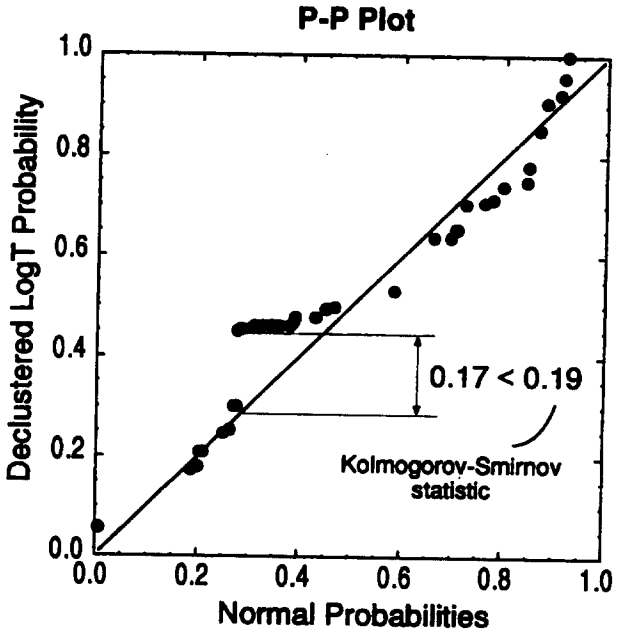

Figure 4.16 The comparison produced by the UPV project team of the probabilities of the declustered values of the logarithm of the transmissivity with a normal probability distribution. The Kolmogorov-Smirnov statistic is just the largest vertical difference between a point on this plot and the line with unit slope. If this statistic is greater than the critical value then it is unlikely that the declustered data are samples from from a normal distribution.

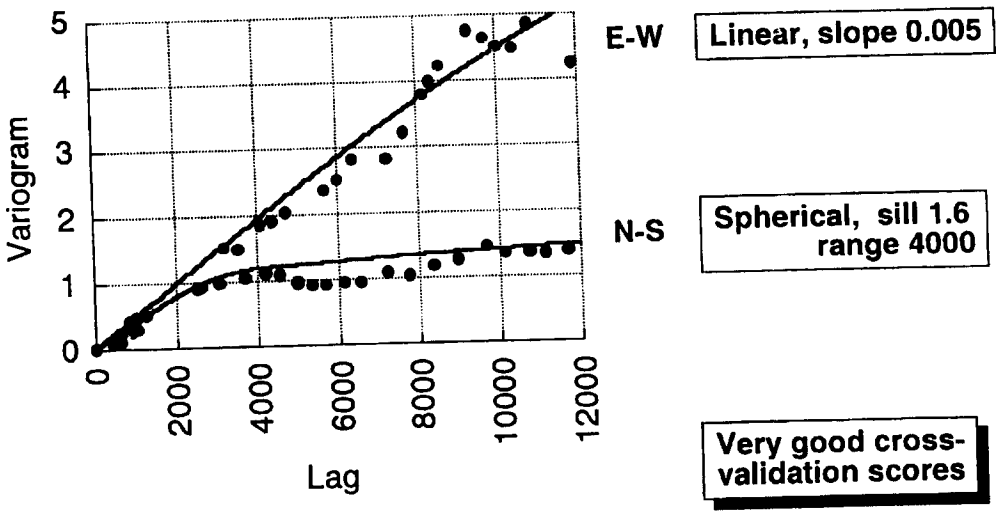

Figure 4.17 The directional variograms obtained by the UPV project team.

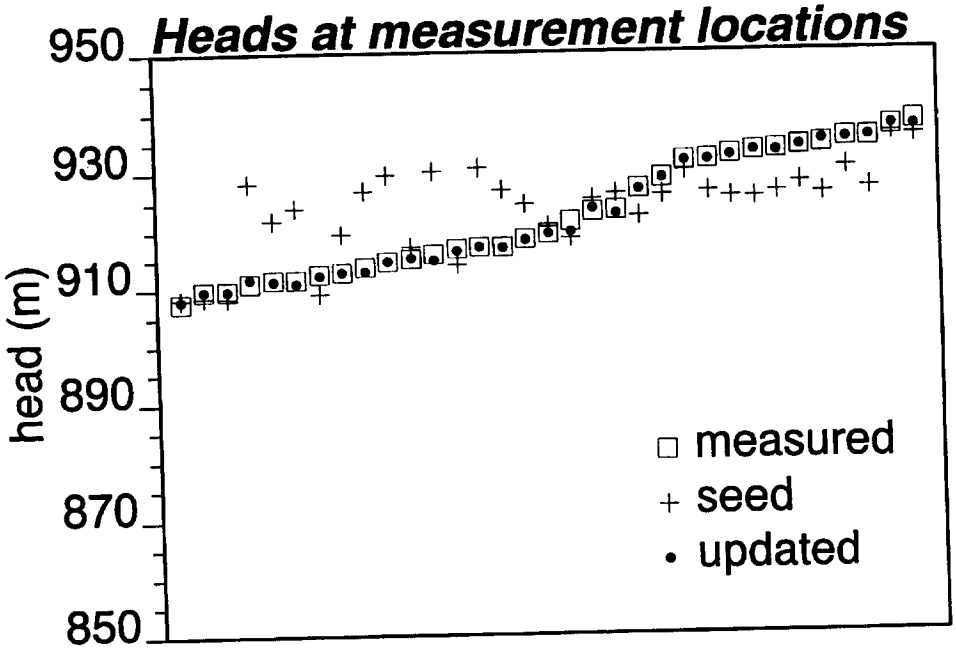

Figure 4.18 Comparison of observed heads and heads calculated by the UPV project team. The Figure presents the measured heads in order of increasing magnitude (shown by a square), the corresponding heads computed for a realization conditioned on measured values of Z only (shown by +), and the corresponding heads computed after the realization was conditioned on measured heads as well using the technique developed by the UPV project team (shown by .). As can be seen the match to observations has been considerably improved by conditioning on the head data.

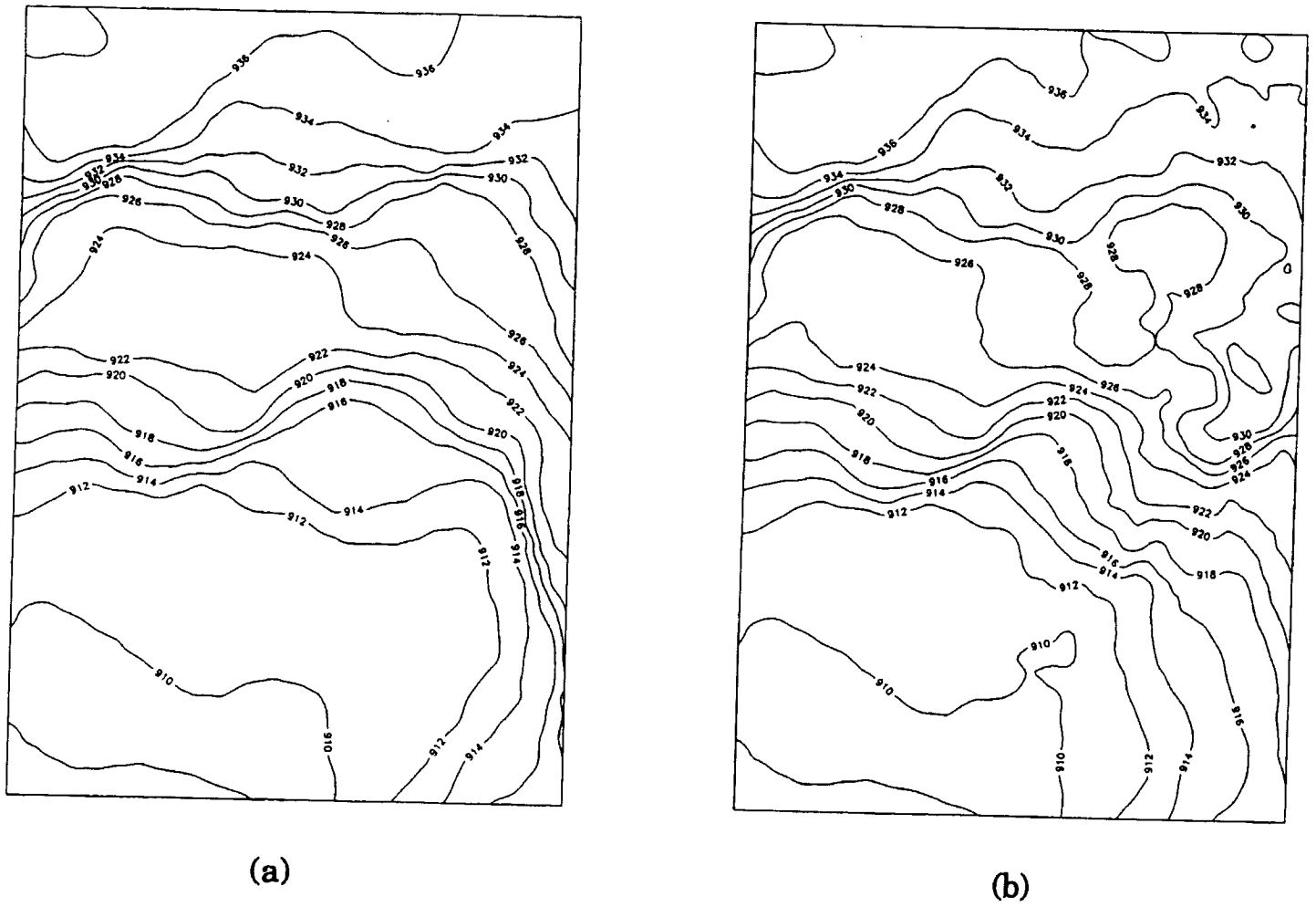

Figure 4.19 Illustration of the effects of taking into account the variation in groundwater density on the head computed by the UPV project team for one realization. (a) density variations not taken into accounty, (b) density variations taken into account.

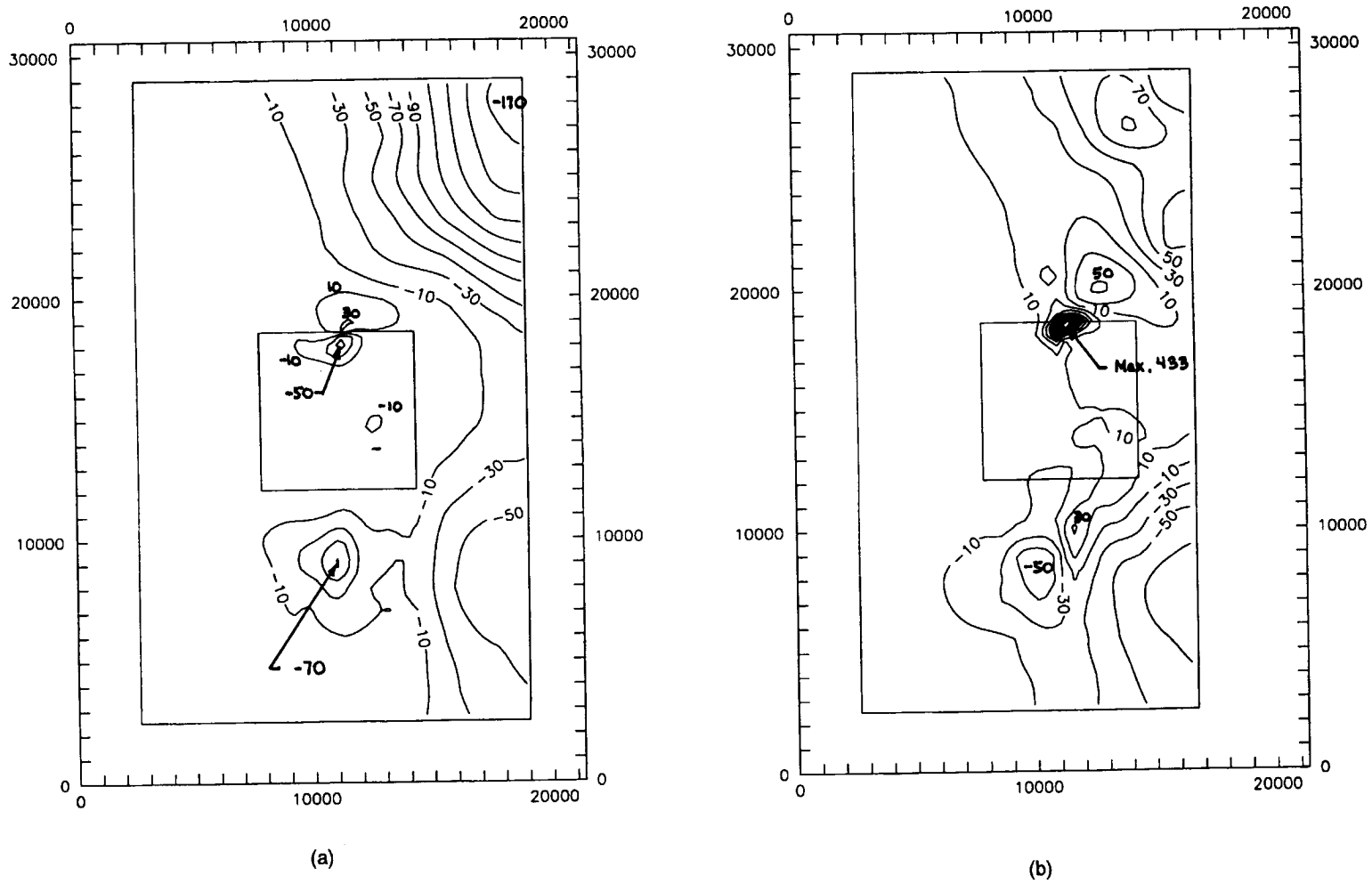

Figure 4.20 The difference between the Darcy flux in the base case and that in the variant with freshwater everywhere as computed by the AECB project team. (a) difference in the direction of the flux (a negative sign corresponds to the direction of the flow in the variant with freshwater everywhere being shifted clockwise relative to the direction of the flow in the base case), (b) difference in the magnitude of the flux.

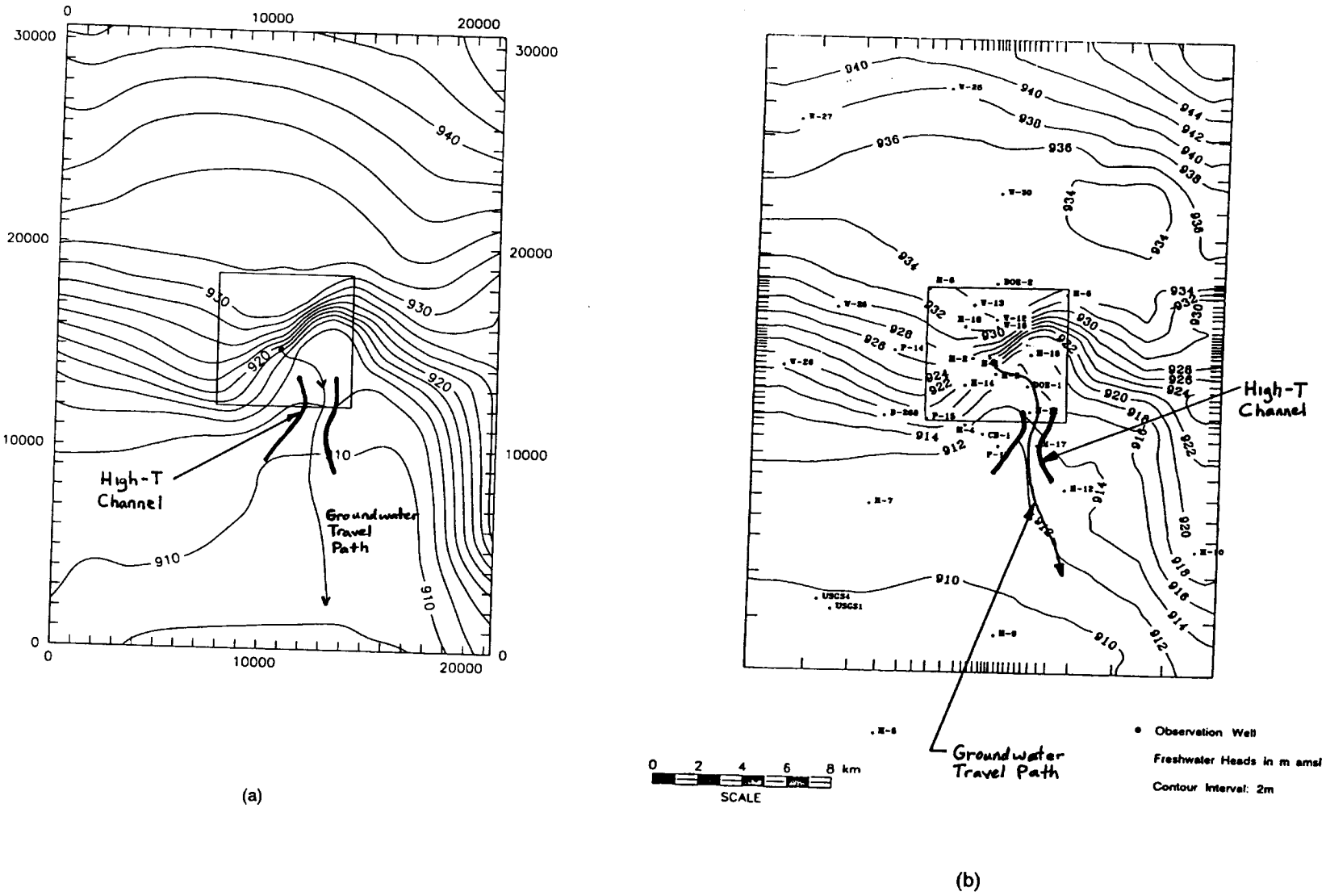

Figure 4.21 Freshwater heads and pathlines from the centre of the WIPP site in the AECB study. (a) for the variant with freshwater everywhere, (b) for the base case from *LaVenue et al. [1990]*.

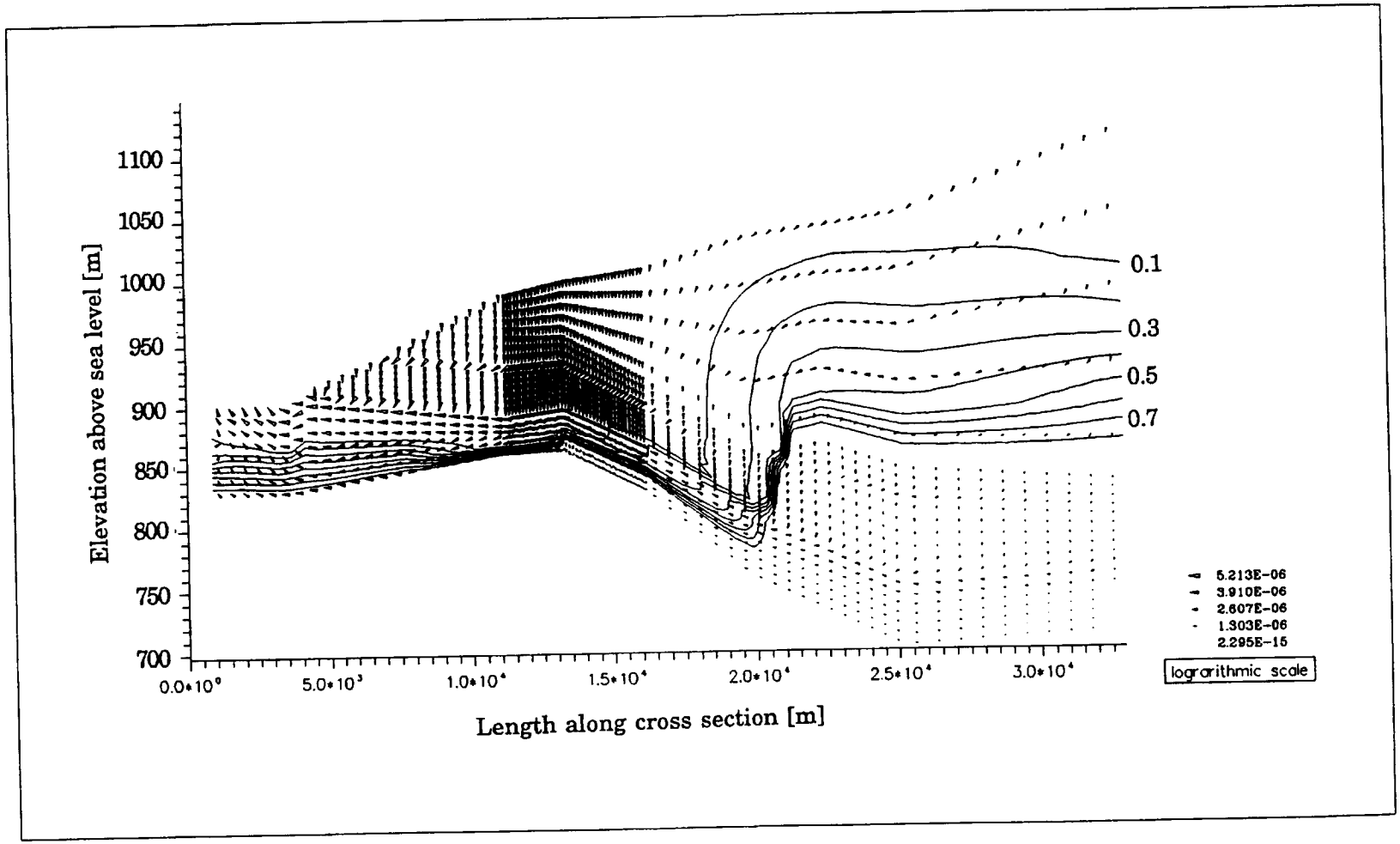

Figure 4.22 The flow field and distribution of salinity at four million years computed by the BGR project team. This was taken to be close to the steady-state. The concentration contours are at 0.1, 0.2, 0.3, 0.3, 0.4, 0.5, 0.6, 0.7, and 0.8 of saturation.

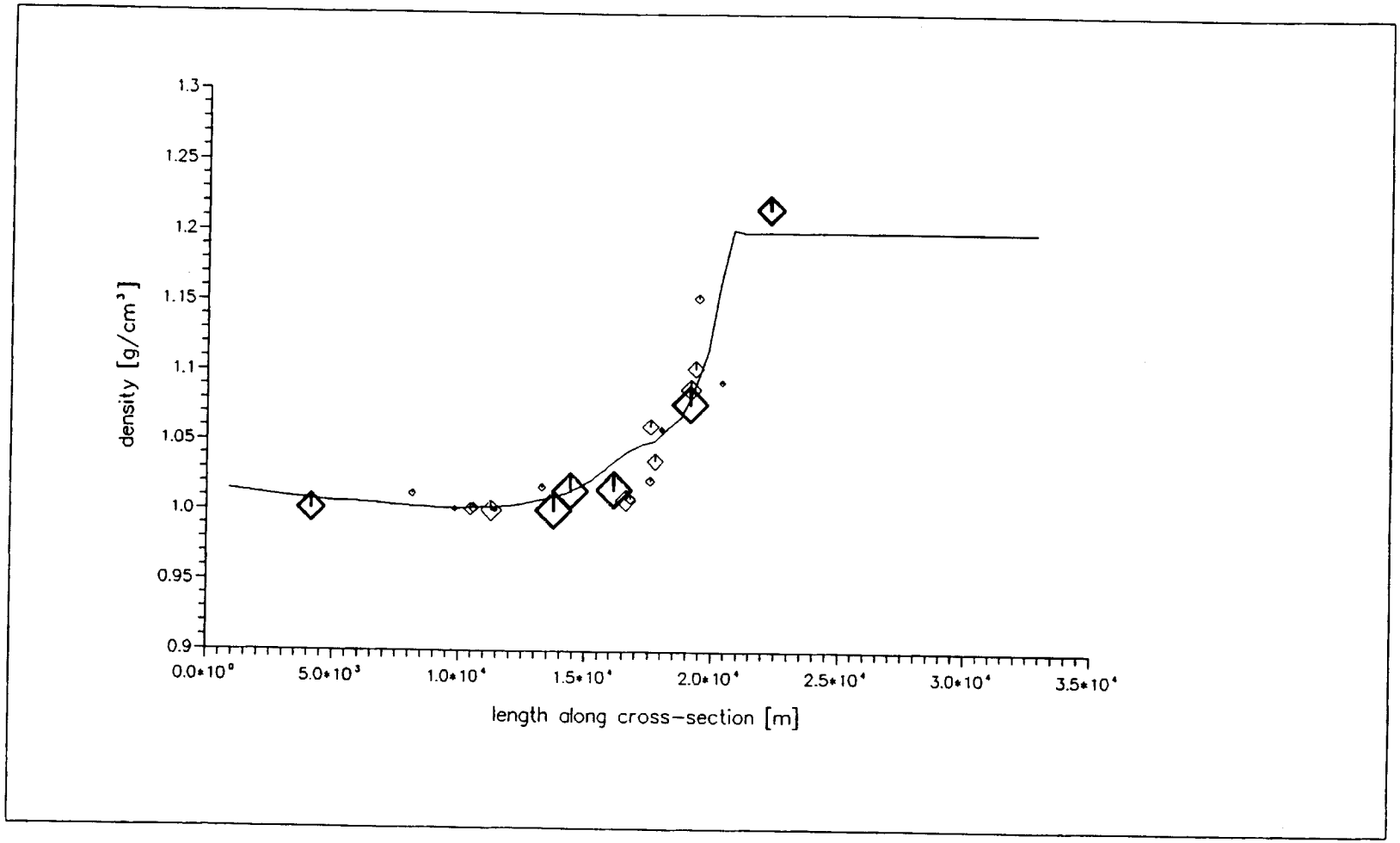

Figure 4.23 Comparison of the measured groundwater density with that computed by the BGR project team using their two-dimensional vertical cross-section model. The size of the markers is inversely proportional to the distance from the cross section of the borehole where the concentration was measured.

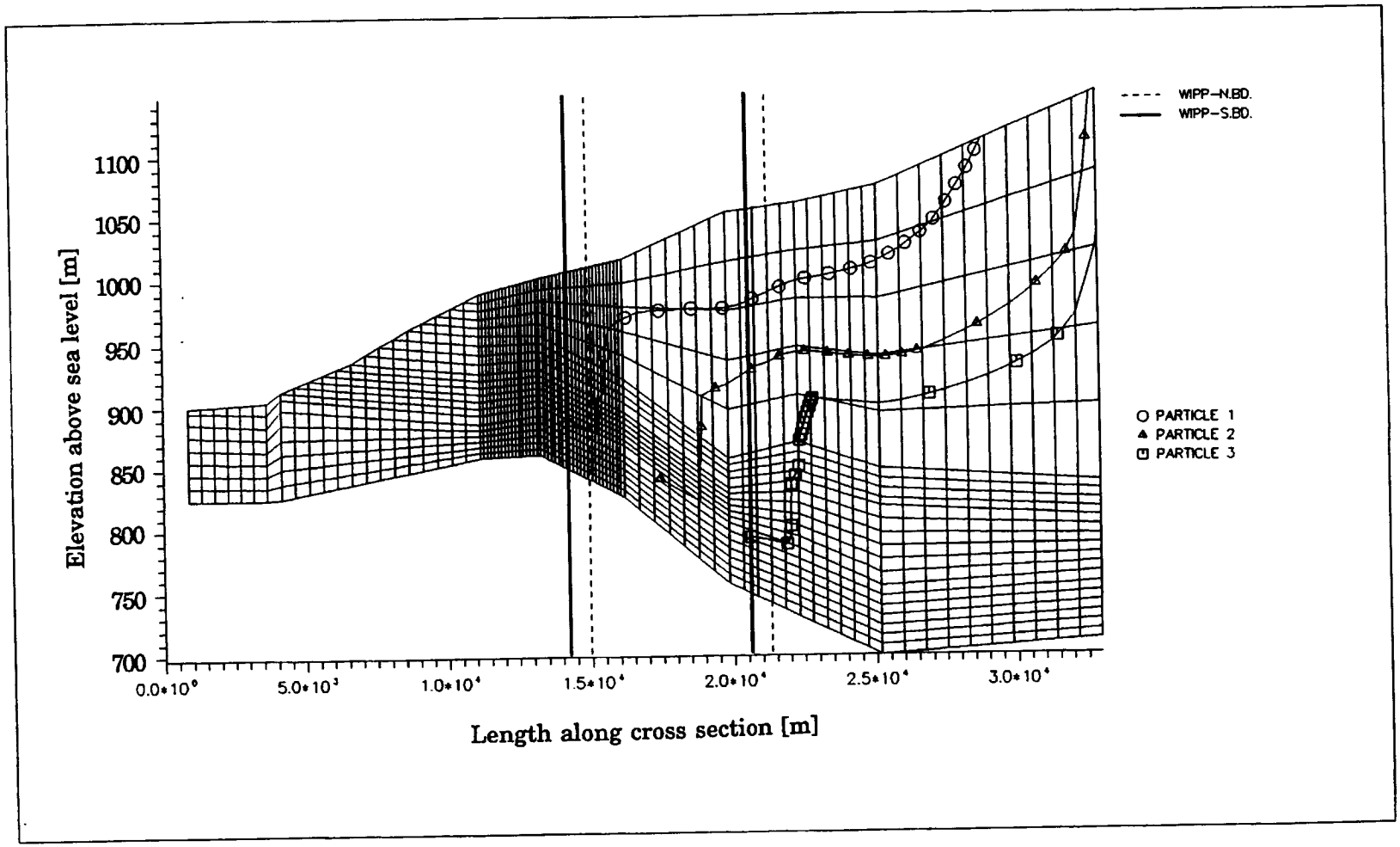

Figure 4.24 The pathlines computed by the BGR project team by tracking back along the flow. (WIPP-NBD denotes the northern corners of the WIPP site and WIPP-SBD denotes the southern corners of the WIPP site.)

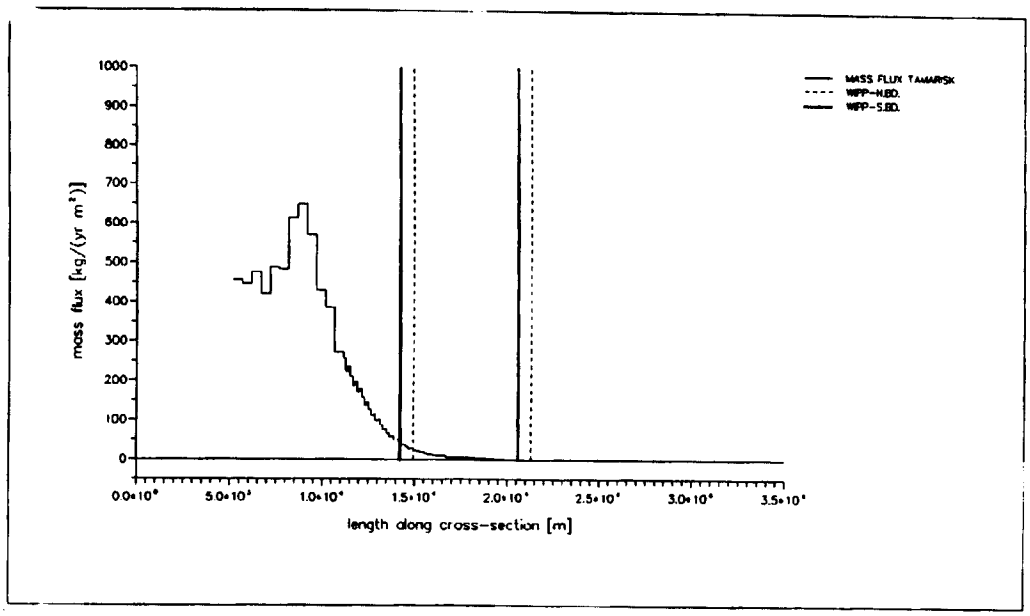

(a)

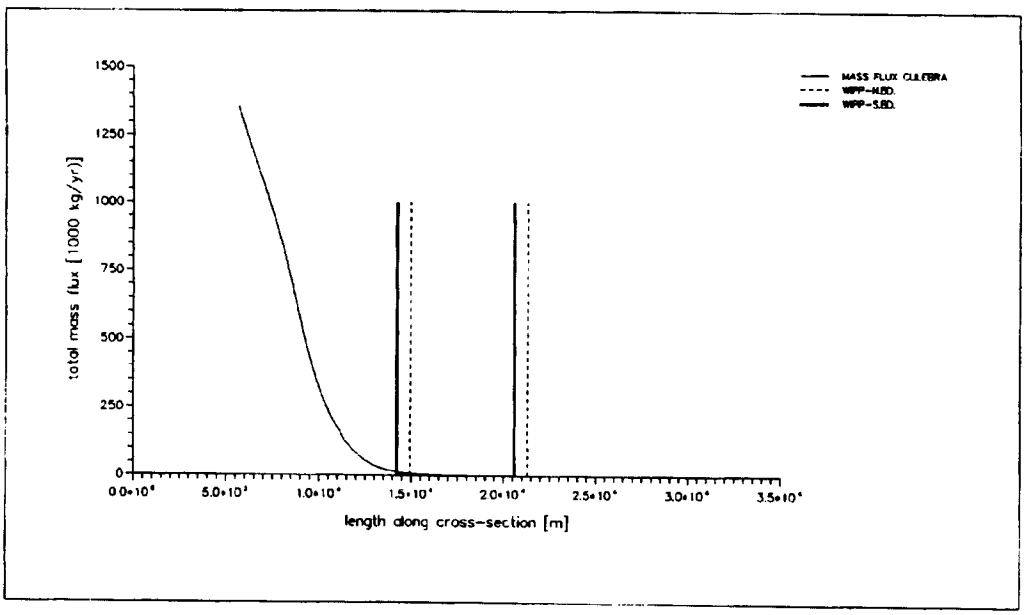

(b)

Figure 4.25 Groundwater fluxes computed by the BGR project team. (a) the vertical flux through the Tamarisk Member (MASS FLUX TAMARISK), and (b) the horizontal flux in the Culebra Dolomite (MASS FLUX CULEBRA). (WIPP-NBD denotes the northern corners of the WIPP site and WIPP-SBD denotes the southern corners of the WIPP site.)

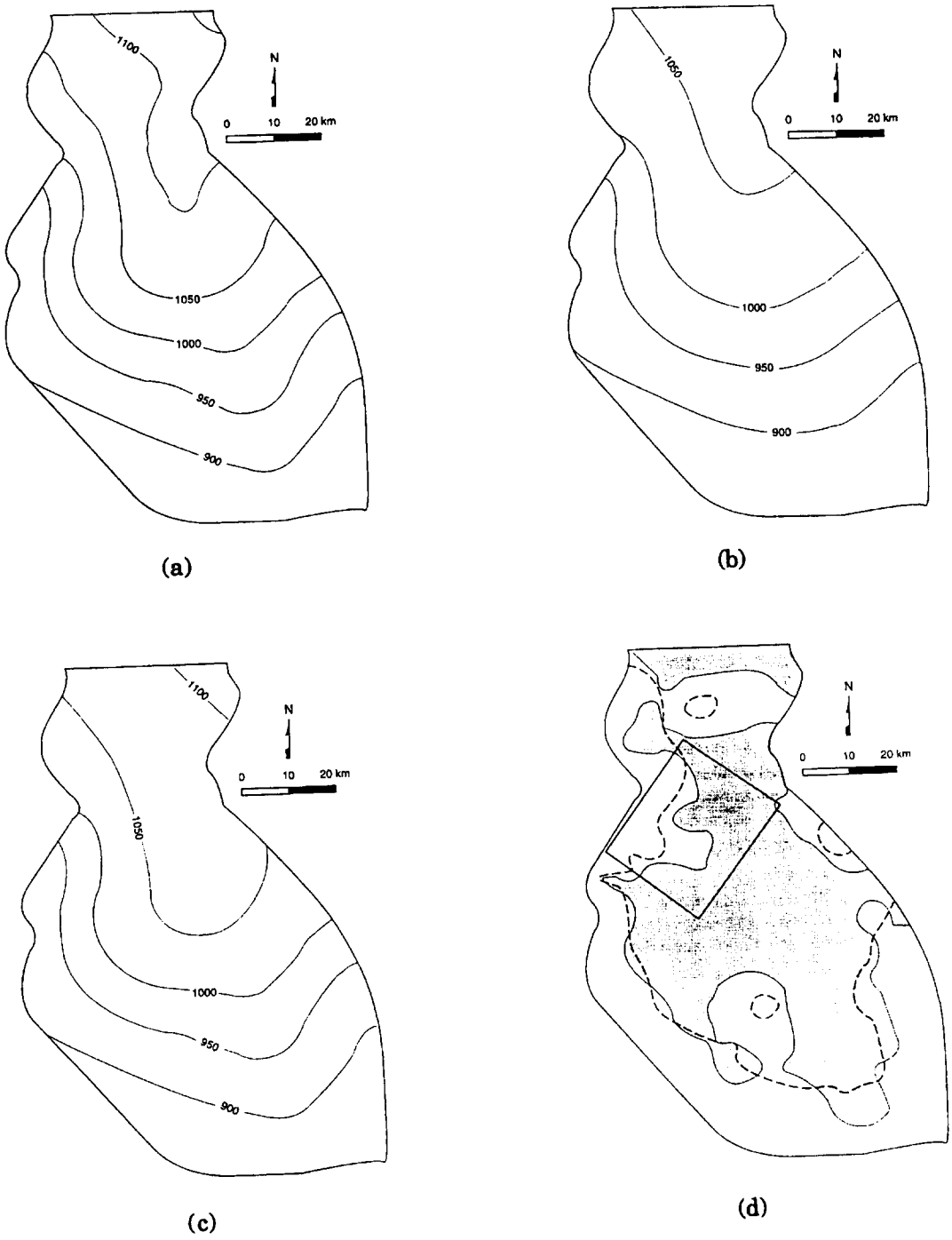

Figure 4.26 Illustration of the results obtained by the SNL project team. (a) the initial calculated head field, (a) the calculated head field after 21000 years (at the end of the dry period), (b) the calculated head after a further 20000 years in which infiltration was maintained at 0.5mm per year, (d) the distribution of vertical leakage (the region of downward flux is shown stippled). The rectangular region in (d) is the region for which horizontal and vertical fluxes were compared by the project team.

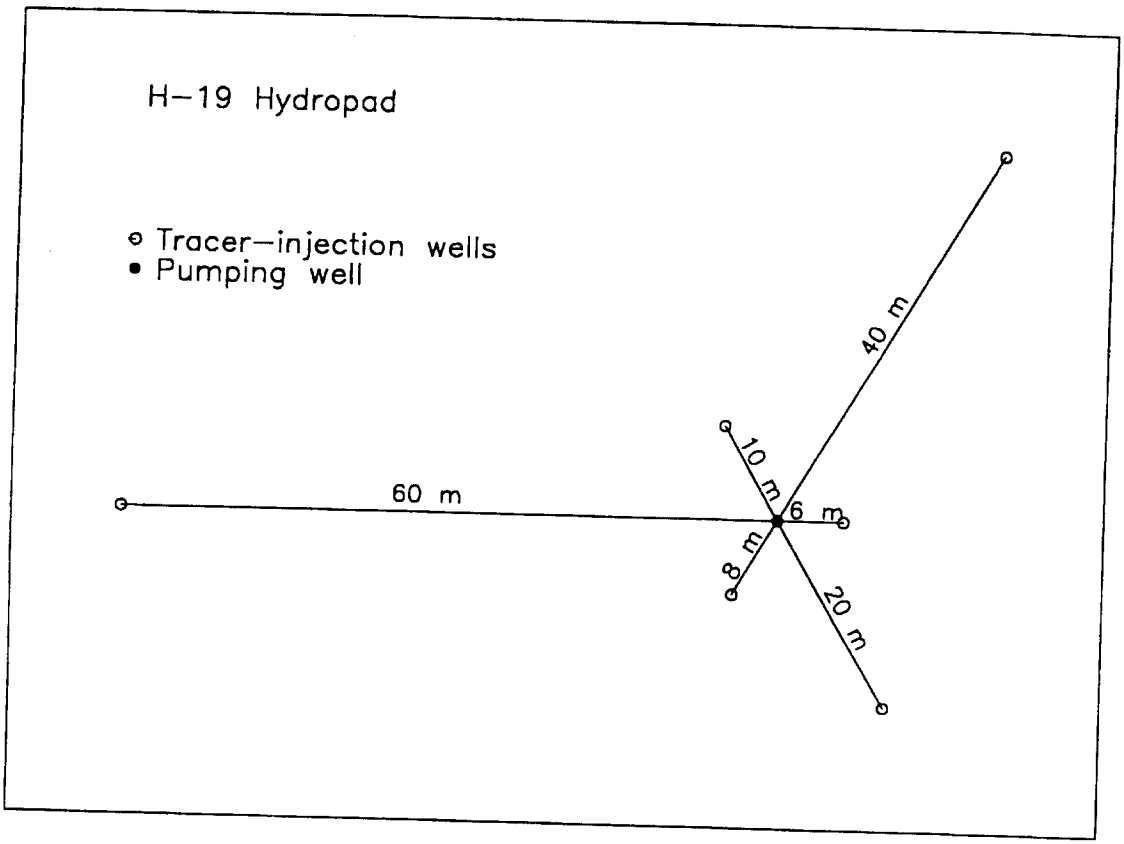

Figure 4.27 The layout of the boreholes in the proposed tracer experiment.

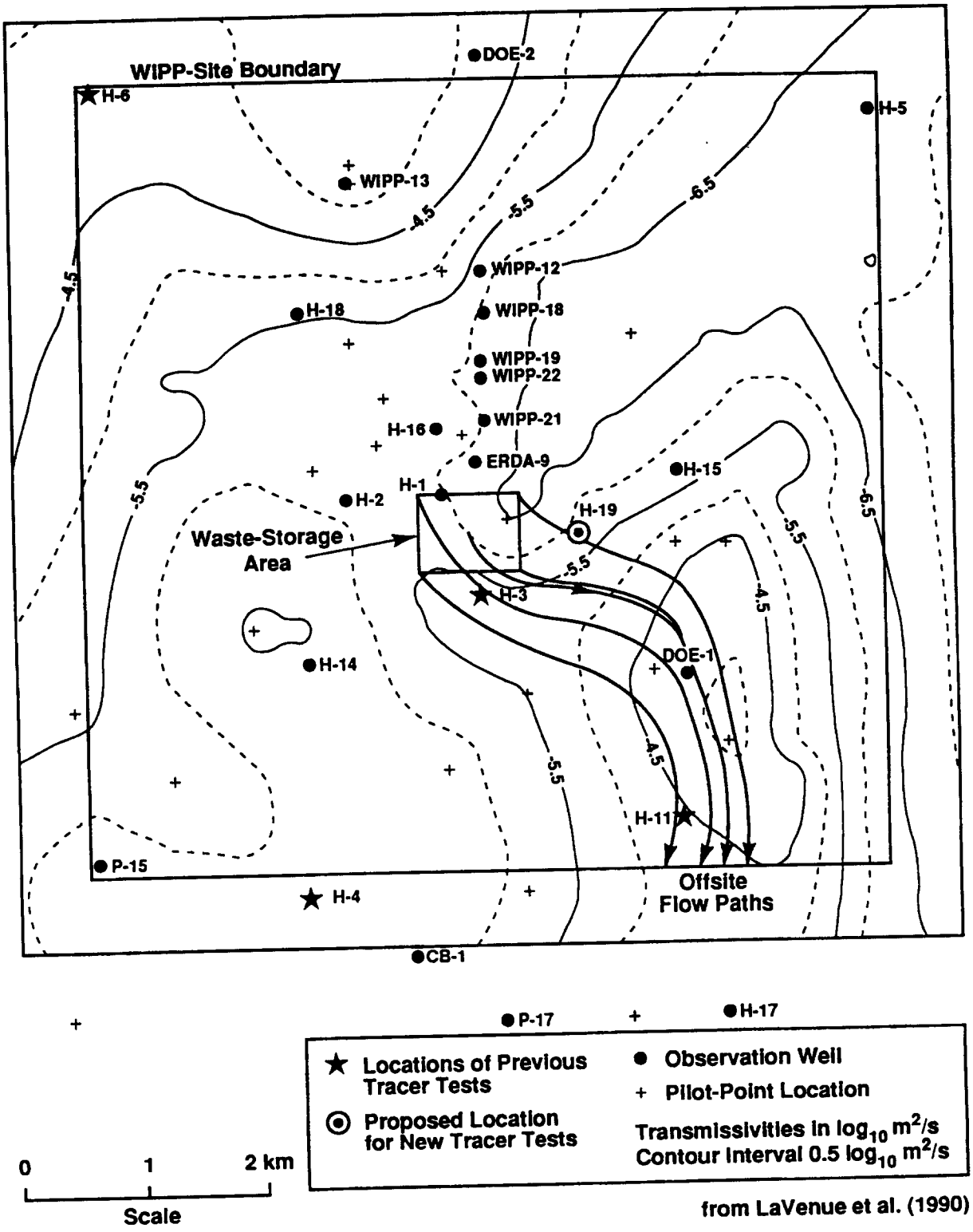

Figure 4.28 The locations of tracer tests at the WIPP site. The locations of previous tests are shown by stars, and possible locations for the proposed new experiment are shown by circles.

References

Ababou R., Sagar B. and Wittmeyer G. (1992): Testing procedure for Spatially Distributed Flow Models. Adv. Water Res., vol. 2 of special issue on model validation, 1992.

Abelin H., Birgersson L., Moreno L., Widén H., Ågren T., and Neretnieks I. (1991): - A large - scale flow and Tracer Experiment in Granite, 2, Results and Interpretation, *Water Resour. Res., 27*(12), 3119-3126.

Abelin H., Birgersson L., Widén H., Ågren T., Moreno L., Neretnieks I. (1990): Channelling Experiment, Stripa Project, Report TR 90-13, 1990.

Abelin H., Birgersson L., Gidlund J., Moreno L., Neretnieks I., Widén H., and Ågren T. (1987): 3D Migration Experiment - Report 3, Part I, Performed Experiments, Results and Evaluation, Stripa Project, Report TR 87-21, Stockholm.

Abelin H., Neretnieks I., Tunbrant S. and Moreno L. (1985): Final Report of the Migration in a Single Fracture - Experimental Results and Evaluation. Dep. Chemical Engineering, Royal Institute of Technology, Stockholm, Sweden Stripa Project Report-85-03.

Andersson J. and Dverstorp B. (1987): Conditional Simulation of Fluid Flow in Three-Dimensional Networks of Discrete Fractures, *Water Resour. Res., 23*(10),1876-1886.

Andersson J-E., Ekman L., Gustafsson E., Nordqvist R. and Tirén S. (1989): Hydraulic Interference Tests and Tracer Tests within the Brändan Area, Finnsjön Study Site - The Fracture Zone Project Phase 3. SKB Technical Report TR 89-12.

Andersson P., Eriksson C-O., Gustafsson E. and Ittner, T. (1990): Dipole Tracer Experiment in a Low-Angle Fracture Zone at the Finnsjön Site, Central Sweden-Experimental Design and Preliminary Results. SKB Progress Report AR 90-24.

Andersson P., Nordqvist R., Persson T., Eriksson C-O., Gustafsson E. and Ittner T. (1993): Dipole Tracer Experiment in a Low-Angle Fracture Zone at Finnsjön - Results and interpretation. The Fracture Zone Project - Phase 3. SKB Technical Report 93-26.

Andersson P. (ed.) (1993): The Fracture Zone Project - Final Report. SKB Technical Report TR 93-20.

Andersson P. and Winberg A. (1994): INTRAVAL Working Group 2 summary report on Phase 2 analysis of the Finnsjön test case. SKB Technical Report TR 94-07.

Baase S. (1978): Computer algorithms Introduction to design and analysis. Addison-Wesley, London, p. 286.

Barker J.A. (1988): A generalized radial flow model for hydraulic tests in fractured rock, *Water Resour. Res., 24* (10),1796-1804.

Barker J.A. (1985): Block geometry function characterizing transport in densely fissured media, *J. of Hydrology, 77*, 263-279.

Billaux D. (1990): Hydrogéologie des milieux fracturés. Géométrie, connectivité et comportement hydraulique, Ph.D. thesis, ENSMP, Paris, 277 p.

Billaux D. and Guerin F. (1993): Connectivity and the continuum approximation in fracture flow modelling. In 4th Int. High-Level Radioactive Waste Management Conference, pp1118-1122, Las Vegas.

Billaux D., Chilès J.P., Hestir K., and Long J. (1989): Three-dimensional statistical modeling of a fracture rock mass - an example from the Fanay-Augères mine, *Int. J. Rock Mech. Min Sci. and Geomech. Abstr.*, 26 (3/4), pp. 281-299.

Billaux D. and Long J.C.S. (1988): Change a numerical model for three dimensional modeling of channelized flow in rock. Theory and design. LBL report, No. 24910, LBL, Berkeley, California.

Birgersson L., Widén H., Ågren T., Neretnieks I. and Moreno L. (1992): Site Characterization and Validation- Tracer migration experiment in the validation drift, Report 2, Part 1 Performed Experiments, Results and Evaluation, Stripa Project, Report TR 92-03.

Bourke P. (1987): Channeling of Flow Through Fractures in Rock, *Proceedings of GEOVAL-87*, International Symposium, Stockholm, Sweden, April 7-9, p. 167-177.

Cacas M.C., de Marsily G., Tillie B., Barbreau A., Durand E., Feuga B., and Peaudecerf P. (1990a): Modelling Fracture Flow With a Stochastic Discrete Fracture Network Calibration and Validation - 1 The Flow Model, *Water Resour. Res,26(3)*, 479-489.

Cacas M.C., Ledoux E., de Marsily G., Barbreau A., Calmels P., Gaillard B., and Margritta R. (1990b): Modelling Fracture Flow with a Stochastic Discrete Fracture Network Calibration and Validation - 2 The Transport Model, *Water Resour. Res., 26(3)*, 491-500.

Cauffman T.L., LaVenue A.M. and McCord J.P. (1990): Ground-Water Flow Modelling of the Culebra Dolomite. Volume II: Model Calibration, Sandia National Laboratories Report SAND89-7068/2.

Charlaix E. (1987): Dispersion en milieu poreux mise en evidence de longueurs caracteristiques. Ph.D thesis, Univ. of Paris 6.

Chilès J.P., and de Marsily G. (1993): Stochastic models of fracture systems and their use in flow and transport modelling. In Flow and Contaminant Transport in Fractured rock (chap. 4), J. Bear, C.F. Tsang and G. de Marsily (Eds.), Academic Press, 560p.

Chilès J.P., Guérin F., and Billaux D. (1992): 3D stochastic simulation of fracture network and flow at Stripa conditioned on observed fractures and calibrated on measured flow rates, *Rock Mechanics*, J.R. Tillerson and W.R. Wawersik (eds), Balkema, Rotterdam, Netherlands, p.533-542.

Cliffe K.A., Jackson C.P. and Impey M.D.: A Preliminary Study of the WIPP-2 Test Case, Nirex Safety Studies Report NSS/R314 (in preparation).

Corbet T.F. and Wallace M.G. (1993): Post-Pleistocene Patterns of Shallow Groundwater Flow in the Delaware Basin, Southeastern New Mexico and West Texas, New Mexico Geological Society Guidebook, 44th Field Conference, Carlsbad Region, New Mexico and West Texas, 321-326.

Davies P.B. (1989): Variable-Density Groundwater Flow and Paleohydrology in the Waste Isolation Pilot Plant (WIPP) Region, Southeastern New Mexico, USGS Open-File Report 88-490, US Geological Survey, Albuquerque, NM.

Dershowitz W.S., Gordon B.M., and Kafritsas J.C. (1985): A New Three Dimensional Model for Flow in Fractured Rock, Hydrogeology of rocks of low permeability, IAH Congress, Tucson, Arizona, Volume 17, p. 441-448.

Dverstorp B., and Andersson J. (1989): Application of discrete fracture network concept with field data possibilities of model calibration and validation, *Water Resour. Res.*, 25(3), 540-550.

Dverstorp B., Andersson J., and Nordqvist W. (1992): Discrete fracture network interpretation of field tracer migration in sparsely fractured rock. *Water Resour. Res.*, 28(9), 2327-2343.

Endo H.K., Long J.C.S., Wilson C.R., and Witherspoon P.A. (1984): A model for investigating mechanical transport in fracture networks, *Water Resour. Res.*, vol 20(10), 1390-1400.

Endo H.K. and Witherspoon P.A. (1985): Mechanical transport and porous media equivalence in anisotropic fracture networks. Hydrogeology of Rocks of low permeability. IAH congress, vol 17, Tucson, Arizona, p. 527-535.

Gentier S. (1986): Morphologie et Comportement Hydromécanique d'une Fracture naturelle dans un Granite sous Contrainte Normale. Etude Expérimentale et Théorique, Thèse de Doctorat à l'Université d'Orléans.

Gómez-Hernández J.J. and Srivastava R.M. (1990): ISIM3D: an ANSI-C Three-dimensional Multiple Indicator Conditional Simulation Program. Computers and Geosciences, vol. 16, no. 4, pp. 395-440.

Gómez-Hernández J.J. (1991): A Stochastic Approach to the Simulation of Block Conductivity Values Conditioned upon Data Measured at a Smaller Scale. PhD Thesis, Stanford University, U.S.A.

Gómez-Hernández J.J. and Journel A.G. (1993): Joint Sequential Simulation of Multi-Gaussian Fields, in Geostatistics Troia 92, Volume 1, Ed A Soares, Kluwer Academic Publishers.

Gonzales M.M. (1989): Compilation and Comparison of Test Hole Location Surveys in the Vicinity of the Waste Isolation Pilot Plant (WIPP) Site. Sandia National Laboratories Report SAND88-1065.

Grindrod P, Herbert A., Roberts D., and Robinson P. (1991): NAPSAC Technical Document. Stripa Project, Report TR 91-31.

Guérin F., and Billaux D. (1993): On the relationship between connectivity and the continuum approximation in fracture flow and transport modeling. Hydrogeology of hard rocks, XXIVth IAH Congress, p. 215-224, Oslo.

Guérin F., and Billaux D.: Chaine de calcul FETICHE,Fracturation Ecoulement Transport en mIlieu CHEnalise, Mode d'emploi. Technical Note BRGM 93 EAU 024.

Guérin F., and Billaux D. (1993): Analyzing flow and transport in the Stripa 3D site Influence of connectivity, Intraval workshop, San Antonio.

Gustafsson E. and Klockars C-E. (1981): Studies on groundwater transport in fractured crystalline rock under controlled conditions using non-radioactive tracers. SKBF/KBS Technical Report TR 81-07.

Gustafsson E. and Klockars C-E. (1984): Study of strontium and cesium migration in fractured crystalline rock. SKBF/KBS Technical Report TR 84-07.

Gustafsson E., Andersson P., Eriksson C-O. and Nordqvist R. (1990): Radially Converging Tracer Experiment in a Low Angle Fracture Zone at the Finnsjön Site, Central Sweden. The Fracture Zone Project Phase 3. SKB Progress Report AR 90-27.

Gustafsson E. and Andersson P. (1991): Groundwater flow conditions in a low-angle fracture zone at Finnsjön, Sweden. Journal of hydrology, Vol 126, pp 79-111.

Gustafsson E. and Nordqvist R. (1993): Radially Converging Tracer Experiment in a Low Angle Fracture Zone at the Finnsjön Site, Central Sweden. The Fracture Zone Project Phase 3. SKB Technical Report 93-25.

Hartley L.J. and Jackson C.P.: NAMMU (release 6.1) User Guide, AEA Report

Hatanaka K. and Mukai S. (1993a): Preliminary Modelling of the Effect of Heterogeneity on Tracer Transport at Finnsjön Site. Presentation at the third INTRAVAL Phase 2 Workshop, San Antonio, Texas, November 9-13, 1992.

Hatanaka K. and Mukai S. (1993b): Study on Estimation of Hydraulic Conductivity and Tracer Transport at Finnsjön Site. Presentation at the Fourth INTRAVAL Phase 2 Workshop, Stockholm, Sweden, August 30-September 3, 1993.

Hautojärvi A. (1993): Do Break-trough curves in field tests reveal matrix diffusion. Research Report no. YDI 12/93, March 1993.

Hautojärvi A. and Taivassalo V. (1988): INTRAVAL PROJECT. Test case 5: Tracer tests at Finnsjön. Predictive modelling of the radially converging experiment. Report YJT-88-13.

Hautojärvi A. and Coworkers. (1992): VTT Analysis of Tracer Data. In Tsang and Neuman (editors). The International INTRAVAL Project. NEA/SKI 1992.

Hautojärvi A. (1993): Summary of VTT analysis of Finnsjön. Presentation at the INTRAVAL Phase II Working Group 2 meeting, Berkeley, California, 15-16/3, 1993.

Herbert A.W, Gale J.E, Lanyon G.W, and MacLeod B. (1991): Modelling for the Stripa Site Characterization and Validation. Drift inflow prediction of flow through fractured rock. Stripa Project, Report TR 91-35, SKB.

Herbert A.W. and Lanyon G.W. (1992): "Discrete fracture network modelling of flow and transport within a fracture zone at Stripa", in Proceedings of the ISRM regional conference on Fractured and Jointed Rock Masses, Lake Tahoe, June 1992. Vol. 3, pp 699-708. Berkeley, California, Lawrence Berkeley Laboratory.

Hodgkinson D., and Grindrod P. (Eds). (1991): The International Intraval Project. Phase 1, test case 4. Flow and tracer experiment in crystalline rock based on the Stripa 3-D experiment. OECD/NEA and SKI, Paris.

Ilvonen M., Hautojärvi A. and Peatero P. (1993): Analysis of Stripa 3D Data by a deconvolution technique, Draft Report, 42 p, July 1993.

Jakob A. and Hadermann J. (1994): INTRAVAL Finnsjön Test - modelling results for some tracer experiments. PSI-Bericht Nr 94-12, Würenlingen, 1994.

Javandel I., Doughty C., and Tsang C.F. (1984): Groundwater transport Handbook of Mathematical Models. Water Resour. Monogr. Ser., vol 10, AGU, Washington, D.C.

Journel A. (1974): Geostatistics for Conditional Simulation of Orebodies, Economic Geology, 69, 673-680.

Journel A.G. (1989): Fundamentals of Geostatistics in Five Lessons, volume 8 of Short Courses in Geology. AGU, Washington D.C.

Journel A.G. and Huijbregts Ch.J. (1990): Mining Geostatistics, Academic Press, 1978. A M LaVenue, T L Cauffman and J F Pickens, Ground-Water Flow Modelling of the Culebra Dolomite. Volume I: Model Calibration, Sandia National Laboratories Report SAND89-7068/1.

Kobayashi A. and Yamashita R. (1993): Heterogeneous Anisotropic Model of Finnsjön Test Case and Seepage and Transport Analyses for Radial Converging Test. Presentation at the Fourth INTRAVAL Phase 2 Workshop, Stockholm, Sweden, August 30-September 3, 1993.

Kröhn K.P. (1987-1990): ROCKFLOW - Theory and Users Manual for the Program System ROCKFLOW; Part 8, 'DM - Gekoppeltes Strömungs- und Transportmodell Einschließlich Dichteeffekte (Dichtemodell)', Inst. für Strömungsmechanik und Elektronisches Rechnen im Bauwesen, Universität Hannover.

Kröhn K.P. and Schelkes K. (1995): Modelling of Density-Dependent Regional Groundwater Movement in the Vicinity of the WIPP Site, New Mexico, USA, Bundesanstalt für Geowissenschaften und Rohstoffe Report No. 113584 (in preparation).

Kung C-S., Cvetkovic V. and Winberg A. (1992): Calibration and Validation of a Stochastic Continuum Model using the Finnsjön Dipole Tracer Test. A Contribution to INTRAVAL Phase 2. SKB Technical Report TR 92-35.

Lambert S.J. and Harvey D.M. (1987): Stable-Isotope Geochemistry of Groundwater in the Delaware Basin of Southeastern New Mexico, Sandia National Laboratories Report SAND87-0138.

Lapidus L., and Amundsen N.R. (1952): Mathematics of adsorption in beds. VII, *J. Phys. Chem., 56*, 984-988.

Long J.C.S. (1983): Investigation of equivalent porous media permeability in networks of discontinuous fractures, Ph.D. thesis, LBL, Univ. of California, Berkeley, CA.

Long J.C.S., and Billaux D. (1987): From field data to fracture network modeling An example incorporating spatial structure, *Water Resour. Res.*, vol. 23(7), p. 1201-1216.

Luis S. and McLaughlin D. (1992): A Stochastic Approach to Model Validation. Adv. Water Res., vol. 1 of special issue on model validation, 1992.

Mantoglou A. and Wilson J.L. (1982): The Turning Bands Method for Simulation of Random Fields using Line Generation by a Spectral Method, Water Resour. Res. 18(5), 1379-1394.

de Marsily G. (1985): Quantitative Hydrogeology, Academic Press, 1985.

Matheron G. (1973): The Intrinsic Random Functions and their Applications, Advances in Applied Probability, 5, 436-468.

McDonald M.G. and Harbaugh A.W. (1988): A Modular Three-Dimensional Finite-Difference Groundwater Flow Model, US Geological Survey Open-File Report 83-875.

Metcalfe D. (1993): Impact of Variable Fluid Density on Groundwater Flow Patterns to the South of the WIPP Site, AECB Report.

Neretnieks I. (1993): Solute transport in fractured rock. Applications to radionuclide waste repositories. In Flow and Contaminant Transport in Fractured rock (Chap. 2). J. Bear, C.F. Tsang and G. de Marsily. (Eds), Academic Press, 560p.

Neretnieks I. (1987): Channeling effects in flow and transport in fractured rocks - Some recent observations and models, Geoval Symposium, Stockholm, pp. 315-335.

Neretnieks I. (1983): A Note on Fracture Flow Mechanisms in the Ground, *Water Resour. Res., 19*, 364-370.

Neretnieks I., Eriksen T., and Tähtinen P. (1982): Tracer Movement in a Single Fissure in Granitic Rock Some Experimental Results and Their Interpretation, *Water Resources Res.*, 18(4), 849.

Neretnieks I. (1980): Diffusion in rock matrix An important factor in radionuclide retardation?. *J. Geophys. Res., 85*, 4379-4397.

Ng T-T. and Kota S. (1993): Interpretation of the Radially Converging Tracer Tests at the Finnsjön Research Site, Sweden. U. of New Mexico Report in prep.

Nordqvist A.W., Tsang Y.W., Tsang C.F., Dverstorp B., Anderson J. (1992): A variable aperture fracture network model for flow and transport in fractured rocks, *Water Resour. Res.*, vol. 28(6), p. 1703-1713.

Robinson P.C. (1984): Connectivity, Flow and Transport in Network Models of Fractured Media, Ph.D. Thesis, St. Catherine's College, Oxford Univ., Ref TP1072.

Schwartz J., Fillon E., Sauty J.P. and Dewiere L. (1993): FINNSJÖN SITE (SWEDEN) - Interpretation of Interference Tests. In : Proceedings International High Level Radioactive Waste Management Conference, Las Vegas, April 26-30, 1993.

Schwartz J. (1993): Participation au test INTRAVAL - Finnsjön - Interprétation des tests de traçage en milieu granitique - Modélisation du test de traçage en radial convergent - Rapport de synthèse. ANDRA report 663 RP BRG 93-014.

Siegel M.D., Lambert S.J., Robinson K.L. (Ed.) (1991): Hydrochemical Studies of the Rustler Formation and Related Rocks in the Waste Isolation Pilot Plant Area, Southeastern New Mexico, Sandia National Laboratories Report SAND88-0196.

SKI (1986): INTRACOIN Final Report Levels 2 and 3. SKI Report 86:2.

SKI/NEA (1990): The International INTRAVAL Project. Background and Results. OECD Paris 1990.

Swift P.N. (1991): Long-Term Climate Variability at the Waste Isolation Pilot Plant, in Sandia National Laboratories Report SAND88-0196.

Tang G.H., Frind E.O and Sudicky E.A. (1981): Contaminant transport in fractured porous media - An analytical solution for a single fracture. *Water Resour. Res., 17,* 555-564.

Thiery D. (1990): Logiciel MARTHE - Modélisation d'Aquiféeres par Maillage Rectangulaire en Régime Transitoire pour le calcul Hydrodynamique des Ecoulments - Release 4.3. BRGM Report no. 32210.

Tompson A.F.B., Ababou R. and Gelhar L.W. (1989): Implementation of the Three-Dimensional Turning Bands Random Field Generator, Water Resour. Res. 25(10), 2227-2243.

Travis B.J. and Birdsell K.H. (1991): TRACR3D: A model of flow and transport in Porous media. Model description and user´s manual. LA-11798-M, Los Alamos.

Tsang C-F and Neuman S. (editors) (1992): The International Intraval Project. Phase 1, Test Case 5. Studies of Tracer Experiments in a Fracture Zone at the Finnsjön Research area. NEA/SKI, OECD Paris 1992.

Tsang C.F., Tsang Y.W. and Hale F.V. (1991): Tracer transport in Fractures Analysis of field data based on a variable-aperture channel model, *Water Resour. Res., 27*(12), 3095-3106.

Tsang Y.W., and Tsang C.F. (1987): Channel Model of Flow Through Fractured Media, *Water Resour. Res.*, 23(3), 467-479.

Tsang Y.W., Tsang C.F., Neretnieks I., and Moreno L. (1988): Flow and Tracer Transport in Fractured Media - A Variable Aperture Channel Model and its Properties, *Water Resour. Res.*, 24(12), 2049-2060.

Van Genuchten M.Th. and Alves W.J. (1982): Analytical solutions of the one-dimensional convective-dispersive solute transport equation, U. S. Dep. Agric. Tech. Bull., 1661.

Voss C.I. (1990): SUTRA - A finite-element simulation model for saturated-unsaturated, fluid-density-dependent groundwater flow with energy transport or chemically-reactive single-species solute transport. Version V06902D. U.S. Geological Survey Water-Resources Investigations Report 84-4369.

MAIN SALES OUTLETS OF OECD PUBLICATIONS
PRINCIPAUX POINTS DE VENTE DES PUBLICATIONS DE L'OCDE

AUSTRALIA – AUSTRALIE
D.A. Information Services
648 Whitehorse Road, P.O.B 163
Mitcham, Victoria 3132 Tel. (03) 9210.7777
Fax: (03) 9210.7788

AUSTRIA – AUTRICHE
Gerold & Co.
Graben 31
Wien I Tel. (0222) 533.50.14
Fax: (0222) 512.47.31.29

BELGIUM – BELGIQUE
Jean De Lannoy
Avenue du Roi, Koningslaan 202
B-1060 Bruxelles Tel. (02) 538.51.69/538.08.41
Fax: (02) 538.08.41

CANADA
Renouf Publishing Company Ltd.
1294 Algoma Road
Ottawa, ON K1B 3W8 Tel. (613) 741.4333
Fax: (613) 741.5439

Stores:
61 Sparks Street
Ottawa, ON K1P 5R1 Tel. (613) 238.8985

12 Adelaide Street West
Toronto, ON M5H 1L6 Tel. (416) 363.3171
Fax: (416)363.59.63

Les Éditions La Liberté Inc.
3020 Chemin Sainte-Foy
Sainte-Foy, PQ G1X 3V6 Tel. (418) 658.3763
Fax: (418) 658.3763

Federal Publications Inc.
165 University Avenue, Suite 701
Toronto, ON M5H 3B8 Tel. (416) 860.1611
Fax: (416) 860.1608

Les Publications Fédérales
1185 Université
Montréal, QC H3B 3A7 Tel. (514) 954.1633
Fax: (514) 954.1635

CHINA – CHINE
China National Publications Import
Export Corporation (CNPIEC)
16 Gongti E. Road, Chaoyang District
P.O. Box 88 or 50
Beijing 100704 PR Tel. (01) 506.6688
Fax: (01) 506.3101

CHINESE TAIPEI – TAIPEI CHINOIS
Good Faith Worldwide Int'l. Co. Ltd.
9th Floor, No. 118, Sec. 2
Chung Hsiao E. Road
Taipei Tel. (02) 391.7396/391.7397
Fax: (02) 394.9176

CZECH REPUBLIC – RÉPUBLIQUE TCHÈQUE
National Information Centre
NIS – prodejna
Konviktská 5
Praha 1 – 113 57 Tel. (02) 24.23.09.07
Fax: (02) 24.22.94.33
(*Contact* Ms Jana Pospisilova, nkposp@dec.niz.cz)

DENMARK – DANEMARK
Munksgaard Book and Subscription Service
35, Nørre Søgade, P.O. Box 2148
DK-1016 København K Tel. (33) 12.85.70
Fax: (33) 12.93.87

J. H. Schultz Information A/S,
Herstedvang 12,
DK – 2620 Albertslung Tel. 43 63 23 00
Fax: 43 63 19 69
Internet: s-info@inet.uni-c.dk

EGYPT – ÉGYPTE
The Middle East Observer
41 Sherif Street
Cairo Tel. 392.6919
Fax: 360-6804

FINLAND – FINLANDE
Akateeminen Kirjakauppa
Keskuskatu 1, P.O. Box 128
00100 Helsinki

Subscription Services/Agence d'abonnements :
P.O. Box 23
00371 Helsinki Tel. (358 0) 121 4416
Fax: (358 0) 121.4450

FRANCE
OECD/OCDE
Mail Orders/Commandes par correspondance :
2, rue André-Pascal
75775 Paris Cedex 16 Tel. (33-1) 45.24.82.00
Fax: (33-1) 49.10.42.76
Telex: 640048 OCDE
Internet: Compte.PUBSINQ@oecd.org

Orders via Minitel, France only/
Commandes par Minitel, France exclusivement :
36 15 OCDE

OECD Bookshop/Librairie de l'OCDE :
33, rue Octave-Feuillet
75016 Paris Tél. (33-1) 45.24.81.81
(33-1) 45.24.81.67

Dawson
B.P. 40
91121 Palaiseau Cedex Tel. 69.10.47.00
Fax: 64.54.83.26

Documentation Française
29, quai Voltaire
75007 Paris Tel. 40.15.70.00

Economica
49, rue Héricart
75015 Paris Tel. 45.75.05.67
Fax: 40.58.15.70

Gibert Jeune (Droit-Économie)
6, place Saint-Michel
75006 Paris Tel. 43.25.91.19

Librairie du Commerce International
10, avenue d'Iéna
75016 Paris Tel. 40.73.34.60

Librairie Dunod
Université Paris-Dauphine
Place du Maréchal-de-Lattre-de-Tassigny
75016 Paris Tel. 44.05.40.13

Librairie Lavoisier
11, rue Lavoisier
75008 Paris Tel. 42.65.39.95

Librairie des Sciences Politiques
30, rue Saint-Guillaume
75007 Paris Tel. 45.48.36.02

P.U.F.
49, boulevard Saint-Michel
75005 Paris Tel. 43.25.83.40

Librairie de l'Université
12*a*, rue Nazareth
13100 Aix-en-Provence Tel. (16) 42.26.18.08

Documentation Française
165, rue Garibaldi
69003 Lyon Tel. (16) 78.63.32.23

Librairie Decitre
29, place Bellecour
69002 Lyon Tel. (16) 72.40.54.54

Librairie Sauramps
Le Triangle
34967 Montpellier Cedex 2 Tel. (16) 67.58.85.15
Fax: (16) 67.58.27.36

A la Sorbonne Actual
23, rue de l'Hôtel-des-Postes
06000 Nice Tel. (16) 93.13.77.75
Fax: (16) 93.80.75.69

GERMANY – ALLEMAGNE
OECD Bonn Centre
August-Bebel-Allee 6
D-53175 Bonn Tel. (0228) 959.120
Fax: (0228) 959.12.17

GREECE – GRÈCE
Librairie Kauffmann
Stadiou 28
10564 Athens Tel. (01) 32.55.321
Fax: (01) 32.30.320

HONG-KONG
Swindon Book Co. Ltd.
Astoria Bldg. 3F
34 Ashley Road, Tsimshatsui
Kowloon, Hong Kong Tel. 2376.2062
Fax: 2376.0685

HUNGARY – HONGRIE
Euro Info Service
Margitsziget, Európa Ház
1138 Budapest Tel. (1) 111.62.16
Fax: (1) 111.60.61

ICELAND – ISLANDE
Mál Mog Menning
Laugavegi 18, Pósthólf 392
121 Reykjavik Tel. (1) 552.4240
Fax: (1) 562.3523

INDIA – INDE
Oxford Book and Stationery Co.
Scindia House
New Delhi 110001 Tel. (11) 331.5896/5308
Fax: (11) 371.8275

17 Park Street
Calcutta 700016 Tel. 240832

INDONESIA – INDONÉSIE
Pdii-Lipi
P.O. Box 4298
Jakarta 12042 Tel. (21) 573.34.67
Fax: (21) 573.34.67

IRELAND – IRLANDE
Government Supplies Agency
Publications Section
4/5 Harcourt Road
Dublin 2 Tel. 661.31.11
Fax: 475.27.60

ISRAEL – ISRAËL
Praedicta
5 Shatner Street
P.O. Box 34030
Jerusalem 91430 Tel. (2) 52.84.90/1/2
Fax: (2) 52.84.93

R.O.Y. International
P.O. Box 13056
Tel Aviv 61130 Tel. (3) 546 1423
Fax: (3) 546 1442

Palestinian Authority/Middle East:
INDEX Information Services
P.O.B. 19502
Jerusalem Tel. (2) 27.12.19
Fax: (2) 27.16.34

ITALY – ITALIE
Libreria Commissionaria Sansoni
Via Duca di Calabria 1/1
50125 Firenze Tel. (055) 64.54.15
Fax: (055) 64.12.57

Via Bartolini 29
20155 Milano Tel. (02) 36.50.83

Editrice e Libreria Herder
Piazza Montecitorio 120
00186 Roma
Tel. 679.46.28
Fax: 678.47.51

Libreria Hoepli
Via Hoepli 5
20121 Milano
Tel. (02) 86.54.46
Fax: (02) 805.28.86

Libreria Scientifica
Dott. Lucio de Biasio 'Aeiou'
Via Coronelli, 6
20146 Milano
Tel. (02) 48.95.45.52
Fax: (02) 48.95.45.48

JAPAN – JAPON

OECD Tokyo Centre
Landic Akasaka Building
2-3-4 Akasaka, Minato-ku
Tokyo 107
Tel. (81.3) 3586.2016
Fax: (81.3) 3584.7929

KOREA – CORÉE

Kyobo Book Centre Co. Ltd.
P.O. Box 1658, Kwang Hwa Moon
Seoul
Tel. 730.78.91
Fax: 735.00.30

MALAYSIA – MALAISIE

University of Malaya Bookshop
University of Malaya
P.O. Box 1127, Jalan Pantai Baru
59700 Kuala Lumpur
Malaysia
Tel. 756.5000/756.5425
Fax: 756.3246

MEXICO – MEXIQUE

OECD Mexico Centre
Edificio INFOTEC
Av. San Fernando no. 37
Col. Toriello Guerra
Tlalpan C.P. 14050
Mexico D.F.
Tel. (525) 665 47 99
Fax: (525) 606 13 07

NETHERLANDS – PAYS-BAS

SDU Uitgeverij Plantijnstraat
Externe Fondsen
Postbus 20014
2500 EA's-Gravenhage
Tel. (070) 37.89.880
Voor bestellingen:
Fax: (070) 34.75.778

Subscription Agency/
Agence d'abonnements :
SWETS & ZEITLINGER BV
Heereweg 347B
P.O. Box 830
2160 SZ Lisse
Tel. 252.435.111
Fax: 252.415.888

NEW ZEALAND – NOUVELLE-ZÉLANDE

GPLegislation Services
P.O. Box 12418
Thorndon, Wellington
Tel. (04) 496.5655
Fax: (04) 496.5698

NORWAY – NORVÈGE

NIC INFO A/S
Ostensjoveien 18
P.O. Box 6512 Etterstad
0606 Oslo
Tel. (22) 97.45.00
Fax: (22) 97.45.45

PAKISTAN

Mirza Book Agency
65 Shahrah Quaid-E-Azam
Lahore 54000
Tel. (42) 735.36.01
Fax: (42) 576.37.14

PHILIPPINE – PHILIPPINES

International Booksource Center Inc.
Rm 179/920 Cityland 10 Condo Tower 2
HV dela Costa Ext cor Valero St.
Makati Metro Manila
Tel. (632) 817 9676
Fax: (632) 817 1741

POLAND – POLOGNE

Ars Polona
00-950 Warszawa
Krakowskie Prezdmiescie 7
Tel. (22) 264760
Fax: (22) 265334

PORTUGAL

Livraria Portugal
Rua do Carmo 70-74
Apart. 2681
1200 Lisboa
Tel. (01) 347.49.82/5
Fax: (01) 347.02.64

SINGAPORE – SINGAPOUR

Ashgate Publishing
Asia Pacific Pte. Ltd
Golden Wheel Building, 04-03
41, Kallang Pudding Road
Singapore 349316
Tel. 741.5166
Fax: 742.9356

SPAIN – ESPAGNE

Mundi-Prensa Libros S.A.
Castelló 37, Apartado 1223
Madrid 28001
Tel. (91) 431.33.99
Fax: (91) 575.39.98

Mundi-Prensa Barcelona
Consell de Cent No. 391
08009 – Barcelona
Tel. (93) 488.34.92
Fax: (93) 487.76.59

Llibreria de la Generalitat
Palau Moja
Rambla dels Estudis, 118
08002 – Barcelona
(Subscripcions) Tel. (93) 318.80.12
(Publicacions) Tel. (93) 302.67.23
Fax: (93) 412.18.54

SRI LANKA

Centre for Policy Research
c/o Colombo Agencies Ltd.
No. 300-304, Galle Road
Colombo 3
Tel. (1) 574240, 573551-2
Fax: (1) 575394, 510711

SWEDEN – SUÈDE

CE Fritzes AB
S–106 47 Stockholm
Tel. (08) 690.90.90
Fax: (08) 20.50.21

For electronic publications only/
Publications électroniques seulement
STATISTICS SWEDEN
Informationsservice
S-115 81 Stockholm
Tel. 8 783 5066
Fax: 8 783 4045

Subscription Agency/Agence d'abonnements :
Wennergren-Williams Info AB
P.O. Box 1305
171 25 Solna
Tel. (08) 705.97.50
Fax: (08) 27.00.71

SWITZERLAND – SUISSE

Maditec S.A. (Books and Periodicals/Livres et périodiques)
Chemin des Palettes 4
Case postale 266
1020 Renens VD 1
Tel. (021) 635.08.65
Fax: (021) 635.07.80

Librairie Payot S.A.
4, place Pépinet
CP 3212
1002 Lausanne
Tel. (021) 320.25.11
Fax: (021) 320.25.14

Librairie Unilivres
6, rue de Candolle
1205 Genève
Tel. (022) 320.26.23
Fax: (022) 329.73.18

Subscription Agency/Agence d'abonnements :
Dynapresse Marketing S.A.
38, avenue Vibert
1227 Carouge
Tel. (022) 308.08.70
Fax: (022) 308.07.99

See also – Voir aussi :
OECD Bonn Centre
August-Bebel-Allee 6
D-53175 Bonn (Germany)
Tel. (0228) 959.120
Fax: (0228) 959.12.17

THAILAND – THAÏLANDE

Suksit Siam Co. Ltd.
113, 115 Fuang Nakhon Rd.
Opp. Wat Rajbopith
Bangkok 10200
Tel. (662) 225.9531/2
Fax: (662) 222.5188

TRINIDAD & TOBAGO, CARIBBEAN TRINITÉ-ET-TOBAGO, CARAÏBES

SSL Systematics Studies Limited
9 Watts Street
Curepe
Trinadad & Tobago, W.I.
Tel. (1809) 645.3475
Fax: (1809) 662.5654

TUNISIA – TUNISIE

Grande Librairie Spécialisée
Fendri Ali
Avenue Haffouz Imm El-Intilaka
Bloc B 1 Sfax 3000
Tel. (216-4) 296 855
Fax: (216-4) 298.270

TURKEY – TURQUIE

Kültür Yayinlari Is-Türk Ltd. Sti.
Atatürk Bulvari No. 191/Kat 13
06684 Kavaklidere/Ankara
Tél. (312) 428.11.40 Ext. 2458
Fax : (312) 417.24.90
et 425.07.50-51-52-53

Dolmabahce Cad. No. 29
Besiktas/Istanbul
Tel. (212) 260 7188

UNITED KINGDOM – ROYAUME-UNI

HMSO
Gen. enquiries
Tel. (0171) 873 0011

Postal orders only:
P.O. Box 276, London SW8 5DT
Personal Callers HMSO Bookshop
49 High Holborn, London WC1V 6HB
Fax: (0171) 873 8463

Branches at: Belfast, Birmingham, Bristol, Edinburgh, Manchester

UNITED STATES – ÉTATS-UNIS

OECD Washington Center
2001 L Street N.W., Suite 650
Washington, D.C. 20036-4922
Tel. (202) 785.6323
Fax: (202) 785.0350
Internet: washcont@oecd.org

Subscriptions to OECD periodicals may also be placed through main subscription agencies.

Les abonnements aux publications périodiques de l'OCDE peuvent être souscrits auprès des principales agences d'abonnement.

Orders and inquiries from countries where Distributors have not yet been appointed should be sent to: OECD Publications, 2, rue André-Pascal, 75775 Paris Cedex 16, France.

Les commandes provenant de pays où l'OCDE n'a pas encore désigné de distributeur peuvent être adressées aux Éditions de l'OCDE, 2, rue André-Pascal, 75775 Paris Cedex 16, France.

8-1996

LES ÉDITIONS DE L'OCDE, 2 rue André-Pascal, 75775 PARIS CEDEX 16 - n° 79496 1996
IMPRIMÉ EN FRANCE